

DISSERTATION

TITANIA NANOTUBE ARRAYS:  
INTERFACES FOR IMPLANTABLE DEVICES

Submitted by

Barbara Symie Smith

Graduate Degree Program in Biomedical Engineering

In partial fulfillment of the requirements

For the Degree of Doctor of Philosophy

Colorado State University

Fort Collins, Colorado

Spring 2012

Doctoral Committee:

Advisor: Ketul Popat

Mercedes Gonzalez-Juarrero

Ashok Prasad

Lakshmi Prasad Dasi

Steven Dow

## ABSTRACT

### TITANIA NANOTUBE ARRAYS: INTERFACES FOR IMPLANTABLE DEVICES

For the 8-10% of Americans (20-25 million people) that have implanted biomedical devices, biomaterial failure and the need for revision surgery are critical concerns. The major causes for failure in implantable biomedical devices promoting a need for re-implantation and revision surgery include thrombosis, post-operative infection, immune driven fibrosis and biomechanical failure. The successful integration of long-term implantable devices is highly dependent on the early events of tissue/biomaterial interaction, promoting either implant rejection or a wound healing response (extracellular matrix production and vasculature). Favorable interactions between the implant surface and the respective tissue are critical for the long-term success of any implantable device. Recent studies have shown that material surfaces which mimic the natural physiological hierarchy of *in vivo* tissue may provide a possible solution for enhancing biomaterial integration, thus preventing infection and biomaterial rejection. Titania nanotube arrays, fabricated using a simple anodization technique, provide a template capable of promoting altered cellular functionality at a hierarchy similar to that of natural tissue. This work focuses on the fabrication of immobilized, vertically oriented and highly uniform titania nanotube arrays to determine how this specific nano-architecture affects skin cell functionality, hemocompatibility, thrombogenicity and the immune response. The results in this work identify enhanced dermal matrix production, altered hemocompatibility, reduced thrombogenicity and a deterred immune response on titania nanotube arrays.

This evidences promising implications with respect to the use of titania nanotube arrays as beneficial interfaces for the successful implantation of biomedical devices.

## ACKNOWLEDGEMENTS

Funding support for this work was provided by the National Science Foundation (NSF) (CBET - 0827827 and 0827845), and the Colorado Office of Economic Development and International Trade. The author would like to thank Dan Bolchen and the staff at Garth Englund Blood Center for their assistance with drawing blood.

## DEDICATION

This work is dedicated to the brilliant individuals who stand as my platform in life: Sylvia K. Delin, Robert B. Smith, David A. Smith and Mark B. Smith. From one rock to another, I thank you.

TABLE OF CONTENTS

**Introduction.....1-2**

**Hypothesis and Specific Aims.....3-5**

**Chapter 1.....6**  
Literature Review.....6-21

**Chapter 2.....22**  
Specific Aim #1.....22-39  
Fabrication and Characterization of Titania Nanotube Arrays.....22-39

**Chapter 3.....40**  
Specific Aim #2.....40-67  
Skin Cell Functionality on Titania Nanotube Arrays.....40-67

**Chapter 4.....68**  
Specific Aim #3.....68-92  
Altered Hemocompatibility on Titania Nanotube Arrays.....68-92

**Chapter 5.....93**  
Specific Aim #4.....93-130  
Reduced Thrombogenicity on Titania Nanotube Arrays.....93-130

**Chapter 6.....131**  
Specific Aim #5.....131-164  
Modulating Immune Responses on Titania Nanotube Arrays.....131-164

**Chapter 7.....165**  
Conclusions and Suggestions for Future Work .....165-170

## LIST OF TABLES

Table 2.1	Numerical analysis of micro- and nano-scale substrate topographies, measured using atomic force microscopy (AFM) ( <b>See Figure 2.6</b> ). Where Ra is the mean roughness, Rq is the standard deviation of the surface heights, Rz is the average maximum profile of the ten greatest peak-to-valley separations in the region of evaluation, and Rt is the vertical distance between the highest and lowest points (length/area).
Table 2.2	Representative images of the water contact angle (degrees) on titania nanotube arrays and biomedical grade titanium. The results indicate that titania nanotube arrays are more hydrophilic than the control surfaces.
Table 2.3	Young's modulus and hardness values for titania nanotube arrays and biomedical grade titanium surfaces, determined using nanoindentation.
Table 3.1	Blocking agents, primary antibodies and secondary antibodies used for immunofluorescence identification of membrane specific marker proteins on HDF and HEK cells.
Table 4.1	N/Ti ratio computed from XPS survey scans for blood serum proteins adsorbed on titania nanotube arrays and biomedical grade titanium.
Table 5.1	Blocking agents, primary antibodies and secondary antibodies used for immunofluorescence identification of membrane specific marker proteins on platelets and leukocytes.
Table 5.2	Summary of results identifying a decrease in thrombogenic effects on titania nanotube arrays as compared to biomedical grade titanium after 2 hours of contact with whole blood plasma.
Table 6.1	(a and b) Summary of CBA results on titania nanotube arrays as compared to the control substrates after 2 hours, 2 and 7 days of culture. The results identify a decrease in long-term cytokine/chemokine expression on titania nanotube arrays as compared to the control substrates after 2 and 7 days of incubation in human whole blood lysate. (* $\rightarrow$ $p < 0.05$ )
Table 6.2	Summary of CBA results for LPS positive samples on titania nanotube arrays as compared to the control substrate after 2 hours, 2 and 7 days of incubation in human whole blood lysate. (* $\rightarrow$ $p < 0.05$ )

## LIST OF FIGURES

- Figure 1.1 Schematic of two fates of intra-osseous transcutaneous biomaterial implantation, either leading to tissue/biomaterial integration or biomaterial rejection via fibrous encapsulation.
- Figure 1.2 Schematic of the complex cascade of events following biomaterial implantation.
- Figure 1.3 Schematic of the natural hierarchy of biological components, including multiple size scales.
- Figure 2.1 Schematic of anodization setup for fabrication of titania nanotube arrays.
- Figure 2.2 Schematic of anodized titanium, for the fabrication of titania nanotube arrays.
- Figure 2.3 Representative SEM images (20000x, 50000x, 75000x magnification) showing the nanoarchitecture of titania nanotube arrays fabricated using an anodization technique.
- Figure 2.4 Representative XRD pattern of titania nanotube arrays showing crystalline phases fabricated using an anodization technique.
- Figure 2.5 Representative atomic force microscopy (AFM) images of surface topographies for titania nanotube arrays and the control substrates. The images include (top) 3D plots and (bottom) surface topography. The resulting images identify a nano-architecture on titania nanotube arrays and a micro-architecture on biomedical grade titanium.
- Figure 2.6 Schematic of the cellular response to the different surfaces, identifying a correlation between increased hydrophilicity and improved cellular integration.
- Figure 2.7 Representative load-displacement curves for titania nanotube arrays and biomedical grade titanium, obtained by nanoindentation, (insert, left corner) Representative SEM image of an indent made by a Beckovich tip on a titania nanotube array substrate
- Figure 2.8 Representative optical microscopy images of scratches at various forces on titania nanotube arrays and smooth titanium surfaces.
- Figure 3.1 Representative SEM images of titania nanotube arrays.
- Figure 3.2 (a) Representative fluorescence microscopy images (10x magnification) of adhered HDF stained with calcein-AM on the control substrate and titania nanotube arrays after 1, 2 and 4 days of culture. The amount of HDF coverage was calculated using the fluorescence images and the ImageJ software. The results indicate a 40% increase in HDF coverage on titania nanotube arrays compared to the control substrate (\*  $\rightarrow$   $p < 0.05$ ).
- (b) Representative fluorescence microscopy images (10x magnification) of adhered HEK stained with calcein-AM on the control substrate and titania

nanotube arrays after 1, 2 and 4 days of culture. The amount of HEK coverage was calculated using the fluorescence images and the ImageJ software. The results indicate a significant 92% decrease in HEK coverage on titania nanotube arrays compared to the control substrate (\*  $\rightarrow p < 0.05$ ).

Figure 3.3 Representative fluorescence microscopy images of HDF and HEK cells stained with DAPI on the control substrate and titania nanotube arrays after 4 days of culture. The HDF cell count indicates a significant 14% increase in HDF cells on titania nanotube arrays (\*  $\rightarrow p < 0.05$ ). The HEK cell count indicates a significant 43% decrease in HEK cells on titania nanotube arrays (\*  $\rightarrow p < 0.05$ ).

Figure 3.4 (a) Cell viability measured using MTT assay for HDF cells on the control substrate and titania nanotube arrays. After 4 days of culture, HDF viability is significantly increased on titania nanotube arrays (\*  $\rightarrow p < 0.05$ ).

(b) Cell viability measured using MTT assay for HEK cells on the control substrate and titania nanotube arrays. After 4 days of culture, HEK viability is significantly decreased on titania nanotube arrays (\*  $\rightarrow p < 0.05$ ).

Figure 3.5 (a) Representative SEM images (2000x and 20000x magnification) of HDF cells on the control substrate and titania nanotube arrays after 4 days of culture. Images show a higher degree of HDF activation and matrix formation on titania nanotube arrays.

(b) Representative SEM images (2000x magnification) of HEK cells on the control substrate and titania nanotube arrays after 1 day of culture. Images show a lower degree of HEK activation and matrix formation on titania nanotube arrays.

Figure 3.6 (a) Representative fluorescence microscopy images (10x and 20x magnification) of HDF stained with DAPI, FITC-conjugated anti-vinculin, and rhodamine-conjugated phalloidin along with consolidated images (from top to bottom respectively) on the control substrate and titania nanotube arrays, after 4 days of culture.

(b) Representative fluorescence microscopy images (10x magnification) of HEK cells stained with DAPI, FITC-conjugated anti-vinculin, and rhodamine-conjugated phalloidin along with consolidated images (from top to bottom respectively) on the control substrate and titania nanotube arrays, after 4 days of culture.

Figure 3.7 (a) Representative fluorescence microscopy images (10x magnification) of HDF cells immuno-stained with collagen-I $\alpha$ 1 and fibrillin-1 on the control substrate and titania nanotube arrays, after 4 days of culture. The images indicate a considerable increase in collagen-I $\alpha$ 1 expression, and a higher degree of fibrillin-1 expression and orientation for HDF cells on titania nanotube arrays.

(b) Representative fluorescence microscopy images (10x magnification) of HDF cells immuno-stained with cytokeratin-19 and laminin- $\beta$ 3 on the control substrate and titania nanotube arrays, after 4 days of culture. The images indicate a decrease in cytokeratin-19 and laminin- $\beta$ 3 expression for HEK cells on titania nanotube arrays.

- Figure 4.1 Schematic of isolation of platelets from whole human blood, obtaining a final concentration of  $8 \times 10^8$  platelets/ml
- Figure 4.2 Representative SEM image showing the nanoarchitecture of titania nanotube arrays fabricated using an anodization technique
- Figure 4.3 Amount of blood serum proteins adsorbed on titania nanotube arrays and biomedical grade titanium was determined using micro-BCA assay. Significantly higher amounts of proteins were adsorbed on titania nanotube arrays compared to biomedical grade titanium (\*, #, @  $\rightarrow p < 0.05$ ).
- Figure 4.4 High resolution C1s scans for blood serum proteins adsorbed on titania nanotube arrays and biomedical grade titanium showing C-N and N=C-O characteristic peaks (a) ALB, (b) FIB and (c) IgG.
- Figure 4.5 Representative fluorescence microscopy images of adhered platelets stained with calcein-AM on biomedical grade titanium [(a) 4 $\times$ , (b) 10 $\times$  and (c) 20 $\times$ ] and titania nanotube arrays [(d) 4 $\times$ , (e) 10 $\times$  and (f) 20 $\times$ ].
- Figure 4.6 Cell viability measured using MTT assay for adhered platelets on titania nanotube arrays and biomedical grade titanium. Platelets viability is significantly higher on titania nanotube arrays compared to biomedical grade titanium (\* $\rightarrow p < 0.05$ ).
- Figure 4.7 Representative SEM images of adhered and activated platelets on biomedical grade titanium [(a), (b) and (c)] and titania nanotube arrays [(d), (e) and (f)].
- Figure 4.8 Distribution of different shapes of adhered platelets on biomedical grade titanium and titania nanotube arrays.
- Figure 4.9 Free hemoglobin concentrations in terms of absorbance on titania nanotube arrays and biomedical grade titanium for up to 60 mins of clotting time.
- Figure 4.10 Representative SEM images of whole blood clotted on (a) biomedical grade titanium and (b)-(c) titania nanotube arrays.
- Figure 5.1 Schematic of the isolation of whole blood plasma, following removal from healthy individuals.
- Figure 5.2 Representative SEM images (10000 $\times$ , 25000 $\times$ , 100000 $\times$  magnification) showing the nanoarchitecture of titania nanotube arrays fabricated using an anodization technique. Titania nanotube arrays were coated with a 10 nm layer of gold and imaged at 15kV.

- Figure 5.3 Representative fluorescence microscopy images of adhered platelets and leukocytes stained with calcein-AM on the control substrate and titania nanotube arrays after 2 hours of incubation in whole blood plasma. The images indicate a decrease in platelet and leukocyte adhesion on titania nanotube arrays.
- Figure 5.4 Cell coverage calculated using the fluorescence microscope images and the ImageJ software. The results indicate a significant 75% decrease in cell coverage on titania nanotube arrays compared to the control substrate (\*  $\rightarrow$   $p < 0.05$ ).
- Figure 5.5 Cell cytotoxicity measured using an LDH Assay on the control substrate and titania nanotube arrays after 2 hours of incubation in whole blood plasma. The results indicate no significant difference in LDH activation on titania nanotube arrays compared to the control substrate.
- Figure 5.6 Representative fluorescence microscope images of adhered platelets and leukocytes stained with DAPI (nucleus) and rhodamine-conjugated phalloidin (actin) on the control substrate and titania nanotube arrays after 2 hours of incubation in whole blood plasma. The images indicate a decrease in platelet-leukocyte adhesion and aggregation on titania nanotube arrays.
- Figure 5.7 Cell count calculated using the fluorescence images and the ImageJ software. The results indicate a significant 69% decrease in total cell count on titania nanotube arrays compared to the control substrate (\*, #, @  $\rightarrow$   $p < 0.05$ ).
- Figure 5.8 Representative fluorescence microscope images of platelets immuno-stained for P-Selectin and leukocytes immuno-stained for CD45 on titania nanotube arrays and the control substrate after 2 hours of incubation in whole blood plasma. The images indicate a considerable decrease in P-Selectin (TR-conjugated) and CD45 (FITC-conjugated) expression on titania nanotube arrays.
- Figure 5.9 Representative fluorescence microscope images of monocytes/macrophages immuno-stained for CD14 and neutrophils immuno-stained CD16 on titania nanotube arrays and the control substrate after 2 hours of incubation in whole blood plasma. The images indicate a decrease in CD14 (TR-conjugated) and CD16 (FITC-conjugated) expression on titania nanotube arrays.
- Figure 5.10 Representative SEM images of adhered platelets and leukocytes on titania nanotube arrays and the control substrate after 2 hours of incubation in whole blood plasma. The substrates were coated with a 10 nm layer of gold and imaged at 15kV. Images show a lower degree of platelet-leukocyte interaction and cellular aggregation on titania nanotube arrays. Neither titania nanotube arrays nor the control substrate showed increased platelet activation as a result of the material surface.

- Figure 5.11 Complement activation measured by the amount of SC5b-9 activation on titania nanotube arrays and the control substrate after 2 hours of incubation in human plasma. The results indicate a slight decrease in complement activation on titania nanotube arrays compared to the control substrate.
- Figure 5.12 Contact activation measured by the amount of kallikrein on titania nanotube arrays and the control substrate after 2 hours of incubation in whole plasma. The results indicate a significant increase in contact activation on titania nanotube arrays compared to the control substrate (\*  $\rightarrow p < 0.05$ ).
- Figure 5.13 Platelet release reaction measured by the amount of PF-4 released from  $\alpha$ -granules within the platelets on titania nanotube arrays and the control substrate after 2 hours of incubation in whole blood plasma. The results indicate no significant difference in PF-4 concentration on titania nanotube arrays compared to the control substrate.
- Figure 5.14 Human fibrinogen antigen concentration measured on titania nanotube arrays and the control substrate after 2 hours of incubation in whole blood plasma. The results indicate a slight increase in fibrinogen concentration in the substrate-exposed whole blood plasma on titania nanotube arrays compared to the control substrate.
- Figure 6.1 Schematic of the isolation of whole human blood lysate.
- Figure 6.2 Representative SEM images (5,000 $\times$ , 20,000 $\times$ , 50,000 $\times$  magnification) showing the nanoarchitecture of titania nanotube arrays fabricated using an anodization technique. Titania nanotube arrays were coated with a 10 nm layer of gold and imaged at 15kV.
- Figure 6.3 Cellular viability measured using an MTT assay to identify adhered immune cells. The results indicate a significant decrease in the number of adhered immune cells on titania nanotube arrays as compared to biomedical grade titanium. ( $\oplus, \star, \otimes, \odot, \blacklozenge \rightarrow p < 0.05$ )
- Figure 6.4 (a) Representative fluorescence microscope images of adhered monocytes, macrophages, neutrophils and foreign body giant cells (FBGC, 3 or more nuclei) stained with DAPI (nucleus) and CMFDA (cytoplasm) on titania nanotube arrays and biomedical grade titanium after 2 hours, 2 and 7 days of incubation in human whole blood lysate. The images show a decrease in cellular adhesion, fusion and the formation of FBGCs (indicated by the circled regions) on titania nanotube arrays. The scale bar represents 50  $\mu\text{m}$ .
- Figure 6.4 (b) Cell count calculated using the fluorescence images and the ImageJ software. The results indicate a significant decrease in the number of adhered immune cells on titania nanotube arrays as compared to biomedical grade titanium. ( $\oplus, \star, \otimes, \odot, \blacklozenge \rightarrow p < 0.05$ )

- Figure 6.5 Representative fluorescence microscope images of adhered monocytes, macrophages, neutrophils and foreign body giant cells (3 or more nuclei) stained with DAPI (nucleus) and rhodamine-conjugated phalloidin (actin, cytoskeleton) on titania nanotube arrays and biomedical grade titanium after 2 hours, 2 and 7 day of incubation in human whole blood lysate. The images indicate a decrease in immune cell adhesion, activation and fusion on titania nanotube arrays. The scale bar represents 50  $\mu\text{m}$ .
- Figure 6.6 Representative SEM images of adhered immune cells on titania nanotube arrays and biomedical grade titanium after 2 hours, 2 and 7 days of incubation in human whole blood lysate. The substrates were coated with a 10 nm layer of gold and imaged at 15kV. The images indicate constrained cellular morphology on titania nanotube arrays, while showing increased cell-substrate integration and cell-cell interaction leading to the formation of foreign body giant cells on biomedical grade titanium.
- Figure 6.7 Nitric oxide release was measure by a Griess reagent. The results indicate a significant increase in long-term NO presence in substrate-exposed supernatant on titania nanotube arrays as compared to biomedical grade titanium. (⊙, ★, ⊕, ■, ⊛ →  $p < 0.05$ )
- Figure 6.8 Schematic of various cell exocytosis and endocytosis of cytokine/chemokine paths.
- Figure 6.9 Cytokine/chemokine expression was identified using a CBA assay and flow cytometry. The results identify the presence of 10 different cytokines/chemokines including IL-1 $\beta$ , IL-6, IL-8, IL-10, IL-12p70, TNF, TGF- $\beta$ 1, IFN- $\gamma$ , MCP-1 and MIP-1 $\beta$ . The long-term results after 2 and 7 days of incubation in human whole blood lysate show significant reductions in protein expression on titania nanotube arrays as compared to biomedical grade titanium. (■, ⊙, ○, ⊕, ★, ⊛ →  $p < 0.05$ )
- Figure 6.10 Cytokine/chemokine expression was identified using a CBA assay and flow cytometry. Human whole blood lysate incubated in RPMI medium with and without LPS tested for cytokine/chemokine expression after 2 hours, 2 and 7 days of incubation in human whole blood lysate on titania nanotube arrays as compared to the biomedical grade titanium. The results indicate altered short- and long-term cytokine/chemokine expression with the addition of LPS positive medium. (◆, ✦, ⊕, ⊕, ⊙, ○, ■, ⌘, ★, ⊛ →  $p < 0.05$ )

## LIST OF KEYWORDS

Titania Nanotube Arrays  
Nanotechnology  
Biomaterials  
Fibroblasts  
Keratinocytes  
Platelets  
Leukocytes  
Whole Blood Clotting  
Hemocompatiblility  
Thrombogenicity  
Immune Reaction  
Implantable Biomedical Devices  
Intra-Osseous Transcutaneous Implants

## INTRODUCTION

This research evaluates the effect of titania nanotube arrays on skin cell functionality, hemocompatibility, thrombogenicity and the immune response. Vertically oriented, immobilized, high aspect ratio and uniform titania nanotube arrays, fabricated using a simple anodization technique, were utilized in all subsequent studies. Biomedical grade titanium (as-received, non-polished) was used as the control. In brief, this bottom-up process of anodization results in substrate-derived (titania) nanotube fabrication, as opposed to a top-down process such as that seen in material deposition techniques. Nanotubes with pore diameters of 70-170 nm and tube lengths of 1-1.5  $\mu\text{m}$  were selected based on previous studies that identified increased osseointegration, reduced bacterial response and a capability for localized drug delivery. In this study, the physiological effect of titania nanotube arrays was investigated to better understand the punctual response, between hours and days, of natural human physiology/nano-biomaterial interaction. The time points were selected based on cell-specific adhesion, proliferation, activation, differentiation and protein expression. This work has investigated the protein, blood, immune and skin cell response to titania nanotube arrays *in vitro* as opposed to *in vivo*. These criteria were utilized in order to answer fundamental questions with respect to this specific and precise nano-architecture, prior to testing in live animal models.

The progressive nature of this work has been arranged into five research aims. Where, specific aim 1 focuses on nano-biomaterial fabrication and structural/mechanical characterization for use with *in vivo* applications. The aims of this research then identify four levels of interaction with intra-osseous transcutaneous implantable devices (amputee

prosthesis). These levels begin with the skin cell/nanotube interaction, moving further into the body and identifying the protein, blood clotting and isolated platelet affect. A more physiologically relevant model of cell and protein rich, whole human plasma then takes all of these interactions to the next level when thrombogenicity is identified through platelet-leukocyte interaction, cytoskeletal reorganization and cell-specific protein expression. This work culminates with evaluating the immune cell response through cellular functionality, differentiation, nitric oxide release and cytokine/chemokine expression. Through this work, a thorough evaluation of titania nanotube arrays has been investigated for use as interfaces in implantable biomedical devices.

This Ph.D. document addresses the hypothesis that titania nanotube arrays provide a favorable template for cell/nano-biomaterial interaction. The results of this work identify enhanced dermal matrix production, altered hemocompatibility, reduced thrombogenicity and a deterred immune response on titania nanotube arrays. This evidences promising implications with respect to the use of titania nanotube arrays as beneficial interfaces for the successful implantation of biomedical devices.

## HYPOTHESIS AND SPECIFIC AIMS

Fundamental Hypothesis: Titania nanotube arrays provide an advantageous interface for skin cell functionality, hemocompatibility, thrombogenicity and the immune response; leading to enhanced biomaterial integration.

Hypothesis (1): Titania nanotube arrays will be engineered to have vertically oriented, immobilized, high aspect ratio and a bioactivity suitable as interfaces for biomedical implantable devices.

Specific Aim 1: Fabricate and characterize a highly oriented, vertical array of immobilized titania nanotube arrays for biomedical applications. This research is discussed in **Chapter 2**.

- (a) Fabricate well controlled, highly reproducible titania nanotube arrays using an anodization process.
- (b) Evaluate the surface characteristics of titania nanotube arrays.
- (c) Evaluate the mechanical characteristics of titania nanotube arrays.

Hypothesis (2): Titania nanotube arrays will provide a favorable template for skin cell functionality.

Specific Aim 2: Determine the effect of titania nanotube arrays on skin cell functionality. This research is discussed in **Chapter 3**.

- (a) Evaluate the effect of titania nanotube arrays on the functionality (adhesion, proliferation, viability, and morphology) of human dermal fibroblast cells and human epidermal keratinocyte cells.
- (b) Evaluate the effect of titania nanotube arrays on cytoskeletal organization of human dermal fibroblast cells and human epidermal keratinocyte cells.
- (c) Evaluate the effect of titania nanotube arrays on protein expression by human dermal fibroblast cells and human epidermal keratinocyte cells.

Hypothesis (3): Titania nanotube arrays will enhance hemocompatibility; proving to be an effective interface for blood-contacting implantable biomedical devices.

Specific Aim 3: Determine the effect of titania nanotube array surface on the behavior of protein adsorption, platelet adhesion and activation and whole blood clotting. This research is discussed in **Chapter 4**.

- (a) Evaluate the effect of titania nanotube arrays on the adsorption of key blood proteins (fibrinogen, albumin and immunoglobulin-G).
- (b) Evaluate the effect of titania nanotube arrays on platelet adhesion and activation.
- (c) Evaluate the effect of titania nanotube arrays on the blood clotting kinetics by measuring the free hemoglobin concentration.

Hypothesis (4): Titania nanotube arrays will provide a beneficial interface for reduced thrombogenicity.

Specific Aim 4: Determine the effect of titania nanotube arrays on the behavior of whole blood plasma with respect to platelet/leukocyte interaction and cell specific protein expression. This research is discussed in **Chapter 5**.

- (a) Evaluate the effect of titania nanotube arrays on platelet/leukocyte interaction, through the use of whole blood plasma.
- (b) Identify cellular functionality and cell specific protein expression on titania nanotube arrays.
- (c) Evaluate the effect of titania nanotube arrays on PF-4 and fibrinogen expression.
- (d) Evaluate the effect of titania nanotube arrays on the activation of complement and contact proteins.

Hypothesis (5): Titania nanotube arrays can reduce the immune response; leading to enhanced biomaterial integration.

Specific Aim 5: Determine the *in vitro* immune response to titania nanotube arrays based on leukocyte activation, cytokine/chemokine secretion, protein expression and nitric oxide release. This research is discussed in **Chapter 6**.

- (a) Evaluate the effect of titania nanotube arrays on monocyte, macrophage and neutrophil functionality (viability, morphology and differentiation).
- (b) Identify macrophage fusion and formation into foreign body giant cells.
- (c) Evaluate the effect of titania nanotube arrays on the degree of nitric oxide release.
- (d) Evaluate the effect of titania nanotube arrays on cytokine / chemokine expression.

# CHAPTER 1

## LITERATURE REVIEW

### 1.1 Introduction

As the demand for injury and illness related implantable biomedical devices continue to rise, there exists a need for the development of compatible and effective materials<sup>1-3</sup>. For the 8-10% of Americans (20-25 million people) that have implanted biomedical devices, biomaterial failure and the need for revision surgery are critical concerns<sup>4,5</sup>. The major causes for failure in implantable biomedical devices promoting a need for re-implantation and revision surgery include thrombosis, post-operative infection, immune driven fibrosis and biomechanical failure. In fact, the greatest shortcoming has been the lack of complete biocompatibility, leading to poor tissue/biomaterial integration and further biomaterial rejection<sup>6,7</sup>. The successful integration of long-term implantable devices is highly dependent on the early events of tissue/biomaterial interaction, promoting either implant rejection or a wound healing response (extracellular matrix production and vasculature)<sup>8</sup> (See **Figure 1.1**). The physiological reaction to implanted biomaterials has been well documented, identifying a complex cascade of events which often result in a foreign body reaction on the surface of the biomaterial and in the surrounding tissue<sup>4,6,9</sup>. The cells required for healthy tissue regeneration are compromised through this adverse immune reaction<sup>10</sup>, thus hindering the natural wound healing response and the long-term success of implantable biomedical devices such as intra-osseous transcutaneous implants<sup>11,12</sup> and stent grafts<sup>13,14</sup>. Favorable interactions between the implant surface and the respective tissue are critical

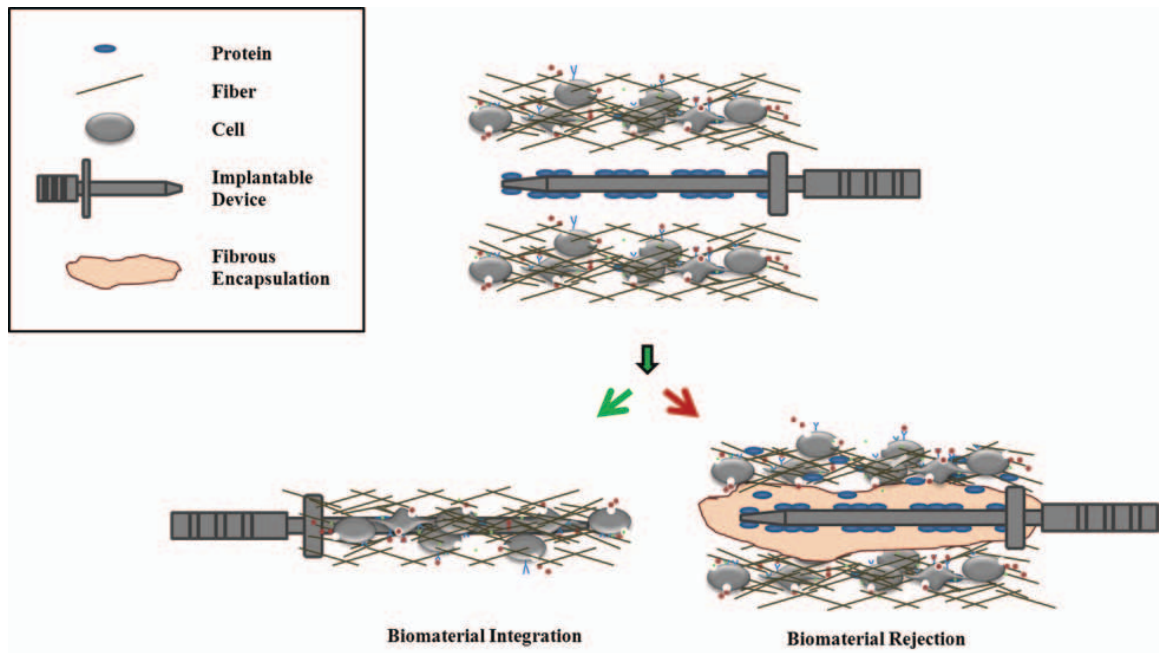


Figure 1.1 Schematic of two fates of intra-osseous transcuteaneous biomaterial implantation, either leading to tissue/biomaterial integration or biomaterial rejection via fibrous encapsulation.

for the long-term success of any implantable device. Recent studies have shown that material surfaces which mimic the natural physiological hierarchy of *in vivo* tissue may provide a possible solution for enhancing biomaterial integration, thus preventing infection and biomaterial rejection<sup>15-18</sup>. A thorough understanding of the effect of nanotopographical cues, at a hierarchy similar to that of natural tissue, on altered cellular functionality is essential for determining how nano-biomaterials can direct the tissue/biomaterial integration, thereby affecting the foreign body and wound healing responses.

## 1.2 Titanium as a Biomaterial

Titanium and titanium-based alloys have been among the most widely utilized materials for use in implantable biomedical devices since the mid-1900s, when titanium was found to possess tissue-compatible properties<sup>19,20</sup>. The main factors contributing to the widespread use of titanium in biomedical implants include their impressive mechanical and biocompatible properties<sup>20,21</sup>, non-toxicity<sup>22</sup>, corrosion resistance<sup>23</sup> and ease of process-ability<sup>21,24</sup>. Titanium reacts naturally with atmospheric oxygen to produce a passive oxide layer on the outside surface, known as titania<sup>25</sup>. This oxide-rich layer creates a hard and scratch-resistant material surface which protects the metal from environmental factors, improves corrosion and wear resistance, enables a low coefficient of friction and provides a favorable biocompatible interface for tissue integration<sup>21,24</sup>. These materials have been used in a variety of clinical devices including prosthesis<sup>23,26</sup>, hard and soft tissue grafts<sup>27</sup>, dental<sup>28,29</sup> and craniofacial implants<sup>30,31,32</sup> and cardiovascular stents<sup>33,34</sup>. However, the constant exposure of implanted biomaterials to blood and tissue introduces serious and ongoing concerns regarding poor biomaterial integration<sup>5,35,36</sup>. Although titanium and titanium-based alloys are among the better choices for implantable biomedical devices, to date, all long-term implanted biomaterials have the potential of initiating physiological events in the form of inflammation, infection, thrombosis and fibrosis<sup>37,38</sup>; potentially leading to complete implant rejection. The degree of biocompatibility, or the ability of a material to coexist with natural tissue or organs without initiating harm, may therefore be determined by characterizing the extent of a physiological reaction acting to neutralize or sequester the implanted biomedical device from the natural tissue<sup>39</sup>.

### 1.3 Physiological Response to Implanted Materials

Recent studies have identified a correlation relating the nanoscale surface topographies with enhanced cellular adhesion<sup>40-43</sup> and increased protein adsorption<sup>44, 45</sup>. However, cells are not the first responders to implantable biomedical devices. Immediately following implantation, biomaterials initiate a complex cascade of events<sup>4, 6, 46</sup>. (See Figure 1.2)

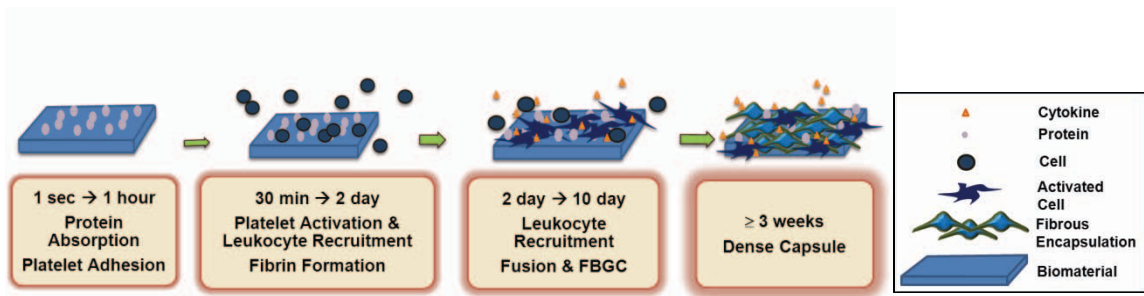


Figure 1.2 Schematic of the complex cascade of events following biomaterial implantation.

Within seconds to minutes, key blood serum proteins are adsorbed and undergo conformational changes on the surface. This layer of adsorbed proteins will direct subsequent adhesion and activation of platelets, which play an essential role in both the formation of a fibrin clot as well as the recruitment of leukocytes (including monocytes and neutrophils) to the site of injury through biochemical cues. The inflammatory cell infiltration subsequently leads to acute and chronic inflammation, promoting additional cellular activation (monocyte differentiation into macrophages), apoptosis and intercellular communication (cytokine/chemokine). This cascade of events perpetuates additional cellular infiltration and activation (lymphocytes and fibroblasts) initiating

granulocyte recruitment. The formation of foreign body giant cells (FBGC) potentially lead to fibrous encapsulation and complete implant rejection<sup>6, 7</sup>. This foreign body response has been proven to be a major hindrance to the integration of the natural tissue with the implanted biomaterial. Thus, the ability to modulate the cell-specific interaction with the titanium surface is critical for the long-term success of implantable devices.

#### 1.4 Nanomaterials and Biocompatibility

The human body is composed of a hierarchy of biological structures from the smallest molecule to the largest tissue (See Figure 1.3).

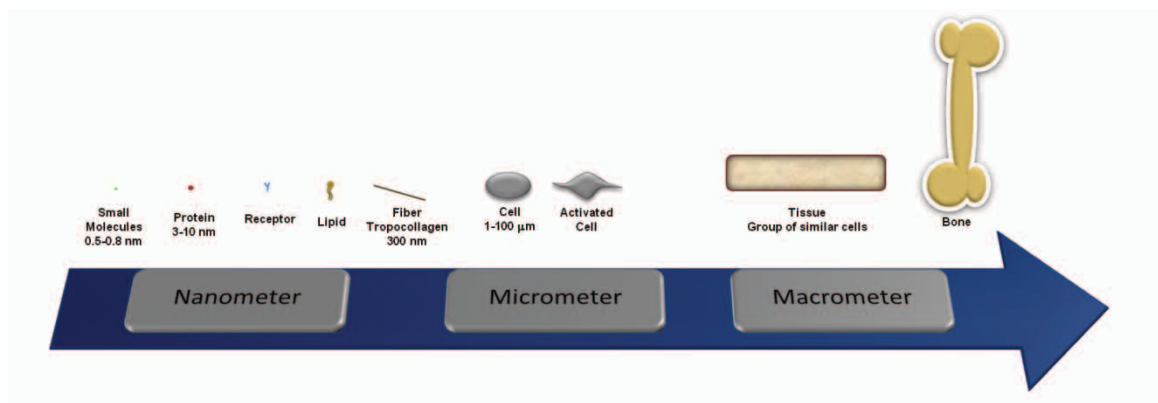


Figure 1.3 Schematic of the natural hierarchy of biological components, including multiple size scales.

Therefore, when micro-scale cells interact with their macro-scale environment, they do so through countless nano-scale topographical and biochemical cues. In fact, cells are in constant interaction with their surroundings, comprised of nano-scale subcellular structures including fibers, pits, pores and protrusions. Thus, material surfaces with biochemical<sup>47, 48 49, 50</sup> or topographical<sup>40, 51-53</sup> modifications similar to that of the natural

*in vivo* environment have been shown to elicit cell-specific functionality, enabled through biomimetic cues. Recent studies have shown increased cellular functionality on peptide modified<sup>54,55</sup> and growth factor functionalized<sup>56,57</sup> surfaces. State of the art advances in technology have enabled the fabrication of unique nanostructures on biomaterial surfaces such as nanoparticles<sup>58</sup>, nanofibers<sup>59,60</sup>, nanopores<sup>61,62</sup>, nanowires<sup>63,64</sup>, nanostructured hydrogels<sup>65</sup> and nanotube arrays<sup>66,67</sup>. The goal of these nanostructures is to provide nano-scale cues for a variety of cell types. Studies have identified a correlation between nano-scale surface architectures and cellular functionality including improved osseointegration<sup>59,63,66,68</sup>, augmented mesenchymal stem cell differentiation<sup>69-71</sup>, enhanced neuronal activation<sup>72,73</sup> and increased growth rate of endothelial cells<sup>74-77</sup>. In addition, these nano-architectures have been shown to promote the activation of signaling pathways that mediate cell adhesion, proliferation and activation, regulate cytokine expression, differentiation and cellular fusion. Thus, promoting the development of important structural and functional components of healthy tissue-biomaterial integration, preventing infection and biomaterial rejection<sup>18,40,52,53,78-84</sup>. These studies point out the benefit of nano-scale architectures on the surface of implantable biomedical devices<sup>40,53,40</sup>. In addition, titania nanotube arrays have been identified as providing a favorable interface for improved cellular functionality. Previous studies have demonstrated improved mesenchymal stem cell functionality<sup>85</sup>, hemocompatibility<sup>44</sup>, osteoblast phenotypic behavior<sup>15,85,86</sup>, selective behavioral responses of stem cells<sup>69,87</sup> and the production of endothelial cell ECM on titania nanotube arrays<sup>33</sup>. In addition, these nanotube arrays can be filled with various drugs such as antibiotics<sup>88</sup> and/or growth factors<sup>89</sup> that can be delivered locally at the site of implantation, thus preventing

infection and encouraging tissue integration. Titania nanotube arrays therefore, are attractive candidate as interfaces for implantable biomedical devices.

### **1.5 Nano-Scale Surface Modifications on TiO<sub>2</sub>**

Current technological advances have enabled the fabrication of nano-scale architectures on the surface of titanium and titanium-based alloys<sup>24, 51, 85, 90-94</sup>. Synthetic methods for producing surface nanostructures include sol-gel, micelle and inverse micelle, hydro- and solvo-thermal, direct oxidation/anodization, chemical and physical vapor deposition, electrodeposition, sonochemical and microwave<sup>95</sup>. These techniques have been shown to yield nano-scale features such as nanoparticles, nanorods, nanotubes and nanowires. Of these nano-scale fabrications, titania nanotube arrays have been identified as strong prospects for interfaces on implantable devices due to their ability to elicit altered cellular functionality, provide a method of localized drug delivery<sup>88</sup> and establish a foundation capable of incorporating biofunctional coatings<sup>96</sup>. The fabrication of titania nanotube arrays has been accomplished using hydrothermal, direct oxidation/anodization and microwave processes<sup>95, 97</sup>. However, vertically oriented, uniform, immobilized, high aspect ratio titania nanotube arrays have only been successfully developed by direct oxidation/anodization. Due to the proven biocompatibility, strong mechanical properties and high surface area of the nanotube arrays, current studies are beginning to evaluate this specific nano-architecture for use in biomedical<sup>67, 77, 89, 92, 94</sup> and solar cell<sup>98-101</sup> applications.

## 1.7 Dimension-Specific Cellular Functionality

Previous research has evaluated the biocompatibility of titania nanotube arrays, demonstrating enhanced osseointegration<sup>66,85</sup>, improved endothelialization<sup>77</sup>, increased protein adsorption<sup>44, 102</sup> and an altered hemocompatibility<sup>44</sup>, preferential fibroblast orientation and increased dermal matrix deposition<sup>51,92</sup>, selective behavioral responses of stem cells<sup>69,87</sup> and localized drug delivery<sup>103,104</sup>. In addition, these nanotube arrays can be filled with various drugs such as antibiotics<sup>88</sup> and growth factors<sup>89</sup> that can be delivered locally at the site of implantation, thus preventing infection and encouraging tissue integration<sup>15, 86, 88</sup>. Recent studies have correlated enhanced fibroblast functionality on titania nanotube arrays of 30-70 nm in pore diameter, showing decreased cell/nano-biomaterial interaction on nanotube arrays with diameters larger than 150 nm in dimensions<sup>67,70,92</sup>. Cellular functionality may be tuned and optimized by changing the size parameters of titania nanotube arrays<sup>66,69,70,87,94</sup>. Thus, providing a foundation that effectively moderates cell-specific functionality<sup>53,105-107</sup>. This interface may allow for regionally selective cell/nano-biomaterial interaction.

## 1.8 References

1. Bhat, S. V., *Biomaterials*. Second ed.; Alpha Science International Ltd.: 2005.
2. Ratner, B. D.; Hench, L., Perspectives on biomaterials. *Current Opinion in Solid State and Materials Science* **1999**, *4* (4), 379.
3. Langer, R., Biomaterials and biomedical engineering. *Chemical Engineering Science* **1995**, *50* (24), 4109.
4. Jones, J. A. Biomaterials and the foreign body reaction: Surface chemistry dependent macrophage adhesion, fusion, apoptosis, and cytokine production. 3263192, Case Western Reserve University, United States -- Ohio, 2007.
5. Mooney, V.; Predecki, P. K.; Renning, J.; Gray, J., Skeletal extension of limb prosthetic attachments—problems in tissue reaction. *Journal of Biomedical Materials Research* **1971**, *5* (6), 143-159.
6. Anderson, J. M.; Rodriguez, A.; Chang, D. T., Foreign body reaction to biomaterials. *Seminars in Immunology* **2008**, *20* (2), 86.
7. Jackson, C. M.; Nemerson, Y., Blood Coagulation. *Annual Review of Biochemistry* **1980**, *49* (1), 765-811.
8. Remes, A.; Williams, D. F., Immune response in biocompatibility. *Biomaterials* **1992**, *13* (11), 731-743.
9. Hu, W.-J.; Eaton, J. W.; Ugarova, T. P.; Tang, L., Molecular basis of biomaterial-mediated foreign body reactions. *Blood* **2001**, *98* (4), 1231-1238.
10. Stadelmann, W. K.; Digenis, A. G.; Tobin, G. R., Impediments to wound healing. *The American Journal of Surgery* **1998**, *176* (2, Supplement 1), 39S-47S.
11. Cohen, J., Assay of Foreign-Body Reaction. *The Journal of Bone & Joint Surgery* **1959**, *41* (1), 152-166.
12. DiCarlo, E. F.; Bullough, P. G., The biologic responses to orthopedic implants and their wear debris. *Clinical Materials* **1992**, *9* (3-4), 235-260.
13. Mani, G.; Feldman, M. D.; Patel, D.; Agrawal, C. M., Coronary stents: A materials perspective. *Biomaterials* **2007**, *28* (9), 1689-1710.
14. Peuster, M.; Hesse, C.; Schloo, T.; Fink, C.; Beerbaum, P.; von Schnakenburg, C., Long-term biocompatibility of a corrodible peripheral iron stent in the porcine descending aorta. *Biomaterials* **2006**, *27* (28), 4955-4962.
15. Porter, J. R.; Ruckh, T. T.; Papat, K. C., Bone tissue engineering: a review in bone biomimetics and drug delivery strategies. *Biotechnol Prog* **2009**, *25* (6), 1539-60.
16. Seunarine, K.; Curtis, A. S. G.; Meredith, D. O.; Wilkinson, C. D. W.; Riehle, M. O.; Gadegaard, N., A Hierarchical Response of Cells to Perpendicular Micro- and Nanometric Textural Cues. *NanoBioscience, IEEE Transactions on* **2009**, *8* (3), 219-225.

17. Yeo, I.-S.; Oh, J.-E.; Jeong, L.; Lee, T. S.; Lee, S. J.; Park, W. H.; Min, B.-M., Collagen-Based Biomimetic Nanofibrous Scaffolds: Preparation and Characterization of Collagen/Silk Fibroin Bicomponent Nanofibrous Structures. *Biomacromolecules* **2008**, *9* (4), 1106-1116.
18. Zhang, L.; Webster, T. J., Nanotechnology and nanomaterials: Promises for improved tissue regeneration. *Nano Today* **2009**, *4* (1), 66.
19. John E, D., Bone bonding at natural and biomaterial surfaces. *Biomaterials* **2007**, *28* (34), 5058-5067.
20. Wang, K., The use of titanium for medical applications in the USA. *Materials Science and Engineering: A* **1996**, *213* (1-2), 134.
21. Niinomi, M., Mechanical biocompatibilities of titanium alloys for biomedical applications. *Journal of the Mechanical Behavior of Biomedical Materials* **2008**, *1* (1), 30-42.
22. Tengvall, P.; Lundström, I., Physico-chemical considerations of titanium as a biomaterial. *Clinical Materials* **1992**, *9* (2), 115.
23. Van Noort, R., Titanium: The implant material of today. *Journal of Materials Science* **1987**, *22* (11), 3801-3811.
24. Cáceres, D.; Munuera, C.; Ocal, C.; Jiménez, J. A.; Gutiérrez, A.; López, M. F., Nanomechanical properties of surface-modified titanium alloys for biomedical applications. *Acta Biomaterialia* **2008**, *4* (5), 1545-1552.
25. Effah, E. A. B.; Bianco, P. D.; Ducheyne, P., Crystal structure of the surface oxide layer on titanium and its changes arising from immersion. *Journal of Biomedical Materials Research* **1995**, *29* (1), 73-80.
26. Long, M.; Rack, H. J., Titanium alloys in total joint replacement--a materials science perspective. *Biomaterials* **1998**, *19* (18), 1621-1639.
27. Speroni, S.; Briguglio, F.; Maridat, i. P.; Beretta, M.; Maiorana, C., Hard and soft tissue augmentation in implant surgery: a case report. *Minerva Stomatologica* **2011**, *60* (3), 123-31
28. Wang, R.; Fenton, A., Titanium for prosthodontic applications: a review of the literature. *Quintessence Int* **1996**, *27* (6), 401-408.
29. Jokstad, A.; Braegger, U.; Brunski, J. B.; Carr, A. B.; Naert, I.; Wennerberg, A., Quality of Dental Implants. *International journal of Prosthodontics* **2004**, *17*, 607-641.
30. Heo, S. J.; Odersjö, M.; Granström, G.; Tjellström, A.; Meredith, N., Stability measurements of craniofacial implants by means of resonance frequency analysis. A clinical pilot study. *The Journal of Laryngology & Otology* **1998**, *112* (06), 537-542.
31. Eufinger, H.; Wehmöller, M., Individual Prefabricated Titanium Implants in Reconstructive Craniofacial Surgery: Clinical and Technical Aspects of the First 22 Cases. *Plastic and Reconstructive Surgery* **1998**, *102* (2), 300-308.

32. Healy, K. E.; Ducheyne, P., Hydration and preferential molecular adsorption on titanium in vitro. *Biomaterials* **1992**, *13* (8), 553-561.
33. Peng, L.; Eltgroth, M. L.; LaTempa, T. J.; Grimes, C. A.; Desai, T. A., The effect of TiO<sub>2</sub> nanotubes on endothelial function and smooth muscle proliferation. *Biomaterials* **2009**, *30* (7), 1268-72.
34. Fine, E.; Zhang, L.; Fenniri, H.; Webster, T. J., Enhanced endothelial cell functions on rosette nanotube-coated titanium vascular stents. *Int J Nanomedicine* **2009**, *4*, 91-7.
35. Winter, G. D., Transcutaneous implants: Reactions of the skin-implant interface. *Journal of Biomedical Materials Research* **1974**, *8* (3), 99-113.
36. Tillander, J.; Hagberg, K.; Hagberg, L.; Brånemark, R., Osseointegrated Titanium Implants for Limb Prostheses Attachments: Infectious Complications. *Clinical Orthopaedics and Related Research*® **2010**, 1-8.
37. Smith, C. M.; Roy, T. D.; Bhalkikar, A.; Li, B.; Hickman, J. J.; Church, K. H., Engineering a Titanium and Polycaprolactone Construct for a Biocompatible Interface Between the Body and Artificial Limb. *Tissue Engineering Part A* **2010**, *16* (2), 717-724.
38. Kang, N. V.; Pendegrass, C.; Marks, L.; Blunn, G., Osseocutaneous Integration of an Intraosseous Transcutaneous Amputation Prosthesis Implant Used for Reconstruction of a Transhumeral Amputee: Case Report. *The Journal of Hand Surgery* **2010**, *35* (7), 1130-1134.
39. Luttkhuizen, D. T.; Harmsen, M. C.; Van Luyn, M. J., Cellular and molecular dynamics in the foreign body reaction. *Tissue Engineering* **2006**, *12* (7), 1955-70.
40. Curtis, A. S. G.; Gadegaard, N.; Dalby, M. J.; Riehle, M. O.; Wilkinson, C. D. W.; Aitchison, G., Cells react to nanoscale order and symmetry in their surroundings. *IEEE Trans Nanobioscience* **2004**, *3* (1), 61-5.
41. Decuzzi, P.; Ferrari, M., Modulating cellular adhesion through nanotopography. *Biomaterials* **2010**, *31* (1), 173-179.
42. Khang, D.; Carpenter, J.; Chun, Y.; Pareta, R.; Webster, T., Nanotechnology for regenerative medicine. *Biomedical Microdevices* **2010**, *12* (4), 575-587.
43. Valiev, R. Z.; Semenova, I. P.; Latysh, V. V.; Rack, H.; Lowe, T. C.; Petruzelka, J.; Dluhos, L.; Hrusak, D.; Sochova, J., Nanostructured Titanium for Biomedical Applications. *Advanced Engineering Materials* **2008**, *10* (8), B15-B17.
44. Smith, B. S.; Yoriya, S.; Grissom, L.; Grimes, C. A.; Popat, K. C., Hemocompatibility of titania nanotube arrays. *Journal of Biomedical Materials Research Part A* **2010**, *95A* (2), 350-360.
45. Lord, M. S.; Foss, M.; Besenbacher, F., Influence of nanoscale surface topography on protein adsorption and cellular response. *Nano Today* **2010**, *5* (1), 66-78.

46. Gorbet, M. B.; Sefton, M. V. M. V., Biomaterial-associated thrombosis: roles of coagulation factors, complement, platelets and leukocytes. *Biomaterials* **2004**, *25* (26), 5681-5703.
47. Morra, M., Biochemical Modification of Titanium Surfaces: Peptides and eCM Proteins. *European Cells and Materials* **2006**, *12*, 1-15.
48. Dee, K. C.; Andersen, T. T.; Bizios, R., Design and function of novel osteoblast-adhesive peptides for chemical modification of biomaterials. *Journal of Biomedical Materials Research* **1998**, *40* (3), 371-377.
49. Vogel, V.; Sheetz, M. P., Cell fate regulation by coupling mechanical cycles to biochemical signaling pathways. *Current Opinion in Cell Biology* **2009**, *21* (1), 38-46.
50. Dadsetan, M.; Jones, J. A.; Hiltner, A.; Anderson, J. M., Surface chemistry mediates adhesive structure, cytoskeletal organization, and fusion of macrophages. *Journal of Biomedical Materials Research Part A* **2004**, *71A* (3), 439-448.
51. Puckett, S. D.; Lee, P. P.; Ciombor, D. M.; Aaron, R. K.; Webster, T. J., Nanotextured titanium surfaces for enhancing skin growth on transcutaneous osseointegrated devices. *Acta Biomaterialia* **2010**, *6* (6), 2352-2362.
52. Riehle, M., Biocompatibility: Nanomaterials for cell- and tissue engineering. *NanoBioTechnology* **2005**, *1* (3), 308-309.
53. Biggs, M. J. P.; Richards, R. G.; Dalby, M. J., Nanotopographical modification: a regulator of cellular function through focal adhesions. *Nanomedicine: Nanotechnology, Biology and Medicine* **2010**, *6* (5), 619-633.
54. Werner, S.; Huck, O.; Frisch, B.; Vautier, D.; Elkaim, R.; Voegel, J.-C.; Brunel, G.; Tenenbaum, H., The effect of microstructured surfaces and laminin-derived peptide coatings on soft tissue interactions with titanium dental implants. *Biomaterials* **2009**, *30* (12), 2291-2301.
55. Grafahrend, D.; Heffels, K. H.; Möller, M.; Klee, D.; Groll, J., Electrospun, Biofunctionalized Fibers as Tailored in vitro Substrates for Keratinocyte Cell Culture. *Macromolecular Bioscience* **2010**, *10* (9), 1022-1027.
56. Clark, R. A., Growth factors and wound repair. *J Cell Biochem* **1991**, *46* (1), 1-2.
57. Gailit, J.; Clarke, C.; Newman, D.; Tonnesen, M. G.; Mosesson, M. W.; Clark, R. A., Human fibroblasts bind directly to fibrinogen at RGD sites through integrin alpha(v)beta3. *Exp Cell Res* **1997**, *232* (1), 118-26.
58. Kunzler, T. P.; Huwiler, C.; Drobek, T.; Vörös, J.; Spencer, N. D., Systematic study of osteoblast response to nanotopography by means of nanoparticle-density gradients. *Biomaterials* **2007**, *28* (33), 5000-5006.
59. Khang, D.; Sato, M.; Price, R. L.; Ribbe, A. E.; Webster, T. J., Selective adhesion and mineral deposition by osteoblasts on carbon nanofiber patterns. Dove Medical Press: 2006; Vol. 1, pp 65-72.

60. Ruckh, T. T.; Kumar, K.; Kipper, M. J.; Popat, K. C., Osteogenic differentiation of bone marrow stromal cells on poly(epsilon-caprolactone) nanofiber scaffolds. *Acta Biomater* **2010**, *6* (8), 2949-59.
61. La Flamme, K. E.; Popat, K. C.; Leoni, L.; Markiewicz, E.; La Tempa, T. J.; Roman, B. B.; Grimes, C. A.; Desai, T. A., Biocompatibility of nanoporous alumina membranes for immunoisolation. *Biomaterials* **2007**, *28* (16), 2638-2645.
62. Popat, K. C.; Leary Swan, E. E.; Mukhatyar, V.; Chatvanichkul, K.-I.; Mor, G. K.; Grimes, C. A.; Desai, T. A., Influence of nanoporous alumina membranes on long-term osteoblast response. *Biomaterials* **2005**, *26* (22), 4516-4522.
63. Porter, J. R.; Henson, A.; Popat, K. C., Biodegradable poly(epsilon-caprolactone) nanowires for bone tissue engineering applications. *Biomaterials* **2009**, *30* (5), 780-8.
64. Bechara, S.; Wadman, L.; Popat, K. C., Electroconductive polymeric nanowire templates facilitates in vitro C17.2 neural stem cell line adhesion, proliferation and differentiation. *Acta Biomaterialia* **2011**, *7* (7), 2892-2901.
65. Jayawarna, V.; Ali, M.; Jowitt, T. A.; Miller, A. F.; Saiani, A.; Gough, J. E.; Ulijn, R. V., Nanostructured Hydrogels for Three-Dimensional Cell Culture Through Self-Assembly of Fluorenylmethoxycarbonyl-Dipeptides. *Advanced Materials* **2006**, *18* (5), 611-614.
66. Brammer, K. S.; Oh, S.; Cobb, C. J.; Bjursten, L. M.; Heyde, H. v. d.; Jin, S., Improved bone-forming functionality on diameter-controlled TiO<sub>2</sub> nanotube surface. *Acta Biomaterialia* **2009**, *5* (8), 3215.
67. Park, J.; Bauer, S.; von der Mark, K.; Schmuki, P., Nanosize and Vitality: TiO<sub>2</sub> Nanotube Diameter Directs Cell Fate. *Nano Letters* **2007**, *7* (6), 1686-1691.
68. Zhang, L.; Ramsaywack, S.; Fenniri, H.; Webster, T. J., Enhanced osteoblast adhesion on self-assembled nanostructured hydrogel scaffolds. *Tissue Eng Part A* **2008**, *14* (8), 1353-64.
69. Bauer, S.; Park, J.; Faltenbacher, J.; Berger, S.; von der Mark, K.; Schmuki, P., Size selective behavior of mesenchymal stem cells on ZrO<sub>2</sub> and TiO<sub>2</sub> nanotube arrays. *Integrative Biology* **2009**, *1* (8-9), 525-532.
70. Oh, S.; Brammer, K. S.; Li, Y. S. J.; Teng, D.; Engler, A. J.; Chien, S.; Jin, S., Stem cell fate dictated solely by altered nanotube dimension. *Proceedings of the National Academy of Sciences* **2009**, *106* (7), 2130-2135.
71. Porter, J. R.; Henson, A.; Ryan, S.; Popat, K. C., Biocompatibility and mesenchymal stem cell response to poly(epsilon-caprolactone) nanowire surfaces for orthopedic tissue engineering. *Tissue Eng Part A* **2009**, *15* (9), 2547-59.
72. Bechara, S. L.; Judson, A.; Popat, K. C., Template synthesized poly([var epsilon]-caprolactone) nanowire surfaces for neural tissue engineering. *Biomaterials* **2010**, *31* (13), 3492-3501.

73. Brunetti, V.; Maiorano, G.; Rizzello, L.; Sorce, B.; Sabella, S.; Cingolani, R.; Pompa, P. P., Neurons sense nanoscale roughness with nanometer sensitivity. *Proceedings of the National Academy of Sciences* **2010**, *107* (14), 6264-6269.
74. Buttiglieri, S.; Pasqui, D.; Migliori, M.; Johnstone, H.; Affrossman, S.; Sereni, L.; Wratten, M. L.; Barbucci, R.; Tetta, C.; Camussi, G., Endothelization and adherence of leucocytes to nanostructured surfaces. *Biomaterials* **2003**, *24* (16), 2731-2738.
75. Miller, D. C.; Thapa, A.; Haberstroh, K. M.; Webster, T. J., Endothelial and vascular smooth muscle cell function on poly(lactic-co-glycolic acid) with nanostructured surface features. *Biomaterials* **2004**, *25* (1), 53.
76. Park, J.; Bauer, S.; Schmuki, P.; von der Mark, K., Narrow Window in Nanoscale Dependent Activation of Endothelial Cell Growth and Differentiation on TiO<sub>2</sub> Nanotube Surfaces. *Nano Letters* **2009**, *9* (9), 3157-3164.
77. Peng, L.; Eltgroth, M. L.; LaTempa, T. J.; Grimes, C. A.; Desai, T. A., The effect of TiO<sub>2</sub> nanotubes on endothelial function and smooth muscle proliferation. *Biomaterials* **2009**, *30* (7), 1268-1272.
78. Min, B.-M.; You, Y.; Kim, J.-M.; Lee, S. J.; Park, W. H., Formation of nanostructured poly(lactic-co-glycolic acid)/chitin matrix and its cellular response to normal human keratinocytes and fibroblasts. *Carbohydrate Polymers* **2004**, *57* (3), 285-292.
79. Jones, F. H., Teeth and bones: applications of surface science to dental materials and related biomaterials. *Surface Science Reports* **2001**, *42* (3-5), 75.
80. Healy, K. E.; Thomas, C. H.; Reznia, A.; Kim, J. E.; McKeown, P. J.; Lom, B.; Hockberger, P. E., Kinetics of bone cell organization and mineralization on materials with patterned surface chemistry. *Biomaterials* **1996**, *17* (2), 195-208.
81. Stevens, M. M., Biomaterials for bone tissue engineering. *Materials Today* **2008**, *11* (5), 18.
82. Bonzani, I. C.; George, J. H.; Stevens, M. M., Novel materials for bone and cartilage regeneration. *Current Opinion in Chemical Biology* **2006**, *10* (6), 568.
83. Charest, J. L.; Garcia, A. J.; King, W. P., Myoblast alignment and differentiation on cell culture substrates with microscale topography and model chemistries. *Biomaterials* **2007**, *28* (13), 2202-10.
84. Mata, A.; Kim, E. J.; Boehm, C. A.; Fleischman, A. J.; Muschler, G. F.; Roy, S., A three-dimensional scaffold with precise micro-architecture and surface micro-textures. *Biomaterials* **2009**, *30* (27), 4610-7.
85. Popat, K. C.; Leoni, L.; Grimes, C. A.; Desai, T. A., Influence of engineered titania nanotubular surfaces on bone cells. *Biomaterials* **2007**, *28* (21), 3188-3197.
86. Popat, K. C.; Eltgroth, M.; LaTempa, T. J.; Grimes, C. A.; Desai, T. A., Decreased Staphylococcus epidermidis adhesion and increased osteoblast functionality on antibiotic-loaded titania nanotubes. *Biomaterials* **2007**, *28* (32), 4880-4888.

87. von der Mark, K.; Bauer, S.; Park, J.; Schmuki, P., Another look at “Stem cell fate dictated solely by altered nanotube dimension”. *Proceedings of the National Academy of Sciences* **2009**, *106* (24), E60.
88. Popat, K.; Eltgroth, M.; LaTempa, T.; Grimes, C.; Desai, T., Titania Nanotubes: A Novel Platform for Drug-Eluting Coatings for Medical Implants? *Small* **2007**, *3* (11), 1878-1881.
89. Kodama, A.; Bauer, S.; Komatsu, A.; Asoh, H.; Ono, S.; Schmuki, P., Bioactivation of titanium surfaces using coatings of TiO<sub>2</sub> nanotubes rapidly pre-loaded with synthetic hydroxyapatite. *Acta Biomaterialia* **2009**, *5* (6), 2322-2330.
90. Browne, M.; Gregson, P. J., Surface modification of titanium alloy implants. *Biomaterials* **1994**, *15* (11), 894-898.
91. Kim, S. E.; Lim, J. H.; Lee, S. C.; Nam, S.-C.; Kang, H.-G.; Choi, J., Anodically nanostructured titanium oxides for implant applications. *Electrochimica Acta* **2008**, *53* (14), 4846-4851.
92. Smith, B. S.; Yoriya, S.; Johnson, T.; Popat, K. C., Dermal fibroblast and epidermal keratinocyte functionality on titania nanotube arrays. *Acta Biomaterialia* **2011**, *7* (6), 2686-2696.
93. Tambasco de Oliveira, P.; Nanci, A., Nanotexturing of titanium-based surfaces upregulates expression of bone sialoprotein and osteopontin by cultured osteogenic cells. *Biomaterials* **2004**, *25* (3), 403-413.
94. von Wilmsky, C.; Bauer, S.; Roedl, S.; Neukam, F. W.; Schmuki, P.; Schlegel, K. A., The diameter of anodic TiO<sub>2</sub> nanotubes affects bone formation and correlates with the bone morphogenetic protein-2 expression in vivo. *Clinical Oral Implants Research* **2011**, *23* (3), 359-366.
95. Chen, X.; Mao, S. S., Titanium Dioxide Nanomaterials: Synthesis, Properties, Modifications, and Applications. *Chemical Reviews* **2007**, *107* (7), 2891-2959.
96. Liu, S.; Chen, A., Coadsorption of Horseradish Peroxidase with Thionine on TiO<sub>2</sub> Nanotubes for Biosensing. *Langmuir* **2005**, *21* (18), 8409-8413.
97. Wu, X.; Jiang, Q.-Z.; Ma, Z.-F.; Fu, M.; Shanguan, W.-F., Synthesis of titania nanotubes by microwave irradiation. *Solid State Communications* **2005**, *136* (9-10), 513-517.
98. Mor, G. K.; Varghese, O. K.; Paulose, M.; Shankar, K.; Grimes, C. A., A review on highly ordered, vertically oriented TiO<sub>2</sub> nanotube arrays: Fabrication, material properties, and solar energy applications. *Solar Energy Materials and Solar Cells* **2006**, *90* (14), 2011.
99. Roy, P.; Berger, S.; Schmuki, P., TiO<sub>2</sub> Nanotubes: Synthesis and Applications. *Angewandte Chemie International Edition* **2011**, *50* (13), 2904-2939.
100. Ruan, C.; Paulose, M.; Varghese, O. K.; Mor, G. K.; Grimes, C. A., Fabrication of Highly Ordered TiO<sub>2</sub> Nanotube Arrays Using an Organic Electrolyte. *The Journal of Physical Chemistry B* **2005**, *109* (33), 15754-15759.

101. Yoriya, S.; Grimes, C. A., Self-Assembled TiO<sub>2</sub> Nanotube Arrays by Anodization of Titanium in Diethylene Glycol: Approach to Extended Pore Widening. *Langmuir* **2009**, *26* (1), 417-420.
102. Roy, S. C.; Paulose, M.; Grimes, C. A., The effect of TiO<sub>2</sub> nanotubes in the enhancement of blood clotting for the control of hemorrhage. *Biomaterials* **2007**, *28* (31), 4667-4672.
103. Song, Y.-Y.; Schmidt-Stein, F.; Bauer, S.; Schmuki, P., Amphiphilic TiO<sub>2</sub> Nanotube Arrays: An Actively Controllable Drug Delivery System. *Journal of the American Chemical Society* **2009**, *131* (12), 4230-4232.
104. Popat, K. C.; Eltgroth, M.; LaTempa, T. J.; Grimes, C. A.; Desai, T. A., Titania nanotubes: a novel platform for drug-eluting coatings for medical implants? *Small* **2007**, *3* (11), 1878-81.
105. Clark, P.; Connolly, P.; Curtis, A. S. G.; Dow, J. A. T.; Wilkinson, C. D., Cell Guidance By Ultrafine Topography In Vitro. *Journal of Cell Science* **1991**, *99*, 73-77.
106. Curtis, A.; Wilkinson, C., Topographical control of cells. *Biomaterials* **1997**, *18* (24), 1573-1583.
107. Dalby, M. J.; Childs, S.; Riehle, M. O.; Johnstone, H. J. H.; Affrossman, S.; Curtis, A. S. G., Fibroblast reaction to island topography: changes in cytoskeleton and morphology with time. *Biomaterials* **2003**, *24* (6), 927-35.

## CHAPTER 2

### DEVELOPMENT OF TITANIA NANOTUBE ARRAYS AS INTERFACES FOR IMPLANTABLE BIOMEDICAL DEVICES

#### 2.1 Introduction

Common biomedical implant materials include metals or metal alloys, polymers, ceramics and composites. Of these, titanium and titanium-based alloys are the most widely used biomaterials due to their mechanical strength, biocompatibility, non-toxicity, corrosion resistance, and ease of process-ability. They have been used in clinical applications for a variety of implantable devices, including dental implants<sup>1-3</sup>, prosthetic devices<sup>4-6</sup>, materials for craniofacial reconstruction<sup>7, 8</sup> and stent grafts<sup>9, 10</sup>. Titanium forms a passive oxide layer on its surface, titania, which protects it against corrosion and provides a biomechanical interface for appropriate tissue integration<sup>11, 12</sup>. Even though titanium and titanium-based alloys, including other implantable biomaterials, are nontoxic, foreign body reactions are often triggered in the form of inflammation, thrombosis, fibrosis and infection. Several studies report on the cellular functionality of titanium, however little is known about the cellular functionality on nano-textured titanium.

Material surfaces that mimic the natural physiological hierarchy of *in vivo* tissue at a nanoscale provide a possible solution for enhancing biomaterial integration, thus preventing infection and biomaterial rejection<sup>13-17</sup>. Recently, there has been an increased interest in exploring nanoscale surface topographies such as nanotubes<sup>18-20</sup>, nanowires<sup>21</sup>, nanopores<sup>22, 23</sup>, nanoparticles<sup>24, 25</sup>, nanofibers<sup>14, 26, 27</sup>, as biomimetic interfaces for

implantable devices<sup>28</sup>. Several studies have reported enhanced mesenchymal stem cell and osteoblast adhesion along with increased tissue formation on such nanoscale topographies<sup>16, 29, 30</sup>. In this study, titania nanotube arrays (diameter: 70-170 nm, length: 1  $\mu\text{m}$ ) were fabricated using an anodization process, as biomimetic interfaces for transcutaneous implantable devices. Previous studies on titania nanotube arrays have demonstrated improved mesenchymal stem cell functionality<sup>19</sup>, hemocompatibility<sup>20</sup>, osteoblast phenotypic behavior<sup>19, 28, 31</sup>, and localized drug delivery<sup>32</sup>. In addition, these titania nanotube arrays have elicited minimal levels of monocyte activation and cytokine secretion, thus exhibiting very low degree of immunogenicity<sup>33</sup>. Tissue-compatibility is a key consideration for the long-term use of implantable devices<sup>34-36</sup>; therefore, highly oriented, vertical array, high aspect ratio titania nanotube arrays have been fabricated using a simple anodization technique for its potential application as biomaterial interfaces.

## **2.2 Fabrication of Titania Nanotube Arrays**

A simple anodization process was used to fabricate titania nanotube arrays<sup>19, 32, 37</sup>. Titanium foil substrates, 1 cm  $\times$  2.5 cm (0.25 mm thick, 99.7%) were cleaned with soap, acetone, and iso-propanol prior to anodization. An anode-cathode system was fabricated; using a two-electrode cell with titanium foil as the anode and platinum foil as the cathode (See **Figure 2.1**). The electrolyte was prepared by mixing diethylene glycol (DEG, 99.7%) with 2% hydrofluoric acid (HF, 48% solution) and 3% de-ionized water. All experiments were carried out at 60V for 24 hrs at room temperature. Following anodization, the nanotube array substrates were rinsed with iso-propanol and dried with

nitrogen gas. Crystallized substrates were obtained by annealing the as-anodized titania nanotube arrays in oxygen ambient at 530 °C for 3 hrs. Biomedical grade titanium (as-received, non-polished) surfaces were used as controls.

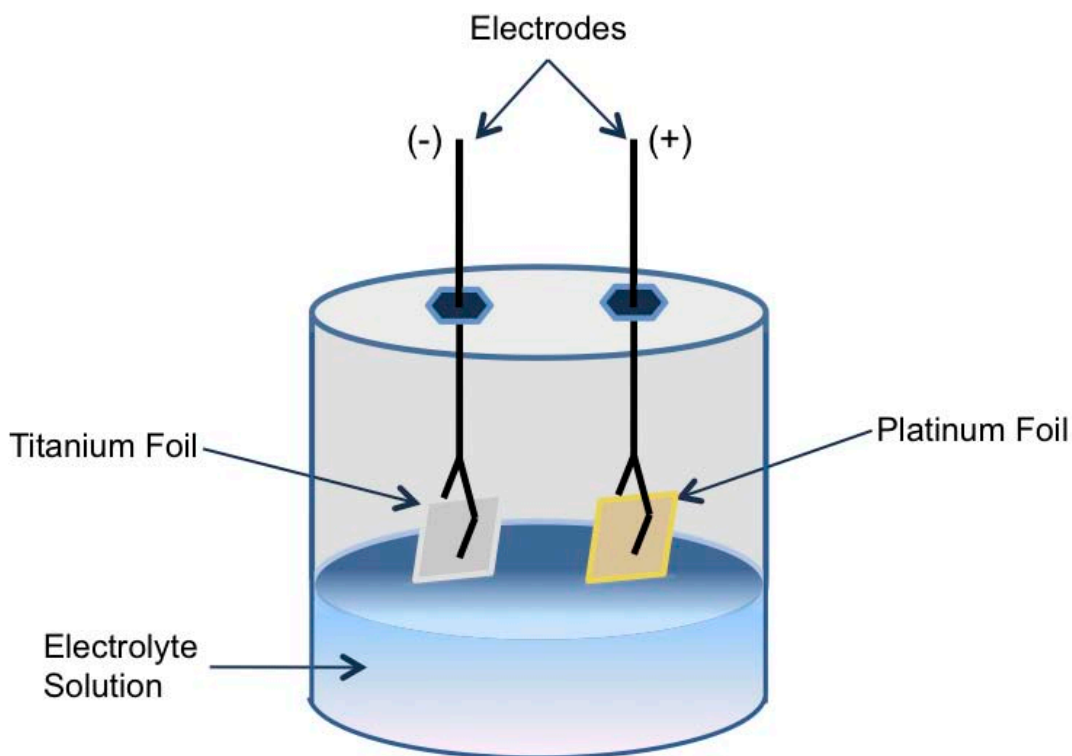


Figure 2.1 Schematic of anodization setup for fabrication of titania nanotube arrays.

### 2.3 Characterization of Titania Nanotube Arrays

The nanotube morphology was examined using a field emission scanning electron microscope (SEM, JEOL JSM-6300). The crystalline phases were identified by glancing angled X-ray diffraction (XRD, SCINTAG 3). A 3-dimensional topographical analysis of the nanotube surface, indicating surface roughness (uniformity and modification), was

examined by atomic force microscopy (AFM) using a confocal micro-Raman microscope alpha300 R (WITec). The material surface wettability was evaluated using a static sessile water-drop method. Images were taken immediately following DI water/substrate contact. A contact angle goniometer was used to identify the degree of phase separation, formed between the liquid/solid interface and the liquid/vapor interface. The images were analyzed to evaluate the degree of surface hydrophobicity/ hydrophilicity, where higher angles correlate with a low surface energy and an increased hydrophobicity of the substrate. In addition, the mechanical properties of the titania nanotube arrays were characterized through nanoindentation (Hysitron) and scratch tests (Micro-Combi Tester, CSEM Instruments). For nanoindentation, a Beckovich tip with a radius of 200 nm was used and a series of 9 indentations were performed on each substrate. Further, a typical load-hold scheme with a peak load of 1000  $\mu\text{N}$ , loading rate of 20  $\mu\text{N}/\text{min}$ , holding time of 60 s and unloading rate of 20  $\mu\text{N}/\text{min}$  was used for all the nanoindentation tests. For scratch tests, a Rockwell diamond tip with a radius of 200  $\mu\text{m}$  was used and a series of 6 scratches were performed on each substrate. The tests were performed by applying loads ranging from 0.03 N to 10 N at a rate of 10 N/min. Biomedical grade titanium (as received) substrates were used as controls.

### **2.3 Results and Discussion**

The anodization of titanium can be explained using a localized dissolution model<sup>38, 39</sup>, where titania nanotube arrays result from the competition between electrochemical etching and chemical dissolution by the fluoride-containing electrolyte solution (See **Figure 2.2**).

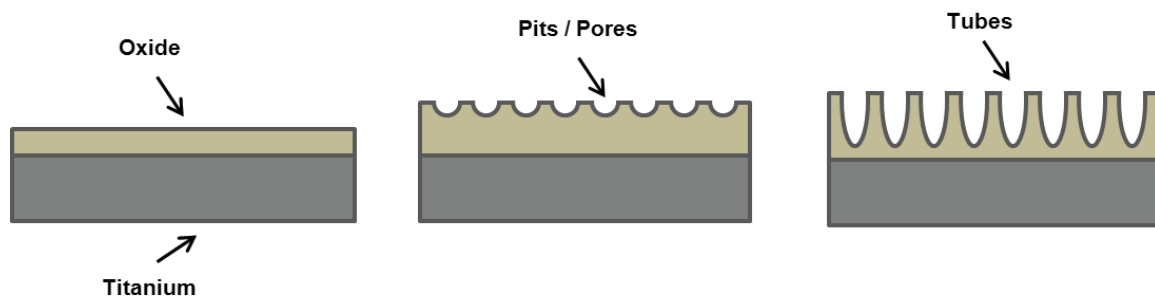


Figure 2.2 Schematic of anodized titanium, for the fabrication of titania nanotube arrays.

A precise correlation exists between the anodization voltage and the pore size<sup>40</sup>. Therefore, by varying anodization parameters (voltage, electrolyte solution and time duration), substrates with different dimensions (pore diameter, wall thickness and nanotube length) can be fabricated. The crystalline (anatase and rutile phases) titania nanotube arrays retain the structure of the as-fabricated amorphous nanotube arrays on annealing in an oxygen ambient environment<sup>20</sup>. Recent studies have shown great variation in the dimensions of titania nanotube arrays ranging in length from 200 nm to 6.5  $\mu\text{m}$ , the pore diameter from 22 nm to 180 nm, and the wall thickness from 9 nm to 34 nm<sup>40-42</sup>. These variations in nanotube dimensions have enabled more in-depth evaluations of size-dependent cell functionality and sustained drug release. Further, the mechanical properties of titania nanotube arrays have been evaluated to better understand their potential in biomedical applications. The uniform and repeatable oxide-rich nanotube architecture has been shown to provide a biomimetic, biocompatible and non-biodegradable interface for implantable biomedical devices.

In this work, we have fabricated vertically oriented, immobilized, high-aspect ratio titania nanotube arrays using a simple anodization technique. The nanoarchitecture of titania nanotube arrays was examined for uniformity and repeatability using SEM (See **Figure 2.3**). SEM images show uniform nanotube arrays with a diameter of 70-170 nm and length of 1-1.5  $\mu\text{m}$ .

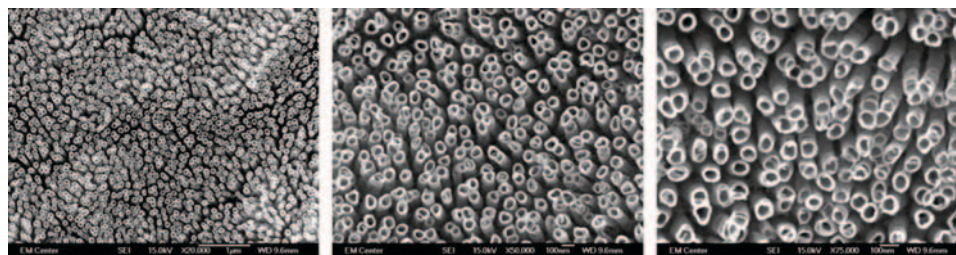


Figure 2.3 Representative SEM images (20000x, 50000x, 75000x magnification) showing the nanoarchitecture of titania nanotube arrays fabricated using an anodization technique.

For this study, titania nanotube arrays with a diameter of 70-170 nm and length of 1-1.5  $\mu\text{m}$  were selected, since previous studies with the same size titania nanotubes arrays have shown enhanced cellular functionality and sustained drug release. The as-fabricated nanotube arrays are amorphous; therefore an annealing step is required to induce crystallization.

Crystallized nanotube arrays were obtained by annealing the anodized titania nanotube arrays in oxygen ambient at 530°C for 3 hrs. The titania nanotube arrays retain their structure on annealing and the crystalline phases were identified by XRD (See **Figure 2.4**). The annealed nanotube arrays show mixed crystallized phases of anatase

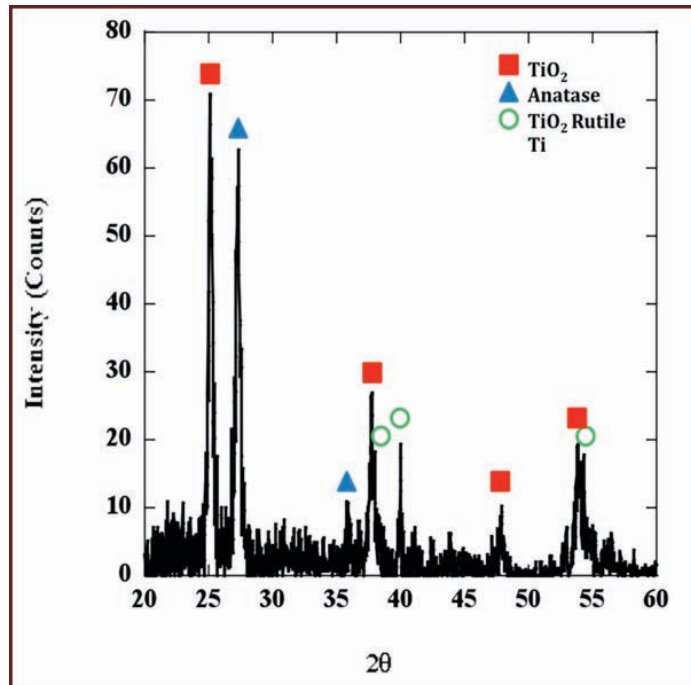


Figure 2.4 Representative XRD pattern of titania nanotube arrays showing crystalline phases fabricated using an anodization technique.

and rutile. The annealing temperature of 530°C selected was to ensure the complete crystallization of titania nanotube arrays.

A 3-dimensional analysis of surface topography was performed using atomic force microscopy (AFM). Where, a precise mechanical probing of the material surface was acquired by tip-to-surface contact. This topographical information, capable of providing measurements with nanometer accuracy, can be utilized to detect variations in topography and identify surface roughness. The results indicate nanometer sized variations on the surface of titania nanotube arrays as compared to the micrometer sized architecture on the surface of control substrates (See Figure 2.5). Further, the nanotube arrays possess a nano-architecture within an overall uniform micro- and macro-scale surface architecture, as shown by the topographical variations limited to the nanometer

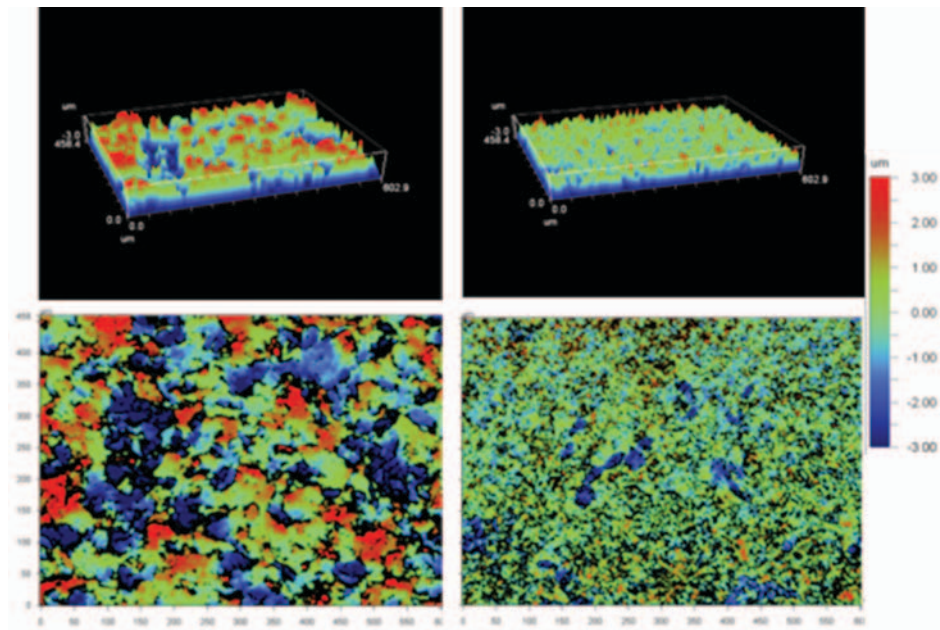


Figure 2.5 Representative atomic force microscopy (AFM) images of surface topographies for titania nanotube arrays and the control substrates. The images include (top) 3D plots and (bottom) surface topography. The resulting images identify a nano-architecture on titania nanotube arrays and a micro-architecture on biomedical grade titanium.

size scale (See Table 2.1). These traits allow for a promising interface for improved cellular interaction due to the increased nano-scale roughness of the material surface.

Within the living body, myriads of hydrophobic (non-polar, water-fearing) and hydrophilic (polar and ionic, water-loving) molecules direct cell function, proving imperative for survival. Biomaterial “wet-ability” has therefore been found to be a considerable factor for tissue integration and the success of implanted devices. Recent studies have shown that biomaterials which possess a heightened degree of hydrophilicity promote improved cellular interactions<sup>43, 44</sup>. Material surface wet-ability was therefore evaluated by contact angle measurement to determine the degree of phase separation, immediately following DI water/substrate contact. Higher contact angles (>90degrees)

Table 2.1 Numerical analysis of micro- and nano-scale substrate topographies, measured using atomic force microscopy (AFM) (See **Figure 2.6**). Where Ra is the mean roughness, Rq is the standard deviation of the surface heights, Rz is the average maximum profile of the ten greatest peak-to-valley separations in the region of evaluation, and Rt is the vertical distance between the highest and lowest points (length/area).

AFM	Titanium	Titania Nanotube Arrays
<b>Ra</b>	1.3 $\mu\text{m}$	667.33 nm
<b>Rq</b>	1.67 $\mu\text{m}$	866.01 nm
<b>Rz</b>	11.34 $\mu\text{m}$	9.23 $\mu\text{m}$
<b>Rt</b>	12.28 $\mu\text{m}$	10.45 $\mu\text{m}$
<b>magnification</b>	10.24 X	
<b>Sampling</b>	820.29 nm	
<b>Array Size</b>	736 x 480	

correlate to a low surface energy and a reduced water-material interaction, indicating hydrophobic surfaces. The opposite is true for hydrophilic surfaces, which possess a high surface energy. The resulting images identified a hydrophilic  $25.8^\circ$  for titania nanotube arrays as compared to the significantly increased hydrophobicity of the control substrates with a contact angle of  $81.8^\circ$  (See **Table 2.2**). These results show titania nanotube arrays as having a hydrophilic interface, which naturally promotes cellular integration (See **Figure 2.6**). Biological interactions at the material interface are sensitive to the physical and mechanical properties of the surfaces presented. Thus, the mechanical properties of titania nanotube arrays were determined using nanoindentation and scratch tests. The nanoindentation tests were performed using a Berkovich tip to determine the Young's modulus and hardness of titania nanotube arrays. SEM was used to determine the projected contact area of indentation made by the Berkovich tip (See **Figure 2.7**).

Table 2.2 Representative images of the water contact angle (degrees) on titania nanotube arrays and biomedical grade titanium. The results indicate that titania nanotube arrays are more hydrophilic than the control surfaces.

	Titanium	Titania Nanotube Arrays
Contact Angle (Degrees)	$81.8 \pm 5.8$	$25.8 \pm 4.8$

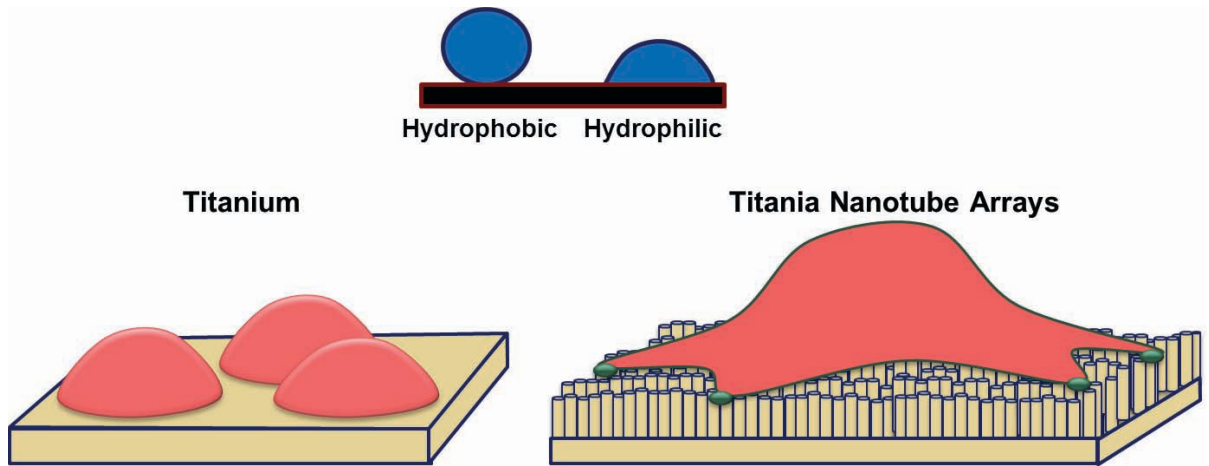



Figure 2.6 Schematic of the cellular response to the different surfaces, identifying a correlation between increased hydrophilicity and improved cellular integration.

The Young's modulus of biomedical grade titanium and titania nanotube arrays are comparable whereas the hardness of titania nanotube arrays is lower than that of biomedical grade titanium (See Table 2.3). However, the relative similarities between

the Young's modulus and hardness are indicative of the potential of the titania nanotube arrays to withstand plastic deformation.

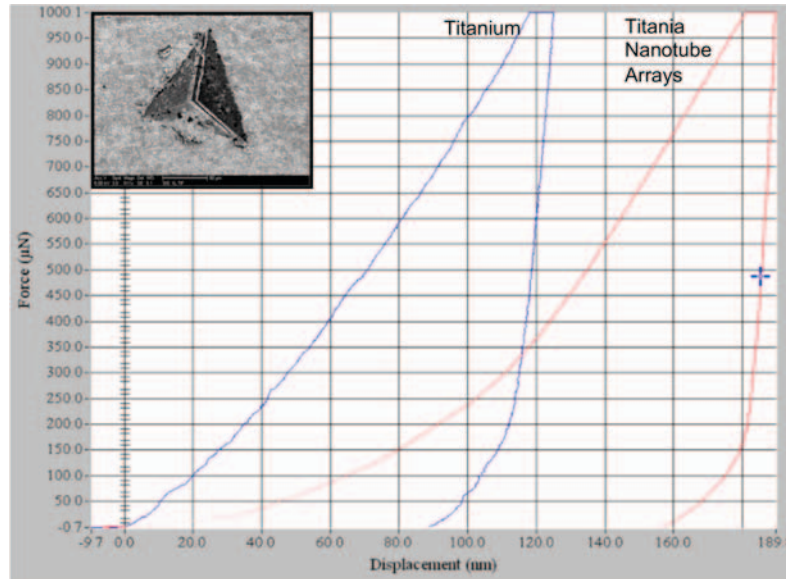
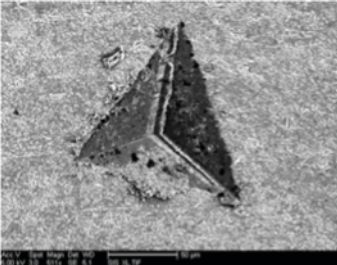


Figure 2.7 Representative load-displacement curves for titania nanotube arrays and biomedical grade titanium, obtained by nanoindentation, (insert – left corner) Representative SEM image of an indent made by a Beckovich tip on a titania nanotube array substrate

Table 2.3 Young's modulus and hardness values for titania nanotube arrays and biomedical grade titanium surfaces, determined using nanoindentation.

	Young's Modulus (GPa)	Hardness (GPa)
<b>Titanium</b>	120 ± 45	3.89 ± 1.88
<b>Titania Nanotube Arrays</b>	111 ± 25	1.02 ± 0.36



The scratch tests were used to characterize the surface mechanical properties of titania nanotube arrays. The tests were performed using a Rockwell tip to determine the delamination characteristics of titania nanotube arrays. Our results indicate that the titanium substrates were able to withstand loads up to 10 N (See **Figure 2.8**). However, the titanium substrate does not have any deposited layer of titania, thus resulting in a scratch on the bulk of the substrate (i.e. no delamination).

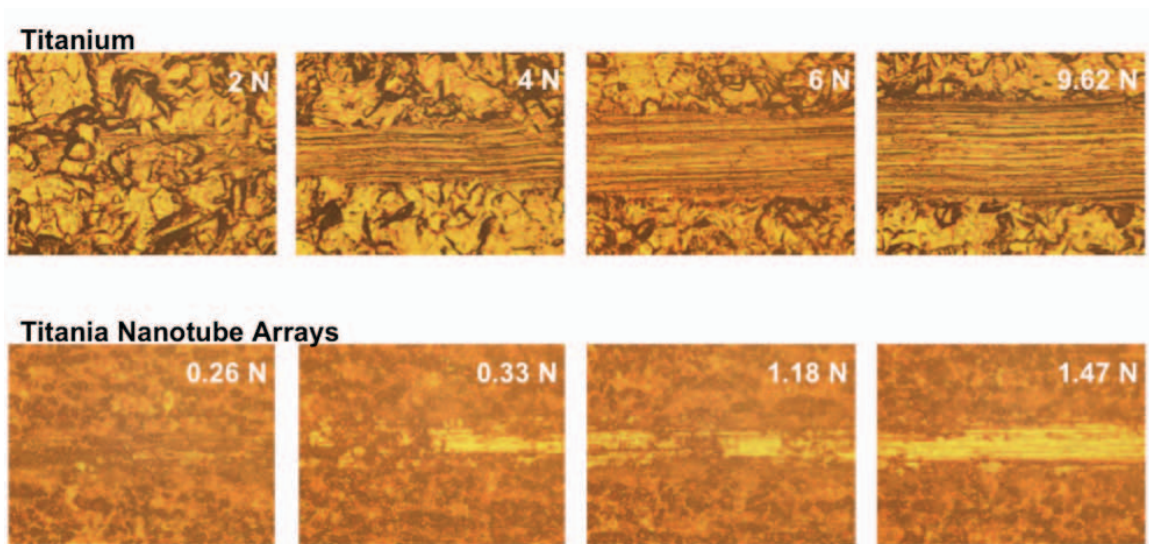


Figure 2.8 Representative optical microscopy images of scratches at various forces on titania nanotube arrays and biomedical grade titanium .

Optical microscopy images show progressive changes in the size of the scratch with an increase in the applied load. In contrast, the titania nanotube arrays show an onset of delamination at a critical load of 0.33 N. A further increase in the applied load results in severe delamination followed by complete failure at 1.47 N. The nanotube arrays exhibit delamination characteristics due to the formation of a layer of titania on the surface of

titanium through the anodization process. These results indicate that the titania nanotube arrays will be able to withstand repeated mechanical wear and abrasion.

## **2.4 Conclusion**

Implanted biomedical devices interact with the human physiology at the biomaterial interface. During implantation biomaterials are often required to withstand abrasive and multi-phase interactions at the material surface. In addition, wear and corrosion resistance are necessary criteria for the lifespan of the implanted device. Thus, surface properties of implantable biomaterials are critical for the long-term success of these devices. With the aim of identifying the capabilities of titania nanotube arrays as interfaces for use in implantable biomedical devices, this research has investigated the characteristics of this specific nanoarchitecture including nanotube morphology, nano-architecture, crystallinity, level of hydrophobicity, hardness and its ability to withstand surface delamination. These characteristics were evaluated using SEM, AFM, XRD, contact angle, nano-indentation and micro-scratch testing respectively.

Titania nanotube arrays were fabricated using a simple anodization technique in HF-based electrolyte solution at 60 V for 24 hours. The resulting SEM images show the production of vertically oriented, high aspect ratio and uniform array of titania nanotubes (diameter 70-170 nm and length 1-1.5  $\mu\text{m}$ ). Further, the results identify a hydrophilic nano-architecture composed of two crystalline phases (anatase and rutile). In addition, these interfaces provide a reduced scratch resistance and a hardness comparable to that of biomedical grade titanium. The simple fabrication, physiologically relevant architecture, strong mechanical properties, low surface energy and large surface area identify titania

nanotube arrays as promising interfaces for implantable biomedical devices. Further studies are now targeted towards understanding the effects of altered anodization process on structural and mechanical nanotube characteristics.

## References

1. Boyan, B. D., The changing face of dental research: blurring the boundaries between industry and academia. *J Dent Res* **1996**, 75 (6), 1426-7.
2. Mendonca, G.; Mendonca, D. B.; Aragao, F. J.; Cooper, L. F., Advancing dental implant surface technology--from micron- to nanotopography. *Biomaterials* **2008**, 29 (28), 3822-35.
3. Werner, S.; Huck, O.; Frisch, B.; Vautier, D.; Elkaim, R.; Voegel, J. C.; Brunel, G.; Tenenbaum, H., The effect of microstructured surfaces and laminin-derived peptide coatings on soft tissue interactions with titanium dental implants. *Biomaterials* **2009**, 30 (12), 2291-301.
4. Naidu, S. H.; Kulkarni, N.; Saunders, M., Titanium Basal Joint Arthroplasty: A Finite Element Analysis and Clinical Study. *The Journal of Hand Surgery* **2006**, 31 (5), 760.
5. Semlitsch, M. F.; Weber, H.; Streicher, R. M.; Schön, R., Joint replacement components made of hot-forged and surface-treated Ti-6Al-7Nb alloy. *Biomaterials* **1992**, 13 (11), 781.
6. Wang, K., The use of titanium for medical applications in the USA. *Materials Science and Engineering: A* **1996**, 213 (1-2), 134.
7. Heissler, E.; Fischer, F. S.; Boiouri, S.; Lehrmann, T.; Mathar, W.; Gebhardt, A.; Lanksch, W.; Bler, J., Custom-made cast titanium implants produced with CAD/CAM for the reconstruction of cranium defects. *International Journal of Oral and Maxillofacial Surgery* **1998**, 27 (5), 334.
8. Blake, G. B.; MacFarlane, M. R.; Hinton, J. W., Titanium in reconstructive surgery of the skull and face. *British Journal of Plastic Surgery* **1990**, 43 (5), 528.
9. Peng, L.; Eltgroth, M. L.; LaTempa, T. J.; Grimes, C. A.; Desai, T. A., The effect of TiO<sub>2</sub> nanotubes on endothelial function and smooth muscle proliferation. *Biomaterials* **2009**, 30 (7), 1268-72.
10. Fine, E.; Zhang, L.; Fenniri, H.; Webster, T. J., Enhanced endothelial cell functions on rosette nanotube-coated titanium vascular stents. *Int J Nanomedicine* **2009**, 4, 91-7.
11. Liu, X.; Chu, P. K.; Ding, C., Surface modification of titanium, titanium alloys, and related materials for biomedical applications. *Materials Science and Engineering: R: Reports* **2004**, 47 (3-4), 49-121.
12. Sul, Y.-T., The significance of the surface properties of oxidized titanium to the bone response: special emphasis on potential biochemical bonding of oxidized titanium implant. *Biomaterials* **2003**, 24 (22), 3893.
13. Biggs, M. J. P.; Richards, R. G.; Dalby, M. J., Nanotopographical modification: a regulator of cellular function through focal adhesions. *Nanomedicine: Nanotechnology, Biology and Medicine* **2010**, 6 (5), 619-633.

14. Min, B.-M.; You, Y.; Kim, J.-M.; Lee, S. J.; Park, W. H., Formation of nanostructured poly(lactic-co-glycolic acid)/chitin matrix and its cellular response to normal human keratinocytes and fibroblasts. *Carbohydrate Polymers* **2004**, *57* (3), 285-292.
15. Riehle, M., Biocompatibility: Nanomaterials for cell- and tissue engineering. *NanoBioTechnology* **2005**, *1* (3), 308-309.
16. Zhang, L.; Webster, T. J., Nanotechnology and nanomaterials: Promises for improved tissue regeneration. *Nano Today* **2009**, *4* (1), 66.
17. Curtis, A. S. G.; Gadegaard, N.; Dalby, M. J.; Riehle, M. O.; Wilkinson, C. D. W.; Aitchison, G., Cells react to nanoscale order and symmetry in their surroundings. *IEEE Trans Nanobioscience* **2004**, *3* (1), 61-5.
18. Martin, C. R.; Kohli, P., The emerging field of nanotube biotechnology. *Nat Rev Drug Discov* **2003**, *2* (1), 29-37.
19. Papat, K. C.; Leoni, L.; Grimes, C. A.; Desai, T. A., Influence of engineered titania nanotubular surfaces on bone cells. *Biomaterials* **2007**, *28* (21), 3188-3197.
20. Smith, B. S.; Yoriya, S.; Grissom, L.; Grimes, C. A.; Papat, K. C., Hemocompatibility of titania nanotube arrays. *Journal of Biomedical Materials Research Part A* **2010**, *95A* (2), 350-360.
21. Bechara, S. L.; Judson, A.; Papat, K. C., Template synthesized poly([var epsilon]-caprolactone) nanowire surfaces for neural tissue engineering. *Biomaterials* **2010**, *31* (13), 3492-3501.
22. Leary Swan, E. E.; Papat, K. C.; Desai, T. A., Peptide-immobilized nanoporous alumina membranes for enhanced osteoblast adhesion. *Biomaterials* **2005**, *26* (14), 1969.
23. Ruckh, T.; Porter, J. R.; Allam, N. K.; Feng, X.; Grimes, C. A.; Papat, K. C., Nanostructured tantalum as a template for enhanced osseointegration. *Nanotechnology* **2009**, *20* (4), 45102.
24. Baroli, B.; Ennas, M. G.; Loffredo, F.; Isola, M.; Pinna, R.; Lopez-Quintela, M. A., Penetration of Metallic Nanoparticles in Human Full-Thickness Skin. *J Invest Dermatol* **2007**, *127* (7), 1701-1712.
25. Zhang, L. W.; Yu, W. W.; Colvin, V. L.; Monteiro-Riviere, N. A., Biological interactions of quantum dot nanoparticles in skin and in human epidermal keratinocytes. *Toxicology and Applied Pharmacology* **2008**, *228* (2), 200-211.
26. Rho, K. S.; Jeong, L.; Lee, G.; Seo, B.-M.; Park, Y. J.; Hong, S.-D.; Roh, S.; Cho, J. J.; Park, W. H.; Min, B.-M., Electrospinning of collagen nanofibers: Effects on the behavior of normal human keratinocytes and early-stage wound healing. *Biomaterials* **2006**, *27* (8), 1452-1461.
27. Ruckh, T. T.; Kumar, K.; Kipper, M. J.; Papat, K. C., Osteogenic differentiation of bone marrow stromal cells on poly(epsilon-caprolactone) nanofiber scaffolds. *Acta Biomater* **2010**, *6* (8), 2949-59.

28. Porter, J. R.; Ruckh, T. T.; Popat, K. C., Bone tissue engineering: a review in bone biomimetics and drug delivery strategies. *Biotechnol Prog* **2009**, *25* (6), 1539-60.
29. Loesberg, W. A.; te Riet, J.; van Delft, F. C. M. J. M.; Schön, P.; Figdor, C. G.; Speller, S.; van Loon, J. J. W. A.; Walboomers, X. F.; Jansen, J. A., The threshold at which substrate nanogroove dimensions may influence fibroblast alignment and adhesion. *Biomaterials* **2007**, *28* (27), 3944-3951.
30. Puckett, S. D.; Lee, P. P.; Ciombor, D. M.; Aaron, R. K.; Webster, T. J., Nanotextured titanium surfaces for enhancing skin growth on transcutaneous osseointegrated devices. *Acta Biomaterialia* **2010**, *6* (6), 2352-2362.
31. Popat, K. C.; Eltgroth, M.; LaTempa, T. J.; Grimes, C. A.; Desai, T. A., Decreased Staphylococcus epidermis adhesion and increased osteoblast functionality on antibiotic-loaded titania nanotubes. *Biomaterials* **2007**, *28* (32), 4880-4888.
32. Popat, K.; Eltgroth, M.; LaTempa, T.; Grimes, C.; Desai, T., Titania Nanotubes: A Novel Platform for Drug-Eluting Coatings for Medical Implants? *Small* **2007**, *3* (11), 1878-1881.
33. Zhao, L.; Mei, S.; Wang, W.; Chu, P. K.; Wu, Z.; Zhang, Y., The role of sterilization in the cytocompatibility of titania nanotubes. *Biomaterials* **2010**, *31* (8), 2055-63.
34. Simpson, D. G., Dermal templates and the wound-healing paradigm: the promise of tissue regeneration. *Expert Review of Medical Devices* **2006**, *3*, 471-484.
35. Winter, G. D., Transcutaneous implants: Reactions of the skin-implant interface. *Journal of Biomedical Materials Research* **1974**, *8* (3), 99-113.
36. Tillander, J.; Hagberg, K.; Hagberg, L.; Brånemark, R., Osseointegrated Titanium Implants for Limb Prostheses Attachments: Infectious Complications. *Clinical Orthopaedics and Related Research*® **2010**, 1-8.
37. Ruan, C.; Paulose, M.; Varghese, O. K.; Mor, G. K.; Grimes, C. A., Fabrication of Highly Ordered TiO<sub>2</sub> Nanotube Arrays Using an Organic Electrolyte. *The Journal of Physical Chemistry B* **2005**, *109* (33), 15754-15759.
38. Gong, D.; Grimes, C. A.; Varghese, O. K.; Hu, W.; Singh, R. S.; Chen, Z.; Dickey, E. C., Titanium oxide nanotube arrays prepared by anodic oxidation. *Journal of Materials Research* **2001**, *16* (12), 3331-34.
39. Mor, G. K.; Varghese, O. K.; Paulose, M.; Mukherjee, N.; Grimes, C. A., Fabrication of tapered, conical-shaped titania nanotubes. *Journal of Materials Research* **2003**, *18* (11), 2588-93.
40. Yoriya, S.; Grimes, C. A., Self-Assembled TiO<sub>2</sub> Nanotube Arrays by Anodization of Titanium in Diethylene Glycol: Approach to Extended Pore Widening. *Langmuir* **2009**, *26* (1), 417-420.
41. Mor, G. K.; Varghese, O. K.; Paulose, M.; Shankar, K.; Grimes, C. A., A review on highly ordered, vertically oriented TiO<sub>2</sub> nanotube arrays: Fabrication, material

- properties, and solar energy applications. *Solar Energy Materials and Solar Cells* **2006**, *90* (14), 2011.
42. Vasilev, K.; Poh, Z.; Kant, K.; Chan, J.; Michelmore, A.; Losic, D., Tailoring the surface functionalities of titania nanotube arrays. *Biomaterials* **2010**, *31* (3), 532-540.
  43. Stevens, M. M.; George, J. H., Exploring and Engineering the Cell Surface Interface. *Science* **2005**, *310* (5751), 1135-1138.
  44. Zhang, S., Fabrication of novel biomaterials through molecular self-assembly. *Nat Biotech* **2003**, *21* (10), 1171-1178.

## CHAPTER 3

### SKIN CELL FUNCTIONALITY ON TITANIA NANOTUBE ARRAYS

#### 3.1 Introduction

Skin interfacing biomaterials are utilized in numerous clinical applications including, but not limited to, prosthetics<sup>1,2</sup>, tissue regeneration<sup>3,4</sup>, wound repair<sup>5,6</sup> and dental implants<sup>7</sup>. Limb loss, for example, a major injury currently affecting nearly 2 million people in the United States, is on the rise due to trauma<sup>8</sup>, diabetes<sup>9</sup>, osteosarcoma<sup>10</sup>, vascular diseases<sup>11</sup>, and the effects of aging<sup>12</sup>. Limb loss and many other conditions are often treated by transcutaneous implants that penetrate through the depth of the skin<sup>1,2,13</sup>. For the long-term success of such implants, the biomaterial must integrate appropriately with the skin. The skin consists of three layers: epidermis (thin outer layer); dermis (thicker inner layer); and hypodermis (consisting of loose connective tissue)<sup>14</sup>. These layers combine to create the largest organ in the human body<sup>6,14</sup>. The multilayered network of skin acts as a protective barrier against infection and toxins, and is a mode of moisture retention, and a network of connective tissue consisting of cells, fibers and the extracellular matrix (ECM)<sup>6,15</sup>. Favorable interactions of a transcutaneous implantable device with the respective skin layers are critical for the long-term use of the biomaterial<sup>16,17</sup>.

Titanium and titanium-based alloys are the most widely used biomaterials for transcutaneous implants due to their mechanical strength, biocompatibility, non-toxicity, corrosion resistance, and ease of process-ability<sup>18,19</sup>. These materials have been used in a variety of clinical devices including prosthesis, wound healing sutures, and dental and

craniofacial implants<sup>20</sup>. The passive oxide layer that forms on the outside surface of titanium, known as titania, protects the surface against corrosion while providing a favorable biocompatible interface for tissue integration<sup>18,19</sup>. Although these materials are among the better choices for transcutaneous implantable devices, all biomaterials have been shown to initiate biological events in the form of inflammatory cell infiltration, granulation tissue formation, foreign body reaction, and fibrosis<sup>21,22</sup>. Wound infection resulting from poor skin-material integration is one of the major causes for the rejection of transcutaneous implantable devices<sup>1,2,13,23</sup>. Recent studies have provided an in-depth look into cellular adhesion and proliferation<sup>24</sup>, cell phenotypic behavior<sup>25</sup>, and cytotoxic effects<sup>26,27</sup> to determine the skin interaction with various biomaterial surfaces<sup>5,28,29</sup>. Numerous studies have shown increased cellular adhesion on microscale surface topographies<sup>30,31</sup>. Further, studies have also shown increased cellular functionality on peptide modified<sup>31,32</sup> and growth factor functionalized<sup>33,34</sup> surfaces. Nonetheless, little is known about the skin cell response to biomaterials with nanoscale architectures.

Material surfaces that mimic the hierarchical structure of *in vivo* tissue at a nanoscale provide a possible solution for enhancing biomaterial integration, thus preventing infection and biomaterial rejection<sup>3,4,17,35,36</sup>. Recently, there has been an increased interest in exploring nanoscale surface topographies such as nanotubes<sup>37-39</sup>, nanowires<sup>40</sup>, nanopores<sup>41,42</sup>, nanoparticles<sup>43,44</sup>, nanofibers<sup>35,45,46</sup>, as biomimetic interfaces for implantable devices<sup>47</sup>. Several studies have reported enhanced dermal fibroblast adhesion along with increased tissue formation on such nanoscale topographies<sup>4,48,49</sup>. In this study, titania nanotube arrays (diameter: 70-90 nm, length: 1  $\mu$ m) were fabricated using an anodization process, as biomimetic interfaces for transcutaneous

implantable devices. Previous studies on titania nanotube arrays have demonstrated improved mesenchymal stem cell functionality<sup>38</sup>, hemocompatibility<sup>39</sup>, osteoblast phenotypic behavior<sup>38, 47, 50</sup>, and localized drug delivery<sup>51</sup>. In addition, these titania nanotube arrays have elicited minimal levels of monocyte activation and cytokine secretion, thus exhibiting a very low degree of immunogenicity<sup>52</sup>. However, few studies report on the interaction of skin cells with titania nanotube arrays. Thus, in this study the compatibility of human dermal fibroblasts (HDF) (responsible for the production of the extracellular matrix and the underlying dermal structure), and human epidermal keratinocytes (HEK) (responsible for creating and retaining the epidermis) with highly uniform titania nanotube arrays is reported. Skin-compatibility is a key consideration for the long-term use of transcutaneous implantable devices<sup>1, 5, 13</sup>; therefore, an understanding of the physiological response elicited from skin/nano-biomaterial interactions is one of immediate concern.

## **3.2 Experimental Methods**

### **3.2.1 *Fabrication and Characterization of Titania Nanotube Arrays***

Titania nanotube arrays were fabricated using a simple anodization process, as described in detail in chapter 2<sup>38, 51, 53</sup>. Biomedical grade titanium (as-received, non-polished) surfaces were used as controls. The nanotube architecture was examined for uniformity and repeatability using SEM imaging.

### **3.2.2 Cell Culture**

HDF and HEK, obtained from neonatal foreskins and purchased from Clonetics, were used in this study. Cryopreserved cell suspensions were transferred to a -80°C freezer, where they were stored until use. Prior to cell culture, they were thawed in a water bath at 37°C. HDF cells were suspended in Medium 106 with low serum growth supplement (LSGS) and gentamicin/amphotericin solution (Cascade Biologics); HEK cells were suspended in EpiLife Medium with human keratinocyte growth supplement (HKGS) and gentamicin/amphotericin solution (Cascade Biologics). The HDF or HEK cell suspensions were added to 75 cm<sup>2</sup> culture flasks and incubated at 37°C and 5% CO<sub>2</sub>. The cell suspensions were subcultured by trypsin digestion (0.025% trypsin/EDTA) when they reached 70-90% confluence. Following a complete cell-surface detachment, a trypsin neutralizer (0.5% fetal bovine serum in phosphate buffered saline (PBS)) was added to arrest the trypsin reaction. The cells were transferred to tubes and centrifuged at 180 g's for 7 mins, forming a cell pellet that was resuspended in the appropriate culture medium. The cell density was determined by trypan blue dye exclusion, using a hemocytometer. For both cell types, a concentration of 5×10<sup>5</sup> cells was suspended in 13 mL of culture medium. The cell suspensions were added to 75 cm<sup>2</sup> culture flasks and incubated at 37°C and 5% CO<sub>2</sub>. The first media change took place between 24-36 hrs after initial culture; subsequent media changes occurred every other day until the cells were 50% confluent, after which the media was changed every day. The experiments for this study were performed using second passage HDF and HEK cells.

### **3.2.3 Cell Culture on Titania Nanotube Arrays**

HDF or HEK cells were seeded on biomedical grade smooth titanium (control) and titania nanotube arrays (both substrates: 0.5 cm<sup>2</sup>) in a 24-well plate. Prior to seeding, all substrates were sterilized and conditioned. The substrates were incubated in 70% ethanol for 30 mins, and washed two times with PBS. Substrates were air dried, subjected to 30 min of *UV* exposure, and conditioned in 500 μL of the appropriate culture medium. HDF cells were seeded at a density of 1×10<sup>4</sup> cells/mL; and HEK cells were seeded at a density of 3×10<sup>4</sup> cells/mL. The substrates were incubated at 37°C and 5% CO<sub>2</sub> in 500 μL of cell rich media and evaluated for adhesion, proliferation, viability, morphology and differentiation after 1, 2 and 4 days of culture.

### **3.2.4 Adhesion and Proliferation of HDF and HEK on Titania Nanotube Arrays**

Cellular adhesion and proliferation was investigated using calcein-AM (Invitrogen) live stain and 4'6-diamidino-2-phenylindole-dihydrochloride (DAPI, Invitrogen) nucleus stain fluorescence microscope imaging, after 1, 2 and 4 days of culture.

Calcein AM live stain fluorescence microscope imaging was observed after 1, 2 and 4 days of culture. Prior to staining, the un-adhered cells were removed by aspirating the cell rich media from the substrates followed by two gentle rinses with PBS. The substrates were then transferred to a new 24-well plate and incubated with 5 μM calcein-AM solution in PBS for 30 min at room temperature. They were rinsed with PBS and imaged with a fluorescence microscope (Zeiss) using filter set 44 FITC BP 530/50 Green

filters (Zeiss). The cell coverage was calculated using the fluorescence images and the ImageJ software.

After 4 days of culture, the cell nuclei were stained with DAPI to determine the number of adherent cells. Prior to staining, the un-adhered cells were removed by aspirating the cell rich media from the substrates followed by two gentle rinses with PBS. The substrates were then transferred to a new 24-well plate. Adherent cells were fixed in 3.7wt % formaldehyde in PBS for 15 min at room temperature and washed three times (5 mins per wash) in PBS. The cell membranes were permeabilized using 1% Triton-X in PBS at room temperature for 3 mins, washed with PBS and incubated in 10% bovine serum albumin (BSA) in PBS for 30 min at room temperature, to block unspecific immune reactions. The substrates were washed three times (5 mins per wash) in PBS. The cell nuclei was stained by DAPI nucleus stain (dilution 1:50) with 2% BSA in PBS for 5 mins. The substrates were washed three times (5 mins per wash) in PBS. The number of cells adhered on the substrates was determined by the number of stained nuclei using the DAPI fluorescence images.

### **3.2.5 Viability of HDF and HEK on Titania Nanotube Arrays**

The cell viability was characterized using a commercially available Methylthiazol Tetrazolium (MTT) assay kit (Sigma). Prior to measuring the MTT activity, the un-adhered cells were removed by aspirating the cell rich media from the substrates followed by two gentle rinses with PBS. Substrates were transferred to a new 24-well plate and incubated in 10% MTT solution in PBS for 3.5 hrs at 37°C and 5% CO<sub>2</sub>. The resulting formazan crystals were dissolved by adding a 10% Triton-X in MTT solvent mixture in

the amounts equal to the MTT solution in PBS, and agitating. The absorbance of the solution was measured at a wavelength of 570 nm using a plate reader (BMG Labtech). The net absorbance was calculated by subtracting the background absorbance at a wavelength of 690 nm. The amount of viable cells was determined by this calculation.

### **3.2.6 Morphology of HDF and HEK on Titania Nanotube Arrays**

The cell morphology was investigated using SEM imaging to visualize the cellular interaction with the nanotube architecture. The un-adhered cells were removed by aspirating the cell rich media from the substrates followed by two gentle rinses with PBS. The substrates were then transferred to a clean petri-dish where the cells were dehydrated and fixed on the substrate surface. The cells were fixed by incubating the substrates in a solution of primary fixative (3% glutaraldehyde (Sigma), 0.1 M sodium cacodylate (Polysciences), and 0.1 M sucrose (Sigma)) for 45 min. They were then incubated in a solution of secondary fixative (primary fixative without glutaraldehyde) for 10 min. Subsequently, the substrates were dehydrated by incubation in consecutive solutions of increasing ethanol concentrations (35%, 50%, 70%, 95%, and 100%) for 10 min each. Further dehydration of the cells was accomplished by incubating the substrates in hexamethyldisilazane (HMDS, Sigma) for 10 min. They were then air dried and stored in a desiccator until further imaging by SEM. The substrates were coated with a 10 nm layer of gold and imaged at 15kV.

### ***3.2.7 Cytoskeletal Organization of HDF and HEK on Titania Nanotube Arrays***

After 4 days of culture, the same samples that were stained for DAPI, were concurrently stained to evaluate the cytoskeleton organization in cells by vinculin and F-actin staining<sup>54</sup>. The substrates were incubated in fluorescein isothiocyanate (FITC)-conjugated monoclonal mouse anti-vinculin IgG (dilution 1:200) with 2% BSA in PBS for 1 hr at room temperature to stain a specific, vinculin-labelled transmembrane protein. The substrates were washed three times (5 mins per wash) in PBS. This was followed by incubating the substrates in rhodamine-conjugated phalloidin (dilution 1:40) with 2% BSA in PBS for 20 min at room temperature to stain the F-actin on the cell membranes. The stained substrates were imaged with a fluorescent microscope using DAPI BP 445/50 Blue filters, HQ Texas Red BP 560/40 Red filters, and HE YFP BP 535/30 Gold filters (Zeiss).

### ***3.2.8 Differentiation of HDF and HEK on Titania Nanotube Arrays***

After 4 days of culture, indirect immunofluorescence staining was used to determine cellular expression and differentiation through the presence of membrane specific marker proteins on HDF or HEK cells<sup>16</sup>. The un-adhered cells were removed by aspirating the cell rich media from the substrates followed by two gentle rinses with PBS. The substrates were then transferred to a new 24-well plate. Adherent cells were fixed in 3.7wt % formaldehyde in PBS for 15 min at room temperature and washed three times (5 mins per wash) in PBS. The cell membranes were permeabilized using 1% Triton-X in PBS at room temperature for 3 mins, and washed in PBS. To block unspecific immune reactions, the substrates were incubated in 10% blocking serum in PBS for 30 min at

room temperature. A primary antibody (dilution 1:50, Santa Cruz Biotechnology) with 2% blocking serum in PBS was administered for 1 hr, at room temperature. The substrates with HDF cells were stained with anti-collagen-I $\alpha$ 1 or anti-fibrillin-1, and the substrates with HEK cells were stained with anti-cytokeratin-19 or anti-laminin- $\beta$ 3. They were then washed three times (5 mins per wash) in PBS, and incubated with an appropriate secondary fluorescently labeled antibody (dilution 1:100, Santa Cruz Biotechnology, Santa Cruz, CA) with 2% blocking serum in PBS for 1 hr, at room temperature. The substrates were washed three times (5 mins per wash) in PBS, and imaged with a fluorescent microscope using HQ Texas Red BP 560/40 Red filters and HE YFP BP 535/30 Gold filters. All images were processed using the ImageJ Software. Images of the HEK substrates, fluorescently-labelled with cytokeratin-19 had their color manipulated from red to green for visual diversity. Cellular differentiation and expression were determined by the presence of cell extensions, increased fluorescence, common orientation, and a heightened cellular size and structure.

### **3.2.9 Statistical Analysis**

Each experiment was reconfirmed on at least three different samples with at least two different cell populations ( $n_{\min} = 6$ ). Further, all the quantitative results were analyzed using an analysis of variance (ANOVA). Statistical significance was considered at  $p < 0.05$ . During the analysis, variances among each group were not assumed to be equal and thus a Welch-Satterthwaite two sample t-test approach was used to test the significance between the control substrates and titania nanotube arrays. This analysis was conducted using the R statistical software.

### 3.3 Results and Discussion

Transcutaneous implantable devices are in constant contact with the thick underlying dermal layer of the skin consisting of fibroblasts; and the thin outer layer of skin consisting of keratinocytes. A favorable cellular interaction with the material surface is critical for the long-term success of such implantable devices. In order to investigate the skin/nano-biomaterial interaction, HDF and HEK cell functionality was investigated on biomedical grade titanium (control) and highly ordered titania nanotube arrays, after 1, 2 and 4 days of culture. Cellular adhesion, proliferation, viability and morphology were evaluated using fluorescence microscope imaging with calcein-AM live stain and DAPI nucleus stain, commercial MTT assay, and SEM imaging respectively. Cytoskeletal organization was examined using fluorescence microscope imaging of vinculin and F-actin membrane proteins. Further, the cellular differentiation was investigated using immunolabeling specific marker proteins and detecting the using fluorescence microscope imaging. The results, as discussed below, indicate an increase in HDF and a significant decrease in HEK functionality on titania nanotube arrays as compared to the control substrate.

Titania nanotube arrays were fabricated using a simple anodization process. Vertically oriented, immobilized, high aspect ratio titania nanotube arrays were fabricated after 24 hrs of anodization at 60 V and annealed, as previously described<sup>38, 39, 53</sup>. Titania nanotube arrays with a diameter of 70-90 nm and length of 1  $\mu\text{m}$  were selected based on previous studies that found enhanced cellular functionality and sustained drug release on the same size titania nanotube arrays<sup>38, 51</sup>. In order to obtain a crystalline structure, the as-anodized titania nanotube arrays were annealed in oxygen ambient at 530°C for 3 hrs.

The crystalline titania nanotube arrays retain the structure of the as-fabricated amorphous nanotube arrays on annealing<sup>39</sup>. The nanotube architecture was examined for uniformity and repeatability (diameter: 70-90 nm, length: 1  $\mu\text{m}$ ) using SEM imaging (See **Figure 3.1**). The titania nanotube arrays provide a biomimetic, biocompatible, and non-biodegradable interface for implantable devices.

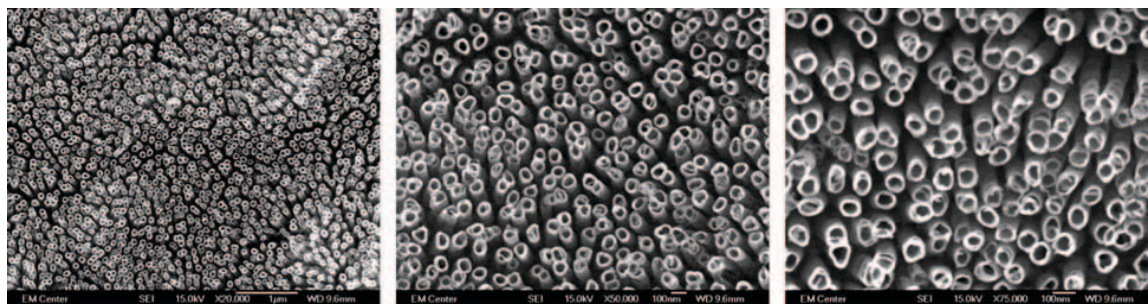


Figure 3.1 Representative SEM images of titania nanotube arrays.

Cellular adhesion and proliferation were investigated using fluorescence microscope imaging of calcein-AM live stain and DAPI nucleus stain after 1, 2 and 4 days of culture. Calcein-AM is cell-permeate stain that labels viable cells by converting the non-fluorescent calcein-AM into a green-fluorescent calcein. This conversion is accomplished through the hydrolyzation of intracellular acetoxymethyl esterases. The results indicate an increase in HDF and a decrease in HEK adhesion and proliferation on titania nanotube arrays as shown in **Figure 3.2a and 3.2b**. In addition, the HDF cells demonstrated a greater order and alignment on titania nanotube arrays as compared to the control substrate (See **Figure 3.2a**). It should be noted that the greatly influenced orientation, elongation and continued proliferation by the HDF cells on the titania nanotube array substrates provide a potential for heightened matrix formation and

enhanced biomaterial integration<sup>15, 48</sup>. The fluorescence microscope images were also analyzed for cell coverage using the ImageJ software. The results indicate a significant 40% increase in HDF cell coverage (See **Figure 3.2a**), and a significant 92% decrease in HEK cell coverage (See **Figure 3.2b**) on titania nanotube arrays as compared to the control substrate. Further, the cells were stained with DAPI nucleus stain and fluorescence microscope images were analyzed using ImageJ software to determine the number of adhered cells after 4 days of culture. The DAPI nucleic acid stain passes through intact membranes and preferentially stains dsDNA with a blue-fluorescence label, capable of being detected by fluorescence microscope imaging. **Figure 3.3** indicates a significant 14% increase in HDF cells and a significant 43% decrease in HEK cells adhered on titania nanotube arrays as compared to the control substrate. Further, the HEK cells did not show any preferential alignment on titania nanotube arrays.

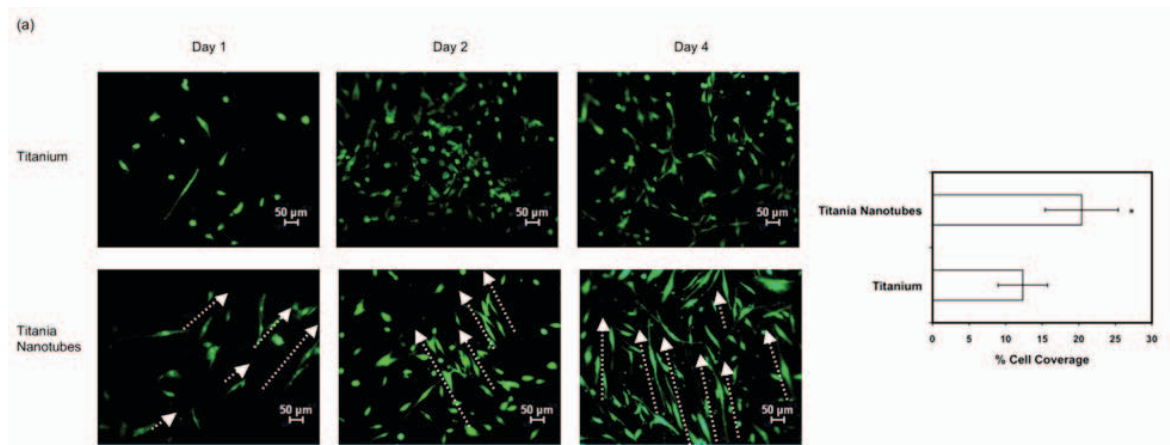


Figure 3.2 (a) Representative fluorescence microscopy images (10x magnification) of adhered HDF stained with calcein-AM on the control substrate and titania nanotube arrays after 1, 2 and 4 days of culture. The amount of HDF coverage was calculated using the fluorescence images and the ImageJ software. The results indicate a significant 40% increase in HDF coverage on titania nanotube arrays compared to the control substrate (\*  $\rightarrow$   $p < 0.05$ ).

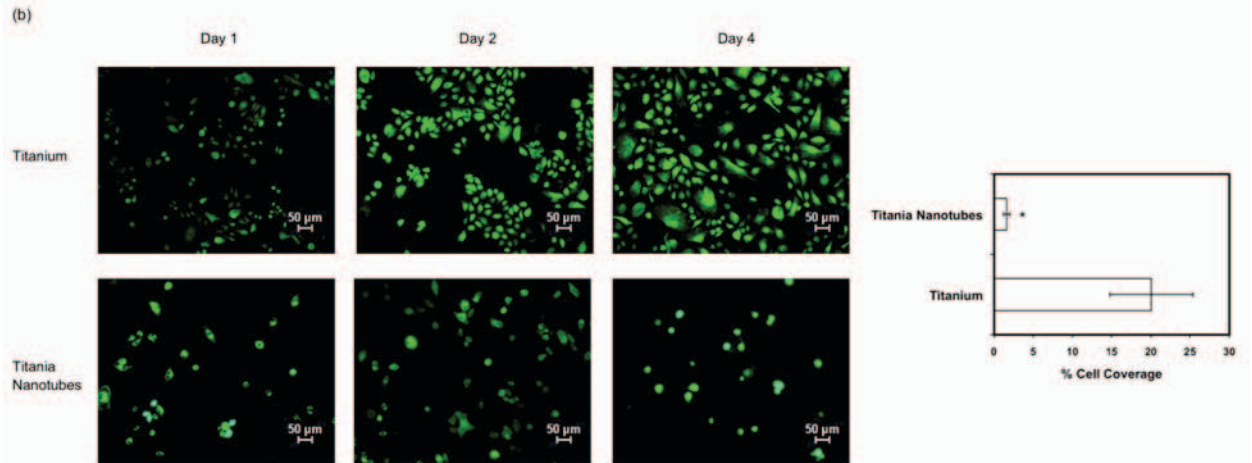


Figure 3.2 (b) Representative fluorescence microscopy images (10x magnification) of adhered HEK stained with calcein-AM on the control substrate and titania nanotube arrays after 1, 2 and 4 days of culture. The amount of HEK coverage was calculated using the fluorescence images and the ImageJ software. The results indicate a significant 92% decrease in HEK coverage on titania nanotube arrays compared to the control substrate (\*  $\rightarrow$   $p < 0.05$ ).

Despite the fact that three times more HEK cells were seeded than HDF cells, the results clearly indicate a higher capacity for HDF cells to adhere and proliferate on titanium substrates than HEK cells.

The cell viability was characterized using a commercially available MTT assay kit after 1, 2 and 4 days of cell culture. MTT is a colorimetric assay that measures the amount of methylthiazol tetrazolium following its reduction into an insoluble form by mitochondrial succinate dehydrogenase, only present in metabolically active cells. Spectrophotometric measurements of the net absorbance were calculated to determine the concentration of viable cells on the substrates. These results indicate a significant

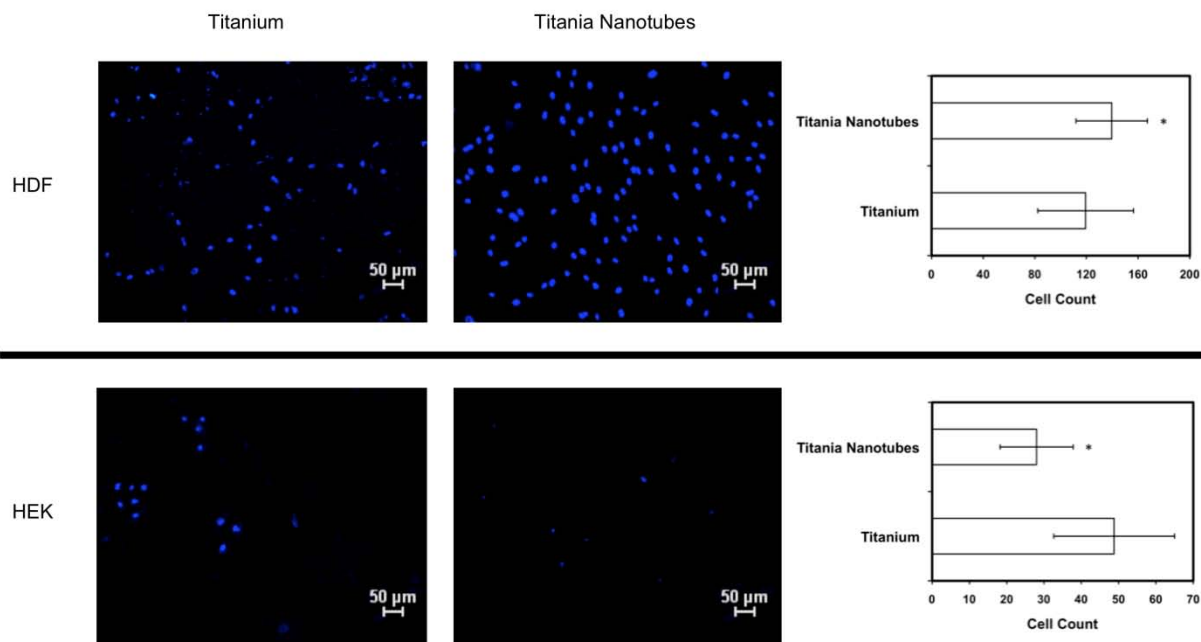


Figure 3.3 Representative fluorescence microscopy images of HDF and HEK cells stained with DAPI on the control substrate and titania nanotube arrays after 4 days of culture. The HDF cell count indicates a significant 14% increase in HDF cells on titania nanotube arrays (\*  $\rightarrow$   $p < 0.05$ ). The HEK cell count indicates a significant 43% decrease in HEK cells on titania nanotube arrays (\*  $\rightarrow$   $p < 0.05$ ).

increase in the viability of HDF cells after 4 days of culture on titania nanotube arrays as compared to the control substrate (See Figure 3.4a). However, there was a significant decrease in the viability of HEK cells after 4 days of culture on titania nanotube arrays as compared to the control substrate (See Figure 3.4b).

The cellular morphology was investigated after 1, 2 and 4 days of culture using SEM imaging to visualize the HDF and HEK interaction with the nanotube architecture (See Figure 3.5a and 3.5b). These images indicate the degree of matrix formation

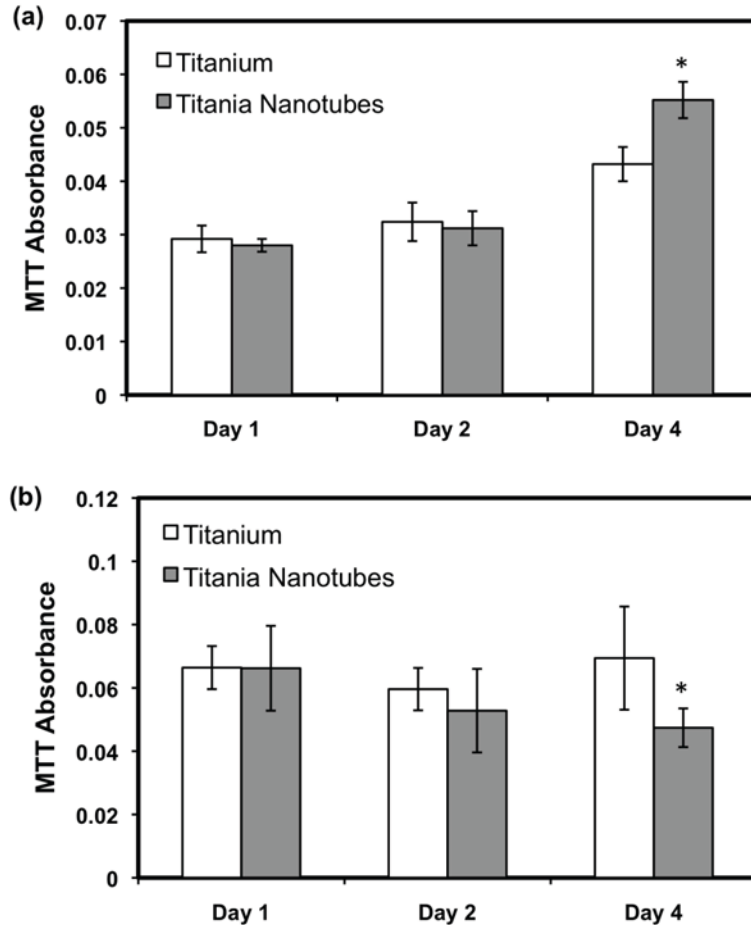


Figure 3.4 (a) Cell viability measured using MTT assay for HDF cells on the control substrate and titania nanotube arrays. After 4 days of culture, HDF viability is significantly increased on titania nanotube arrays (\* $\rightarrow$   $p < 0.05$ ).

(b) Cell viability measured using MTT assay for HEK cells on the control substrate and titania nanotube arrays. After 4 days of culture, HEK viability is significantly decreased on titania nanotube arrays (\* $\rightarrow$   $p < 0.05$ ).

developed by a network of connective tissue consisting of cells, fibers and the ECM produced on the substrates. ECM and fiber production occurs as a result of cell aggregation, excitation, and protein expression. During this process, collagen and cytokeatin along with many other proteins and factors become released by HDF and

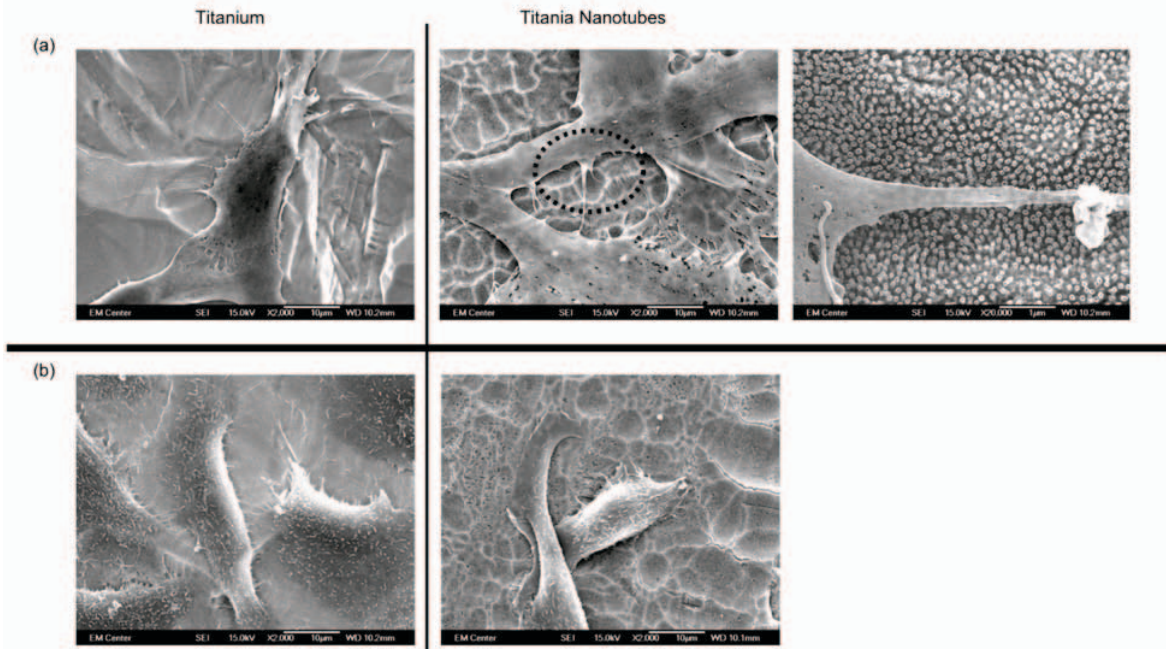


Figure 3.5 (a) Representative SEM images (2000x and 20000x magnification) of HDF cells on the control substrate and titania nanotube arrays after 4 days of culture. Images show a higher degree of HDF activation, cell-cell and cell-surface interaction on titania nanotube arrays.

(b) Representative SEM images (2000x magnification) of HEK cells on the control substrate and titania nanotube arrays after 1 day of culture. Images show a lower degree of HEK activation on titania nanotube arrays.

HEK cells respectively, to create the dermal and epidermal foundation of the skin. The greatest degree of cellular morphology was seen by HDF cells on titania nanotube arrays after 4 days of culture, as evidenced in **Figure 3.5a**. **Figure 3.5b** indicates nearly confluent epidermal coverage by HEK cells on the control substrate after only 1 day of culture; while producing limited epidermal overlay on titania nanotube arrays. These results indicate that the nanotube architecture provides a favorable template for the growth and maintenance of HDF cells while preventing adhesion and proliferation of HEK cells. This translates into an implant interface that allows increased cellular

adhesion and enhanced matrix deposition by the dermal fibroblasts; while preventing competitive adhesion of epidermal keratinocytes. Further providing an interface that restricts HEK cells from traveling downward along the implanted biomaterial, acting to wall off natural dermal matrix integration.

Cellular interactions with titania nanotube arrays may result in cytoskeletal reorganization. The cell cytoskeleton is composed of microfilaments, microtubules and intermediate filaments. When activated these components play important roles by assisting in cell-cell and cell-ECM communication, as well as mediating fundamental cellular events such as cell division, motility, protein trafficking and secretion<sup>55</sup>. After 4 days of culture, cytoskeletal structures were stained and evaluated using anti-vinculin (transmembrane protein, vinculin stain) and rhodamine-conjugated phalloidin (membrane protein, F-actin stain) on the control substrate and titania nanotube arrays. The results indicate a preferential orientation of fibrous extensions in HDF cells on titania nanotube arrays as shown in **Figure 3.6a**. These results indicate enhanced cytoskeletal reorganization and membrane protein expressions; thus enabling favorable cell-material interactions capable of a greater degree of matrix deposition on titania nanotube arrays. Further, the results shown in **Figure 3.6b** indicate altered cytoskeletal reorganization in HEK cells on the control substrates. However, there was no visible cytoskeletal reorganization on titania nanotube arrays. These results confirm the increased HDF functionality, and decreased HEK functionality on titania nanotube arrays reported in this study.

Cellular differentiation is a common indicator of activation, expression and bio-integration of an implant with the tissue. Indirect immunofluorescence staining was

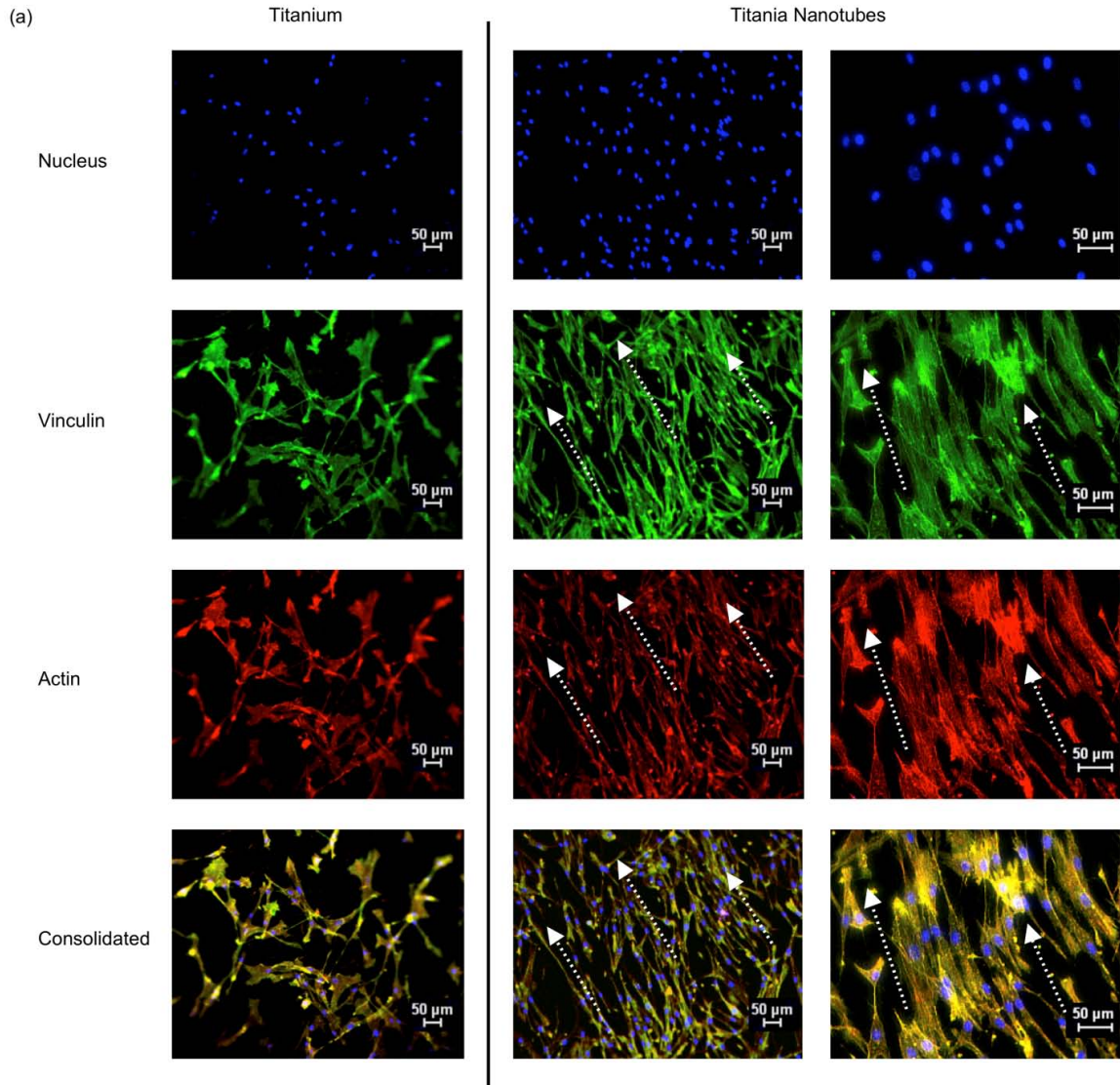


Figure 3.6 (a) Representative fluorescence microscopy images (10x and 20x magnification) of HDF stained with DAPI, FITC-conjugated anti-vinculin, and rhodamine-conjugated phalloidin (actin) along with consolidated images (from top to bottom respectively) on the control substrate and titania nanotube arrays, after 4 days of culture.

utilized to identify the presence of activated proteins within a cell in order to determine cellular differentiation. Previous studies have identified proteins known to be expressed in activated HDF or HEK cells <sup>56</sup>. HDF cells are known to express collagen-I $\alpha$ 1 and

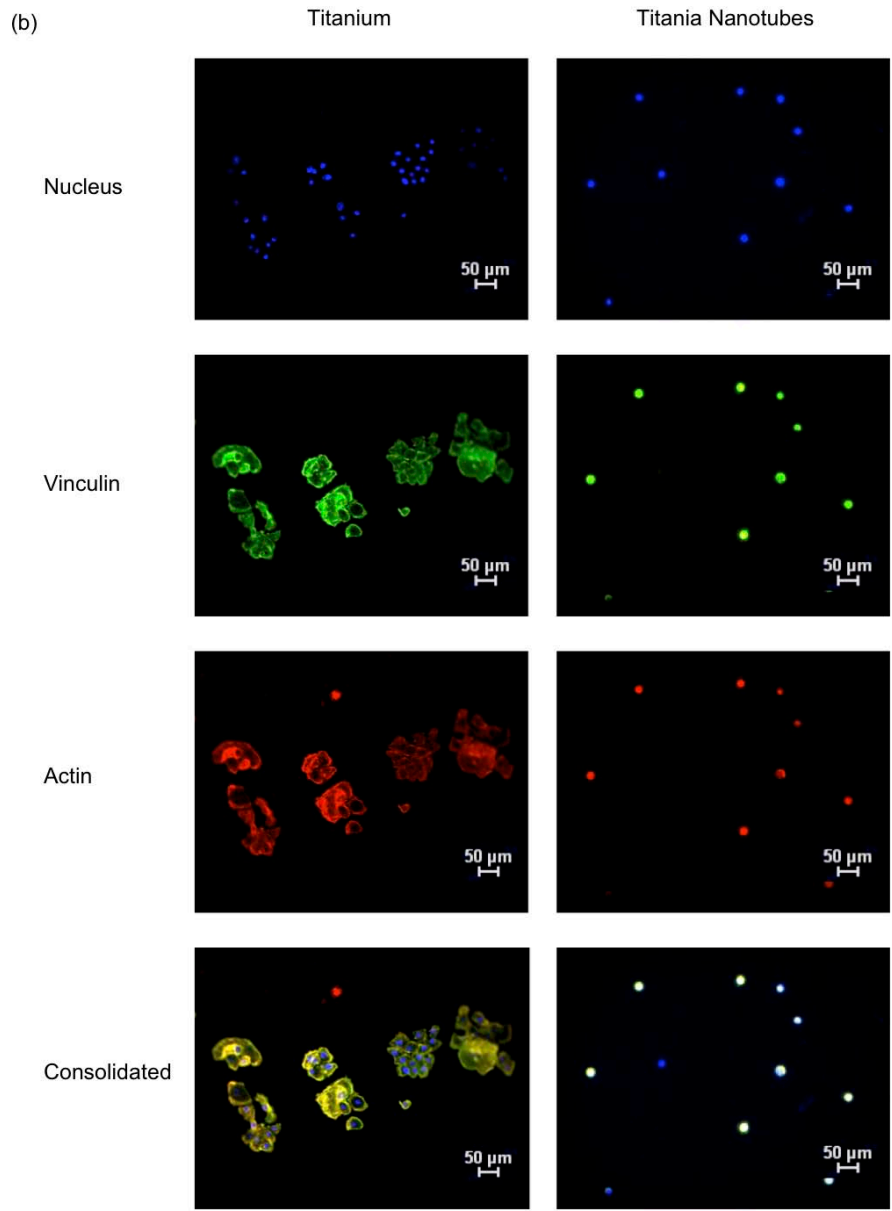


Figure 3.6 (b) Representative fluorescence microscopy images (10x magnification) of HEK cells stained with DAPI, FITC-conjugated anti-vinculin, and rhodamine-conjugated phalloidin (actin) along with consolidated images (from top to bottom respectively) on the control substrate and titania nanotube arrays, after 4 days of culture.

fibrillin-1. Collagen-I $\alpha$ 1 acts as a major component of connective tissue, and is therefore greatly responsible for the formation of the underlying matrix (ECM). When released

from cells, fibrillin-1 enters the ECM where it forms threadlike filaments called microfibrils that bind to elastic fibrils, enabling the skin to stretch. HEK cells are known to express cytokeratin-19 and laminin- $\beta$ 3. Cytokeratin-19 is a member of the keratin family, which acts as an intermediate filament providing a structural integrity specific in epithelial cells. Laminin- $\beta$ 3 regulates cell growth, movement and cell-cell attachment. In addition, it aids in the organization of the basement membrane that underlies the top layer of the skin. Thus, the expression of these marker proteins was determined after 4 days of culture by immunofluorescence for HDF (collagen-1 $\alpha$ 1 and fibrillin-1) and HEK (cytokeratin-19 and laminin- $\beta$ 3) cells (See Table 3.1) on titania nanotube arrays and the control substrate.

Table 3.1 Blocking agents, primary antibodies and secondary antibodies used for immunofluorescence identification of membrane specific marker proteins on HDF and HEK cells.

	Human Dermal Fibroblasts		Human Epidermal Keratinocytes	
	Collagen-1 $\alpha$ 1	Fibrillin-1	Cytokeratin-19	Laminin- $\beta$ 3
<b>Blocking</b>	Normal Donkey Serum	Normal Bovine Serum	Normal Donkey Serum	Normal Bovine Serum
<b>Primary Antibody</b>	Goat anti-collagen-1 $\alpha$ 1 polyclonal antibody	Goat anti-fibrillin-1 polyclonal antibody	Goat anti-cytokeratin-19 polyclonal antibody	Goat anti-laminin- $\beta$ 3 polyclonal antibody
<b>Secondary Antibody</b>	Fluorescein isothiocyanate (FITC)-conjugated donkey anti-goat IgG	Texas red (TR)-conjugated donkey anti-goat IgG	Allophycocyanin-cyanine (F(ab') <sub>2</sub> APC-Cy7)-conjugated donkey anti-goat IgG	Tetramethylrhodamine-5-isothiocyanate (TRITC)-conjugated donkey anti-goat IgG

The results indicate a substantial increase in collagen-1 $\alpha$ 1 expression, along with preferential orientation and expression of fibrillin-1 in HDF cells on titania nanotube arrays (See Figure 3.7a). Further, the results indicate a lower degree of cytokeratin-19 and laminin- $\beta$ 3 expression in HEK cells on titania nanotube arrays (See Figure 3.7b).

These findings confirm the results reported in this study, showing increased HDF and

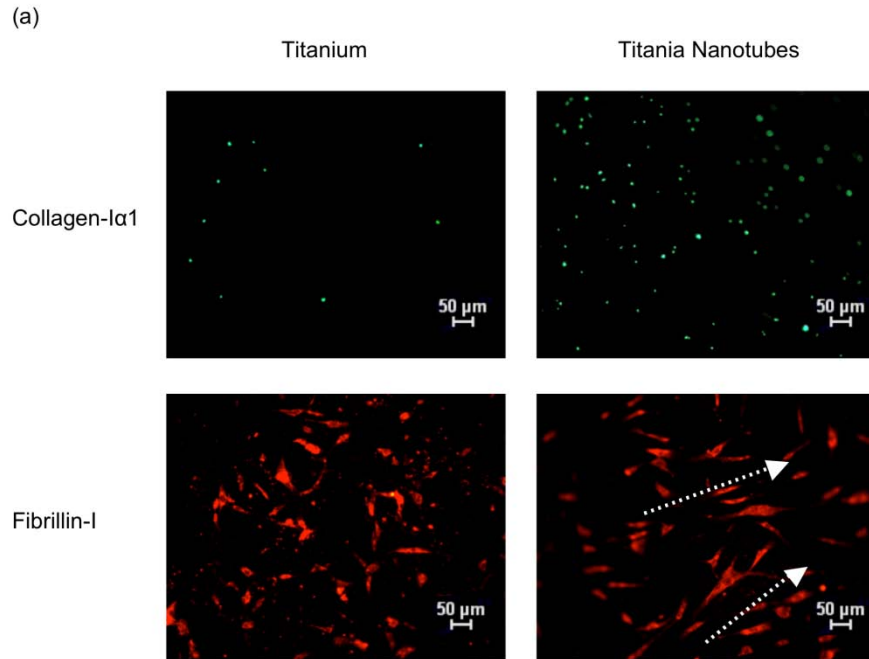


Figure 3.7 (a) Representative fluorescence microscopy images (10x magnification) of HDF cells immuno-stained with collagen-I $\alpha$ 1 and fibrillin-1 on the control substrate and titania nanotube arrays, after 4 days of culture. The images indicate a considerable increase in collagen-I $\alpha$ 1 expression, and a higher degree of fibrillin-1 expression and orientation for HDF cells on titania nanotube arrays.

significantly decreased HEK functionality on titania nanotube arrays as compared to the control substrate. Such cellular behavior is extremely important for inducing fibroblast matrix formation, thus enabling quick healing and wound closure after device implantation. This will allow primary integration between the dermis and the transcutaneous implantable device, followed by secondary epidermal integration based on cell signaling and cell-cell attachment.

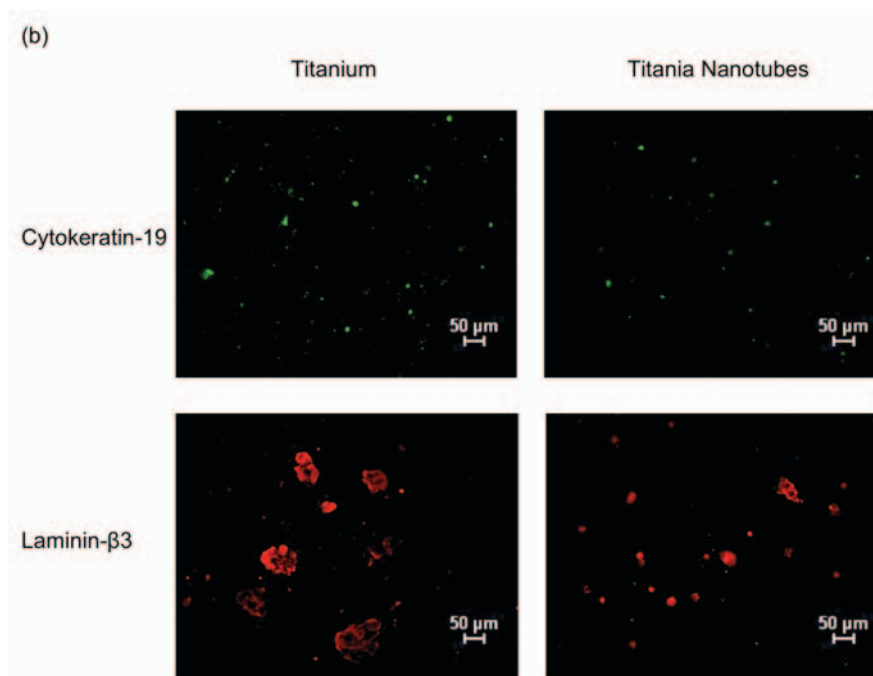


Figure 3.7 (b) Representative fluorescence microscopy images (10x magnification) of HDF cells immuno-stained with cytokeratin-19 and laminin- $\beta$ 3 on the control substrate and titania nanotube arrays, after 4 days of culture. The images indicate a decrease in cytokeratin-19 and laminin- $\beta$ 3 expression for HEK cells on titania nanotube arrays.

### 3.4 Conclusion

Transcutaneous implants that penetrate through the depth of the skin are used in numerous clinical applications including prosthetics and dental implants. Wound infection resulting from poor skin-material integration is one of the major causes for the rejection of such devices. Recently, there has been an increased interest in exploring nanoscale surface topographies as biomimetic interfaces for implantable devices. Several studies have reported favorable cellular response on such nanoscale topographies. However, little is known about the interactions of the respective skin layers to

biomaterials with nanoscale architectures. In this study, titania nanotube arrays were developed for their potential application as interfaces for transcutaneous implantable devices. The results from this study indicate increased dermal fibroblast adhesion, proliferation, orientation, cytoskeletal organization and differentiation on titania nanotube arrays. However, the results show a decrease in epidermal keratinocyte adhesion, proliferation, cytoskeletal organization and differentiation on titania nanotube arrays. The nanotube architecture provides a potentially favorable template for the growth and maintenance of dermal fibroblasts while preventing differentiation of epidermal keratinocytes. Such cellular behavior is extremely important for inducing fibroblast matrix formation, thus enabling quick healing and wound closure after device implantation. This will allow primary integration between the dermis and the transcutaneous implantable device, followed by secondary epidermal integration based on subsequent cell signaling and cell-cell attachment. Further, the cellular response may be tuned and optimized by varying the size parameters of titania nanotube arrays. There is a precise correlation between the anodization voltage and nanotube pore size, thus by varying the voltage and anodization time, nanotubes with different diameters and lengths can be fabricated. Therefore, titania nanotube arrays have the potential of being used as interfaces for transcutaneous implantable devices. Further studies are now targeted towards understanding and evaluating the effects of different size nanotubes on cellular functionality.

### 3.6 References

1. Tillander, J.; Hagberg, K.; Hagberg, L.; Brånemark, R., Osseointegrated Titanium Implants for Limb Prostheses Attachments: Infectious Complications. *Clinical Orthopaedics and Related Research*® **2010**, 1-8.
2. Mooney, V.; Predecki, P. K.; Renning, J.; Gray, J., Skeletal extension of limb prosthetic attachments—problems in tissue reaction. *Journal of Biomedical Materials Research* **1971**, 5 (6), 143-159.
3. Riehle, M., Biocompatibility: Nanomaterials for cell- and tissue engineering. *NanoBioTechnology* **2005**, 1 (3), 308-309.
4. Zhang, L.; Webster, T. J., Nanotechnology and nanomaterials: Promises for improved tissue regeneration. *Nano Today* **2009**, 4 (1), 66.
5. Simpson, D. G., Dermal templates and the wound-healing paradigm: the promise of tissue regeneration. *Expert Review of Medical Devices* **2006**, 3, 471-484.
6. Clark, R. A.; Ghosh, K.; Tonnesen, M. G., Tissue engineering for cutaneous wounds. *J Invest Dermatol* **2007**, 127 (5), 1018-29.
7. Jones, F. H., Teeth and bones: applications of surface science to dental materials and related biomaterials. *Surface Science Reports* **2001**, 42 (3-5), 75.
8. Messinger, S. D., Incorporating the prosthetic: Traumatic, limb-loss, rehabilitation and refigured military bodies. *Disability & Rehabilitation* **2009**, 31 (25), 2130-2134.
9. Byren, I.; Peters, E.; Hoey, C.; Berendt, A.; Lipsky, B., Pharmacotherapy of diabetic foot osteomyelitis. *Expert Opinion on Pharmacotherapy* **2009**, 10 (18), 3033-3047.
10. Robert, R. S.; Ottaviani, G.; Huh, W. W.; Palla, S.; Jaffe, N., Psychosocial and functional outcomes in long-term survivors of osteosarcoma: A comparison of limb-salvage surgery and amputation. *Pediatric Blood & Cancer* **2010**, 54 (7), 990-999.
11. Uustal, H., Prosthetic Rehabilitation Issues in the Diabetic and Dysvascular Amputee. *Physical Medicine and Rehabilitation Clinics of North America* **2009**, 20 (4), 689-703.
12. Prince, R.; Price, R.; Ho, S., Forearm bone loss in hemiplegia: A model for the study of immobilization osteoporosis. *Journal of Bone and Mineral Research* **1988**, 3 (3), 305-310.
13. Winter, G. D., Transcutaneous implants: Reactions of the skin-implant interface. *Journal of Biomedical Materials Research* **1974**, 8 (3), 99-113.
14. Cevc, G.; Vierl, U., Nanotechnology and the transdermal route: A state of the art review and critical appraisal. *Journal of Controlled Release* **2010**, 141 (3), 277-299.

15. Gailit, J.; Clark, R. A., Wound repair in the context of extracellular matrix. *Curr Opin Cell Biol* **1994**, *6* (5), 717-25.
16. Lauer, G.; Wiedmann-Al-Ahmad, M.; Otten, J. E.; Hübner, U.; Schmelzeisen, R.; Schilli, W., The titanium surface texture effects adherence and growth of human gingival keratinocytes and human maxillar osteoblast-like cells in vitro. *Biomaterials* **2001**, *22* (20), 2799-2809.
17. Biggs, M. J. P.; Richards, R. G.; Dalby, M. J., Nanotopographical modification: a regulator of cellular function through focal adhesions. *Nanomedicine: Nanotechnology, Biology and Medicine* **2010**, *6* (5), 619-633.
18. Cáceres, D.; Munuera, C.; Ocal, C.; Jiménez, J. A.; Gutiérrez, A.; López, M. F., Nanomechanical properties of surface-modified titanium alloys for biomedical applications. *Acta Biomaterialia* **2008**, *4* (5), 1545-1552.
19. Niinomi, M., Mechanical biocompatibilities of titanium alloys for biomedical applications. *Journal of the Mechanical Behavior of Biomedical Materials* **2008**, *1* (1), 30-42.
20. Healy, K. E.; Ducheyne, P., Hydration and preferential molecular adsorption on titanium in vitro. *Biomaterials* **1992**, *13* (8), 553-561.
21. Smith, C. M.; Roy, T. D.; Bhalkikar, A.; Li, B.; Hickman, J. J.; Church, K. H., Engineering a Titanium and Polycaprolactone Construct for a Biocompatible Interface Between the Body and Artificial Limb. *Tissue Engineering Part A* **2010**, *16* (2), 717-724.
22. Kang, N. V.; Pendegrass, C.; Marks, L.; Blunn, G., Osseocutaneous Integration of an Intraosseous Transcutaneous Amputation Prosthesis Implant Used for Reconstruction of a Transhumeral Amputee: Case Report. *The Journal of Hand Surgery* **2010**, *35* (7), 1130-1134.
23. Tonel, G.; Conrad, C., Interplay between keratinocytes and immune cells--Recent insights into psoriasis pathogenesis. *The International Journal of Biochemistry & Cell Biology* **2009**, *41* (5), 963.
24. Clark, R. A.; McCoy, G. A.; Folkvord, J. M.; McPherson, J. M., TGF-beta 1 stimulates cultured human fibroblasts to proliferate and produce tissue-like fibroplasia: a fibronectin matrix-dependent event. *J Cell Physiol* **1997**, *170* (1), 69-80.
25. Neuss, S.; Apel, C.; Buttler, P.; Denecke, B.; Dhanasingh, A.; Ding, X.; Grafahrend, D.; Groger, A.; Hemmrich, K.; Herr, A.; Jahnen-Dechent, W.; Mastitskaya, S.; Perez-Bouza, A.; Rosewick, S.; Salber, J.; Wöltje, M.; Zenke, M., Assessment of stem cell/biomaterial combinations for stem cell-based tissue engineering. *Biomaterials* **2008**, *29* (3), 302.
26. Ding, L.; Stilwell, J.; Zhang, T.; Elboudwarej, O.; Jiang, H.; Selegue, J. P.; Cooke, P. A.; Gray, J. W.; Chen, F. F., Molecular Characterization of the Cytotoxic Mechanism of Multiwall Carbon Nanotubes and Nano-Onions on Human Skin Fibroblast. *Nano Letters* **2005**, *5* (12), 2448-2464.

27. Velasco-Ortega, E.; Jos, A.; Cameán, A. M.; Pato-Mourelo, J.; Segura-Egea, J. J., In vitro evaluation of cytotoxicity and genotoxicity of a commercial titanium alloy for dental implantology. *Mutation Research/Genetic Toxicology and Environmental Mutagenesis* **2010**, 702 (1), 17-23.
28. Rosdy, M.; Grisoni, B.; Clauss, L.-C., Proliferation of normal human keratinocytes on silicons substrates. *Biomaterials* **1991**, 12 (5), 511-517.
29. Zhang, Y. Z.; Venugopal, J.; Huang, Z. M.; Lim, C. T.; Ramakrishna, S., Characterization of the Surface Biocompatibility of the Electrospun PCL-Collagen Nanofibers Using Fibroblasts. *Biomacromolecules* **2005**, 6 (5), 2583-2589.
30. Scheideler, L.; Geis-Gerstorfer, J.; Kern, D.; Pfeiffer, F.; Rupp, F.; Weber, H.; Wolburg, H., Investigation of cell reactions to microstructured implant surfaces. *Materials Science and Engineering: C* **2003**, 23 (3), 455-459.
31. Werner, S.; Huck, O.; Frisch, B.; Vautier, D.; Elkaim, R.; Voegel, J.-C.; Brunel, G.; Tenenbaum, H., The effect of microstructured surfaces and laminin-derived peptide coatings on soft tissue interactions with titanium dental implants. *Biomaterials* **2009**, 30 (12), 2291-2301.
32. Grafahrend, D.; Heffels, K. H.; Möller, M.; Klee, D.; Groll, J., Electrospun, Biofunctionalized Fibers as Tailored in vitro Substrates for Keratinocyte Cell Culture. *Macromolecular Bioscience* **2010**, 10 (9), 1022-1027.
33. Clark, R. A., Growth factors and wound repair. *J Cell Biochem* **1991**, 46 (1), 1-2.
34. Gailit, J.; Clarke, C.; Newman, D.; Tonnesen, M. G.; Mosesson, M. W.; Clark, R. A., Human fibroblasts bind directly to fibrinogen at RGD sites through integrin alpha(v)beta3. *Exp Cell Res* **1997**, 232 (1), 118-26.
35. Min, B.-M.; You, Y.; Kim, J.-M.; Lee, S. J.; Park, W. H., Formation of nanostructured poly(lactic-co-glycolic acid)/chitin matrix and its cellular response to normal human keratinocytes and fibroblasts. *Carbohydrate Polymers* **2004**, 57 (3), 285-292.
36. Curtis, A. S. G.; Gadegaard, N.; Dalby, M. J.; Riehle, M. O.; Wilkinson, C. D. W.; Aitchison, G., Cells react to nanoscale order and symmetry in their surroundings. *IEEE Trans Nanobioscience* **2004**, 3 (1), 61-5.
37. Martin, C. R.; Kohli, P., The emerging field of nanotube biotechnology. *Nat Rev Drug Discov* **2003**, 2 (1), 29-37.
38. Papat, K. C.; Leoni, L.; Grimes, C. A.; Desai, T. A., Influence of engineered titania nanotubular surfaces on bone cells. *Biomaterials* **2007**, 28 (21), 3188-3197.
39. Smith, B. S.; Yoriya, S.; Grissom, L.; Grimes, C. A.; Papat, K. C., Hemocompatibility of titania nanotube arrays. *Journal of Biomedical Materials Research Part A* **2010**, 95A (2), 350-360.
40. Bechara, S. L.; Judson, A.; Papat, K. C., Template synthesized poly([var epsilon]-caprolactone) nanowire surfaces for neural tissue engineering. *Biomaterials* **2010**, 31 (13), 3492-3501.

41. Leary Swan, E. E.; Popat, K. C.; Desai, T. A., Peptide-immobilized nanoporous alumina membranes for enhanced osteoblast adhesion. *Biomaterials* **2005**, *26* (14), 1969.
42. Ruckh, T.; Porter, J. R.; Allam, N. K.; Feng, X.; Grimes, C. A.; Popat, K. C., Nanostructured tantalum as a template for enhanced osseointegration. *Nanotechnology* **2009**, *20* (4), 45102.
43. Baroli, B.; Ennas, M. G.; Loffredo, F.; Isola, M.; Pinna, R.; Lopez-Quintela, M. A., Penetration of Metallic Nanoparticles in Human Full-Thickness Skin. *J Invest Dermatol* **2007**, *127* (7), 1701-1712.
44. Zhang, L. W.; Yu, W. W.; Colvin, V. L.; Monteiro-Riviere, N. A., Biological interactions of quantum dot nanoparticles in skin and in human epidermal keratinocytes. *Toxicology and Applied Pharmacology* **2008**, *228* (2), 200-211.
45. Rho, K. S.; Jeong, L.; Lee, G.; Seo, B.-M.; Park, Y. J.; Hong, S.-D.; Roh, S.; Cho, J. J.; Park, W. H.; Min, B.-M., Electrospinning of collagen nanofibers: Effects on the behavior of normal human keratinocytes and early-stage wound healing. *Biomaterials* **2006**, *27* (8), 1452-1461.
46. Ruckh, T. T.; Kumar, K.; Kipper, M. J.; Popat, K. C., Osteogenic differentiation of bone marrow stromal cells on poly(epsilon-caprolactone) nanofiber scaffolds. *Acta Biomater* **2010**, *6* (8), 2949-59.
47. Porter, J. R.; Ruckh, T. T.; Popat, K. C., Bone tissue engineering: a review in bone biomimetics and drug delivery strategies. *Biotechnol Prog* **2009**, *25* (6), 1539-60.
48. Loesberg, W. A.; te Riet, J.; van Delft, F. C. M. J. M.; Schön, P.; Figdor, C. G.; Speller, S.; van Loon, J. J. W. A.; Walboomers, X. F.; Jansen, J. A., The threshold at which substrate nanogroove dimensions may influence fibroblast alignment and adhesion. *Biomaterials* **2007**, *28* (27), 3944-3951.
49. Puckett, S. D.; Lee, P. P.; Ciombor, D. M.; Aaron, R. K.; Webster, T. J., Nanotextured titanium surfaces for enhancing skin growth on transcutaneous osseointegrated devices. *Acta Biomaterialia* **2010**, *6* (6), 2352-2362.
50. Popat, K. C.; Eltgroth, M.; LaTempa, T. J.; Grimes, C. A.; Desai, T. A., Decreased Staphylococcus epidermidis adhesion and increased osteoblast functionality on antibiotic-loaded titania nanotubes. *Biomaterials* **2007**, *28* (32), 4880-4888.
51. Popat, K.; Eltgroth, M.; LaTempa, T.; Grimes, C.; Desai, T., Titania Nanotubes: A Novel Platform for Drug-Eluting Coatings for Medical Implants? *Small* **2007**, *3* (11), 1878-1881.
52. Zhao, L.; Mei, S.; Wang, W.; Chu, P. K.; Wu, Z.; Zhang, Y., The role of sterilization in the cytocompatibility of titania nanotubes. *Biomaterials* **2010**, *31* (8), 2055-63.

53. Ruan, C.; Paulose, M.; Varghese, O. K.; Mor, G. K.; Grimes, C. A., Fabrication of Highly Ordered TiO<sub>2</sub> Nanotube Arrays Using an Organic Electrolyte. *The Journal of Physical Chemistry B* **2005**, *109* (33), 15754-15759.
54. Porter, J. R.; Henson, A.; Ryan, S.; Popat, K. C., Biocompatibility and mesenchymal stem cell response to poly(epsilon-caprolactone) nanowire surfaces for orthopedic tissue engineering. *Tissue Eng Part A* **2009**, *15* (9), 2547-59.
55. Li, S.; Duance, V. C.; Blain, E. J., F-actin cytoskeletal organization in intervertebral disc health and disease. *Biochem Soc Trans* **2007**, *35* (Pt 4), 683-5.
56. Marionnet, C.; Pierrard, C.; Vioux-Chagnoleau, C.; Sok, J.; Asselineau, D.; Bernerd, F., Interactions between Fibroblasts and Keratinocytes in Morphogenesis of Dermal Epidermal Junction in a Model of Reconstructed Skin. *J Invest Dermatol* **2006**, *126* (5), 971-979.

## CHAPTER 4

### ALTERED HEMOCOMPATIBILITY ON TITANIA NANOTUBE ARRAYS

#### 4.1 Introduction

As the number of patients afflicted with traumatic and non-traumatic conditions continues to rise, there is a growing need for the use of efficacious biomaterials in implantable medical devices<sup>1-3</sup>. Biomaterial rejection remains a serious problem, eliciting a need for a more in-depth look at the mechanisms behind material-tissue interactions. Materials with biomolecular or topographical modifications that mimic natural biological tissue hierarchy may provide solutions to the problem of biomaterial rejection<sup>4-9</sup>. Previous research has evaluated the biocompatibility of various biomaterials through an in-depth look into cellular adhesion and proliferation<sup>10, 11</sup>, cell phenotypic behavior<sup>12, 13</sup>, material cytotoxic effects<sup>14, 15</sup> and protein folding and interactions on material surfaces<sup>16, 17</sup>. Several studies have shown increased cellular functionality on peptide-modified<sup>18-21</sup> and growth-factor functionalized surfaces<sup>22, 23</sup>. Moreover, microscale surface topographies have shown increased protein adsorption and cellular adhesion<sup>24-26</sup>. Recently, there has been an increased interest in nanoscale surface topographies such as nanotubes<sup>27, 28</sup>, nanowires<sup>29-31</sup>, nanopores<sup>32, 33</sup>, nanoparticles<sup>34, 35</sup>, nanofibers<sup>36-38</sup>, etc. as biomimetic interfaces for implantable devices. Several studies have reported favorable cellular response on such nanoscale topographies. However, very few studies report the hemocompatibility of nano-biomaterials.

Common biomedical implant materials include metals or metal alloys, polymers, ceramics and composites. Of these, titanium and titanium-based alloys are the most widely used biomaterials due to their mechanical strength, biocompatibility, non-toxicity,

corrosion resistance, and ease of processability. They have been used in clinical applications for a variety of implantable devices, including dental implants<sup>39-41</sup>, prosthetic devices<sup>42-44</sup>, materials for craniofacial reconstruction<sup>45, 46</sup> and stent grafts<sup>47, 48</sup>. Titanium forms a passive oxide layer on its surface, titania, which protects it against corrosion and provides a biomechanical interface for appropriate tissue integration<sup>49, 50</sup>. Even though titanium and titanium-based alloys, including other implantable biomaterials, are nontoxic, foreign body reactions are often triggered in the form of inflammation, thrombosis, fibrosis and infection. Several studies report on the hemocompatibility of biomaterials<sup>51, 52</sup>, however little is known about the hemocompatibility of nano-biomaterials<sup>53, 54</sup>. In order to properly evaluate interactions prevalent at the blood-material interface, it is important to take into account the immunological events that take place during the foreign body reaction. Recent studies have identified a correlation relating the nanoscale surface topographies with enhanced cellular adhesion and increased protein adsorption. However, the cells are not the first responders to blood contacting biomaterial implants. Following implantation of a biomaterial, proteins from blood and the surrounding tissue are immediately adsorbed onto the surface, initiating an immune response. Host proteins adhere on the surface within seconds to minutes after the biomaterial comes in contact with blood or tissue<sup>55</sup>. A conformational change occurs within the adsorbed protein allowing for subsequent biological interactions with the material surface. A continued inflammatory response is activated through this protein-material adhesion followed by platelet adhesion and activation resulting in thrombosis. Thus, hemocompatibility is a key consideration for the

long-term success of blood contacting biomaterials, creating a critical need to understand the physiological response elicited from blood/nano-biomaterial interactions.

In this study, we have investigated the hemocompatibility of highly uniform titania nanotube arrays fabricated using an anodization process with a diameter of 70-80 nm and length of 1  $\mu\text{m}$ <sup>27, 56-58</sup>. Thus, one of the earliest stages in the physiological immune response has been evaluated by considering the adsorption of key blood serum proteins, *in vitro* adhesion and activation of platelets, and clotting kinetics of whole blood on titania nanotube arrays. Biomedical grade titanium were used as controls. Further, we have evaluated the mechanical properties of titania nanotube arrays for identifying their potential applications in implantable biomedical devices. Driven by a need for reduced material rejection and controlled hemocompatibility, this work specifically looks at components that initiate the immune response; thus, providing a basis for identifying potential biomedical and clinical uses for titania nanotube arrays.

## **4.2 Experimental Methods**

### **4.2.1 *Fabrication and Characterization of Titania Nanotube Arrays***

Titania nanotube arrays were fabricated using a simple anodization process, described in detail in chapter 2<sup>27, 54, 59, 60</sup>. Biomedical grade titanium (as-received, non-polished) surfaces were used as controls. The nanotube architecture was examined for uniformity and repeatability using SEM imaging.

### **4.2.2 *Protein Adsorption on Titania Nanotube Arrays***

In order to understand how blood serum proteins interact with materials; fibrinogen (FIB), albumin (ALB) and immunoglobulin-G (IgG) (Sigma) adsorption was

investigated on titania nanotube arrays and biomedical grade titanium. All of the substrates were sterilized by incubating in 70% ethanol for 15 mins followed by *uv* exposure for 15 mins, and rinsed 3 times with phosphate buffer saline (PBS). The substrates were then incubated in a 24-well plate with 100 µg/ml solution of FIB, ALB or IgG in PBS on a horizontal shaker plate (100rpm) at 37°C and 5% CO<sub>2</sub>. After 2 hrs of incubation, the protein solution was aspirated followed by 3 rinses with PBS to remove any non-adherent proteins. The protein adsorption was measured using a commercially available micro-BCA assay (Pierce Biotechnology) and X-ray photoelectron spectroscopy (XPS, ESCA Systems X-ray Photoelectron Spectrometer 5800).

In order to measure the protein adsorption using micro-BCA assay, all of the titania nanotube arrays and biomedical grade titanium were transferred to a fresh 24-well plate and incubated with 1% sodium dodecyl sulfate (SDS, Sigma) solution in PBS on a horizontal shaker plate (100rpm) for 1 hr. Following incubation, the excess SDS solution with solubilized proteins was collected from each well. The SDS incubation was repeated 2 more times and the resulting SDS solution with solubilized proteins was pooled. The concentration of the total adsorbed protein in the pooled SDS solution was then measured colorimetrically using a micro-BCA assay with a plate reader (BMG Labtech)<sup>61</sup>. XPS was used to determine the surface composition of adsorbed proteins on titania nanotube arrays and biomedical grade titanium. Survey spectra were collected from 0 to 1100eV with a pass energy of 187.85 eV, and high-resolution spectra were collected for C1s peak with a pass energy of 10eV. Data for percent elemental composition, elemental ratios and peak fit analysis were calculated using Multipack and XPSPeak 4.1 (Freeware) software.

### 4.2.3 Platelet Adhesion and Activation

Whole blood from healthy individuals, acquired through venopuncture, was drawn into standard vacuum tubes coated with the anti-coagulant, ethylenediaminetetraacetic acid (EDTA) (Fisher Scientific). The blood vials were centrifuged at 150 g for 15 minutes. The plasma from all the tubes was pooled into fresh tubes, and centrifuged for a second time at 900 g for 5 minutes. The supernatant was aspirated off and the remaining pellet was resuspended in HEPES-Tyrode buffer (HTB, Sigma). The platelet solution was diluted with HTB to yield platelet rich plasma (PRP) with a final concentration of  $8 \times 10^8$  platelets/ml (See Figure 4.1). Titania nanotube arrays and biomedical grade titanium were placed into 24-well plates.

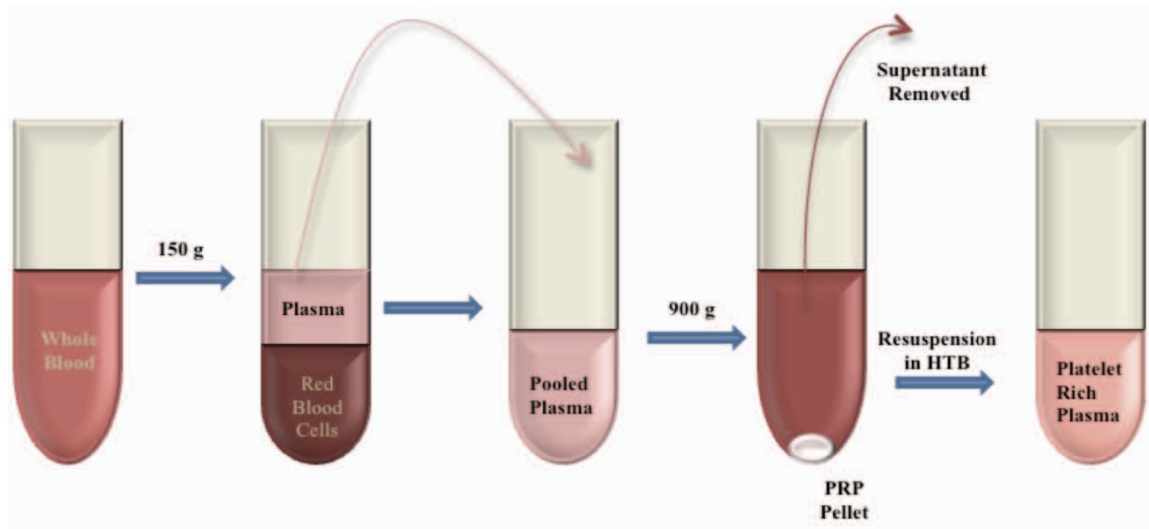


Figure 4.1 Schematic of isolation of platelets from whole human blood, obtaining a final concentration of  $8 \times 10^8$  platelets/ml

All of the substrates were sterilized by incubating in 70% ethanol for 15 mins followed by *uv* exposure for 15 mins, and rinsed 3 times with HTB. The substrates were then

incubated with 500  $\mu$ l of PRP on a horizontal shaker plate (100rpm) at 37°C and 5% CO<sub>2</sub>. Platelet adhesion and activation were investigated after 30 mins of incubation.

Platelet adhesion was characterized by staining the cells with calcein-AM (Invitrogen) live stain. Prior to staining, the un-adhered platelets were removed by aspirating the PRP from the substrates followed by rinsing with PBS. The substrates were incubated with 2  $\mu$ M calcein-AM solution in PBS for 30 mins on a horizontal shaker plate (100 rpm) at 37°C and 5% CO<sub>2</sub>. The substrates were then rinsed with PBS and imaged with a fluorescence microscope (Zeiss) using FITC MF101 Green filters.

Platelet viability was characterized using a commercially available MTT assay kit (Sigma). Prior to measuring the MTT activity, the un-adhered platelets were removed by aspirating the PRP from the substrates followed by rinsing with PBS. The substrates were incubated with 10% MTT solution in HTB for 4 hrs on a horizontal shaker plate (100 rpm) at 37°C and 5% CO<sub>2</sub>. The resulting formazan crystals were dissolved by adding MTT solvent in the amounts equal to the HTB. The absorbance of the solution was measured using a plate reader (BMG Labtech).

Platelet morphology was imaged using SEM. To visualize the platelet interaction with nanotube architecture, they were dehydrated and fixed on the substrates. The platelets were fixed by incubating the substrates in a solution of primary fixative (3% glutaraldehyde (Sigma), 0.1 M sodium cacodylate (Polysciences), and 0.1 M sucrose (Sigma)) for 45 min. The substrates were then incubated in a solution of secondary fixative (primary fixative without glutaraldehyde) for 2 hrs. This was followed by a dehydration step where the substrates were incubated in consecutive solutions of ethanol (35%, 50%, 70% and 100%) for 10 min. Further dehydration of the platelets was

accomplished by incubating the substrates in hexamethyldisilazane (HMDS, Sigma) for 10 min. Prior to imaging, the substrates were coated with a 10 nm layer of gold and imaged at 15kV. The SEM images were then used to determine the percentage of the adhered platelets that were unactivated, or had a short-dendritic or long-dendritic morphology<sup>62</sup>. The following guide was used to determine the morphology of the adhered platelets:

- Unactivated: Platelets that are normal and with compact central body
- Short-dendritic: Platelets with smaller dendrites and partially activated
- Long-dendritic: Platelets with many long dendrites and completely activated

#### **4.2.4 *Whole Blood Clotting on Titania Nanotube Arrays***

In order to evaluate the thrombogenic properties of titania nanotube arrays, their interaction with whole blood was investigated. Whole human blood from healthy individuals was drawn, and 5  $\mu$ l of the blood was immediately dropped on titania nanotube arrays and biomedical grade titanium in a 24-well plate. The droplet of whole human blood was left undisturbed on the substrates for up to 60 mins. The free hemoglobin concentration was measured at 10 min intervals. In order to measure the free hemoglobin concentration, the substrates were transferred into a different 24-well plate with 500  $\mu$ l of deionized (DI) water. The substrates were gently agitated for 30 secs and left in the DI water for 5 mins to release free hemoglobin from red blood cells that were not trapped in the thrombus. The absorbance of the DI water with free hemoglobin was measured at a wavelength of 540 nm using a plate reader. The value of absorbance is directly proportional to the concentration of free hemoglobin in DI water. Further, the

substrates were air dried and coated with a 10 nm layer of gold prior to imaging with SEM at 15kV.

#### **4.2.5 Statistical Analysis**

Each experiment was reconfirmed on three different substrates with at least three different platelet populations ( $n_{\min} = 9$ ). All the quantitative results were analyzed using an analysis of variance (ANOVA). Statistical significance was considered at  $p < 0.05$ .

### **4.3 Results and Discussion**

Hemocompatibility remains a serious concern, eliciting a need for a more thorough study of the mechanisms behind blood-material interactions. Several recent studies have reported on the hemocompatibility of biomaterials<sup>51, 52</sup>, however little is known about the hemocompatibility of nano-biomaterials<sup>53, 54</sup>. In this study, we have investigated the hemocompatibility of titania nanotube arrays for their potential use as interfaces for implantable devices. These titania nanotube arrays can be fabricated using a simple anodization technique<sup>58, 63</sup>, and provide a favorable template for increased cellular functionality and localized drug delivery at a hierarchy similar to that of natural tissue<sup>27, 64</sup>.

In this work, we have fabricated vertically oriented, immobilized, high-aspect ratio titania nanotube arrays using a simple anodization technique. The nanoarchitecture of titania nanotube arrays was examined for uniformity and repeatability using SEM (**See Figure 4.2**). SEM images show uniform nanotube arrays with a diameter of 70-90 nm and length of 1  $\mu\text{m}$ . A localized dissolution model explains the formation of titania nanotube arrays by anodization of titanium<sup>63, 65</sup>. For this study, titania nanotube arrays

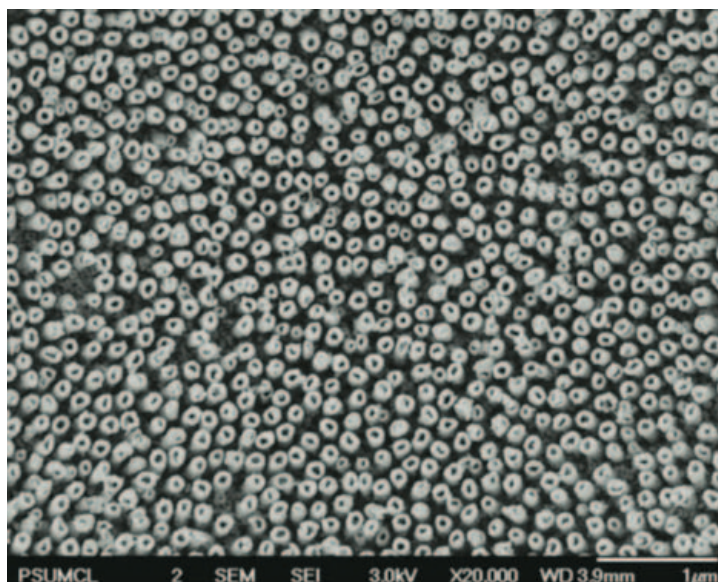


Figure 4.2 Representative SEM image showing the nanoarchitecture of titania nanotube arrays fabricated using an anodization technique

with a diameter of 70-90 nm and length of 1  $\mu\text{m}$  were selected, since previous studies with the same size titania nanotubes arrays have shown enhanced cellular functionality and sustained drug release.

Following implantation of a biomaterial, proteins from blood and the surrounding tissue are immediately adsorbed onto the surface. Host proteins adhere on the surface within seconds to minutes after the biomaterial comes in contact with blood or tissue<sup>55</sup>. Thus, it is important to investigate the adsorption of key blood serum proteins (ALB, FIB and IgG) on titania nanotube arrays. The proteins were adsorbed at a concentration of 100  $\mu\text{g}/\text{ml}$  for 2 hrs and the amount of the proteins adhered were determined using a micro-BCA assay and XPS.

In order to quantify the adsorbed proteins on the surfaces, a micro-BCA assay was used. SDS, an anionic detergent, was used to solubilize the adsorbed protein. The highly

specific chromogenic reagent bicinchoninic acid (BCA) is able to form a complex with the  $\text{Cu}^{1+}$  molecule through a protein mediated reduction reaction in alkaline environment. The production of  $\text{Cu}^{1+}$  is directly proportional to the concentration of the protein and the incubation time in the BCA. Thus, by measuring the absorbance colorimetrically, the protein concentration can be calculated using a pre-determined protein standard curve. Our results suggest that there is an increase in protein adsorption on titania nanotube arrays as compared to biomedical grade titanium (See Figure 4.3).

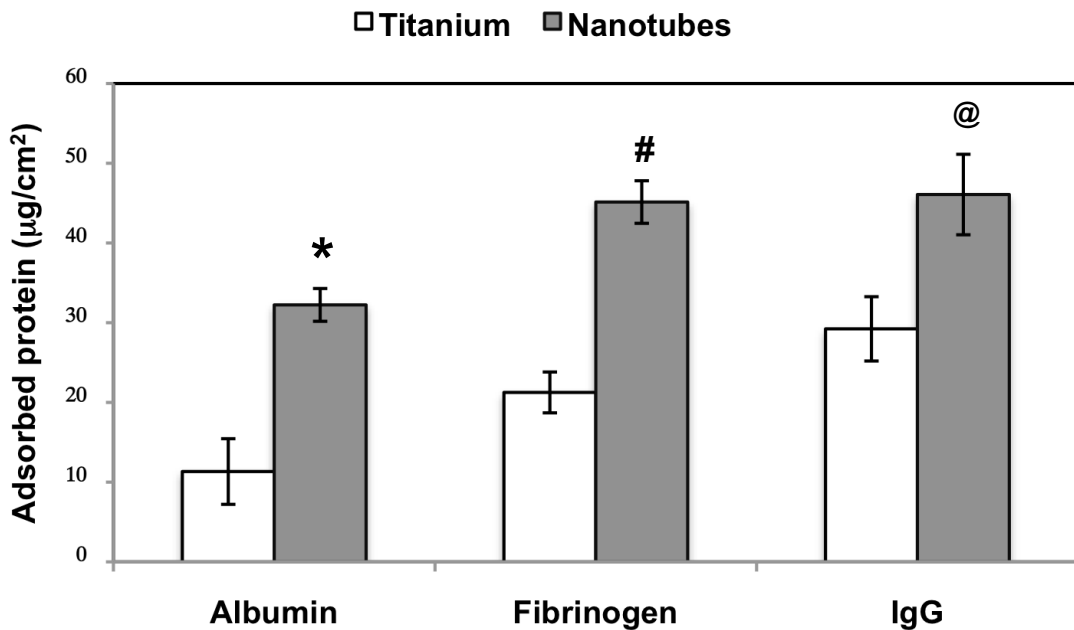


Figure 4.3 Amount of blood serum proteins adsorbed on titania nanotube arrays and biomedical grade titanium was determined using micro-BCA assay. Significantly higher amounts of proteins were adsorbed on titania nanotube arrays compared to biomedical grade titanium (\*, #, @ →  $p < 0.05$ ).

The amounts of proteins adsorbed on titania nanotube arrays are statistically different than that on biomedical grade titanium ( $p < 0.05$ ). Further, the ALB adsorption

was the lowest, followed by the adsorption of FIB and IgG, on both titania nanotube arrays and biomedical grade titanium. Protein adsorption on titania nanotube arrays and biomedical grade titanium was also characterized using XPS. The surface elemental composition was determined using survey scans. Higher amounts of nitrogen were present on titania nanotube arrays as compared to biomedical grade titanium. Since the nitrogen peak is the characteristic for the proteins adsorbed on the surface, our results suggest that the titania nanotube arrays adsorbed higher amounts of protein as compared to biomedical grade titanium (**See Table 4.1**).

Table 4.1 N/Ti ratio computed from XPS survey scans for blood serum proteins adsorbed on titania nanotube arrays and biomedical grade titanium.

	Protein adsorption on titanium				Protein adsorption on nanotube arrays			
	Ti	ALB	FIB	IgG	NT	ALB	FIB	IgG
N/Ti	0	0.39	1.12	1.58	0	1.76	2.15	2.42

A more precise way to characterize proteins adsorbed on the surface is to determine the presence of C-N and N-C=O peaks in the overall C1s peak. The C-N and N-C=O peaks are at a shift of 0.8eV and 1.8eV respectively from the C-C peak. Hence, high-resolution C1s scans were taken and a peak fit analysis was used to determine contribution of C-N and N-C=O peaks in the overall C1s peak. Our results show a significant increase in the intensity of C-N and N-C=O peaks for proteins adsorbed on titania nanotube arrays as compared to biomedical grade titanium (**See Figure 4.4**). The increase in protein adsorption is likely due to the large surface area of nanotube architecture that provides

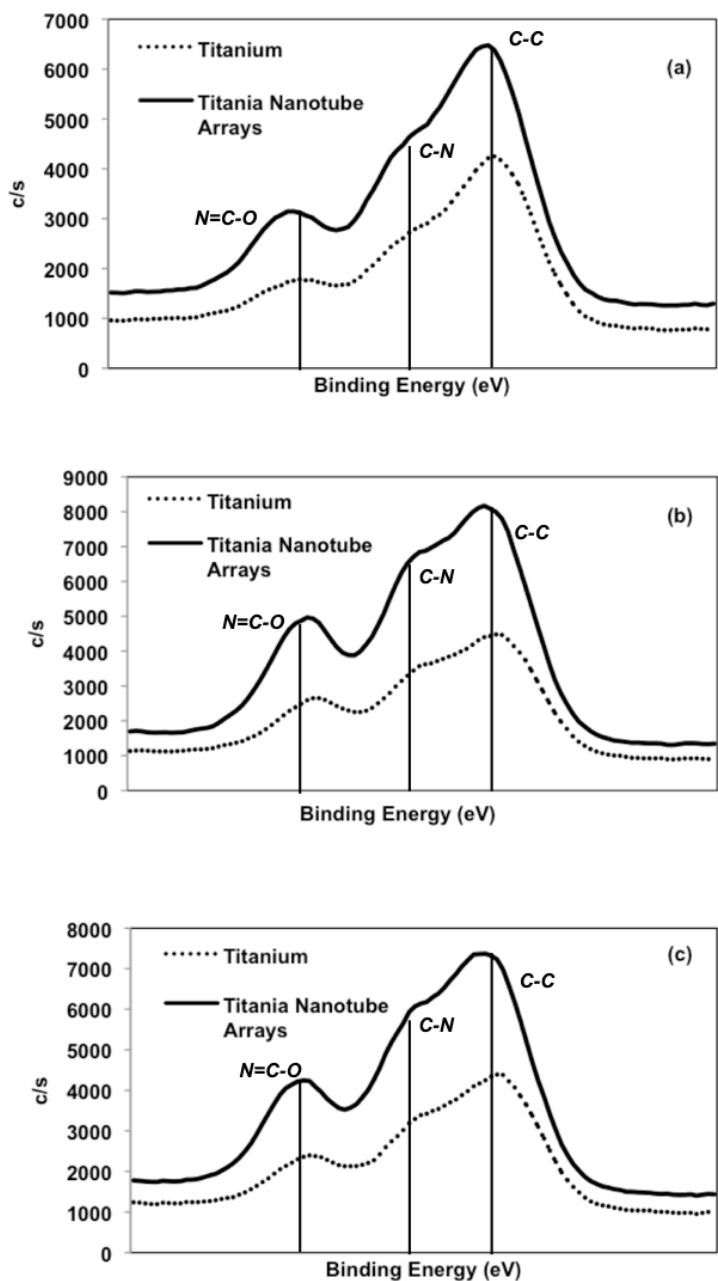


Figure 4.4 High resolution C1s scans for blood serum proteins adsorbed on titania nanotube arrays and biomedical grade titanium showing C-N and N=C-O characteristic peaks (a) ALB, (b) FIB and (c) IgG.

multiple functional sites for the proteins to adsorb. However, the protein adsorption may be optimized for a specific application by precisely tuning the pore size, wall-thickness, and nanotube length by altering the anodization parameters.

Platelet adhesion and activation is a strong indication of the thrombogenicity of biomaterials. In this study, platelets were isolated from whole human blood and their adhesion and activation was investigated on titania nanotube arrays and biomedical grade titanium. Platelet adhesion was evaluated after 30 mins of contact by staining the adhered platelets using calcein-AM stain. Our results show significantly higher platelet adhesion on titania nanotube arrays compared to biomedical grade titanium (**See Figure 4.5**). Low-magnification ( $4\times$  and  $10\times$ ) images indicate increased platelet adhesion on titania nanotube arrays (**See Figure 4.5(d) and (e)**) compared to biomedical grade titanium (**See Figure 4.5(a) and (b)**). Further, high-magnification images ( $20\times$ ) indicate platelet aggregation on titania nanotube arrays (**See Figure 4.5(f)**), compared to minimal aggregation on biomedical grade titanium (**See Figure 4.5(c)**).

Platelet viability was measured using an MTT assay (**See Figure 4.6**). The MTT assay measures mitochondrial activity of live cells via dehydrogenase activity. Our results indicate that the adhered platelets on titania nanotube arrays displayed significantly higher viability than that on smooth titanium for up to 30 mins of contact time ( $p < 0.05$ ). These results confirm the findings from the fluorescence microscopy images that there is higher platelet adhesion on titania nanotube arrays compared to biomedical grade titanium.

Platelet morphology after 30 mins of contact time was investigated using SEM imaging. Low-magnification SEM images show significantly higher platelet adhesion

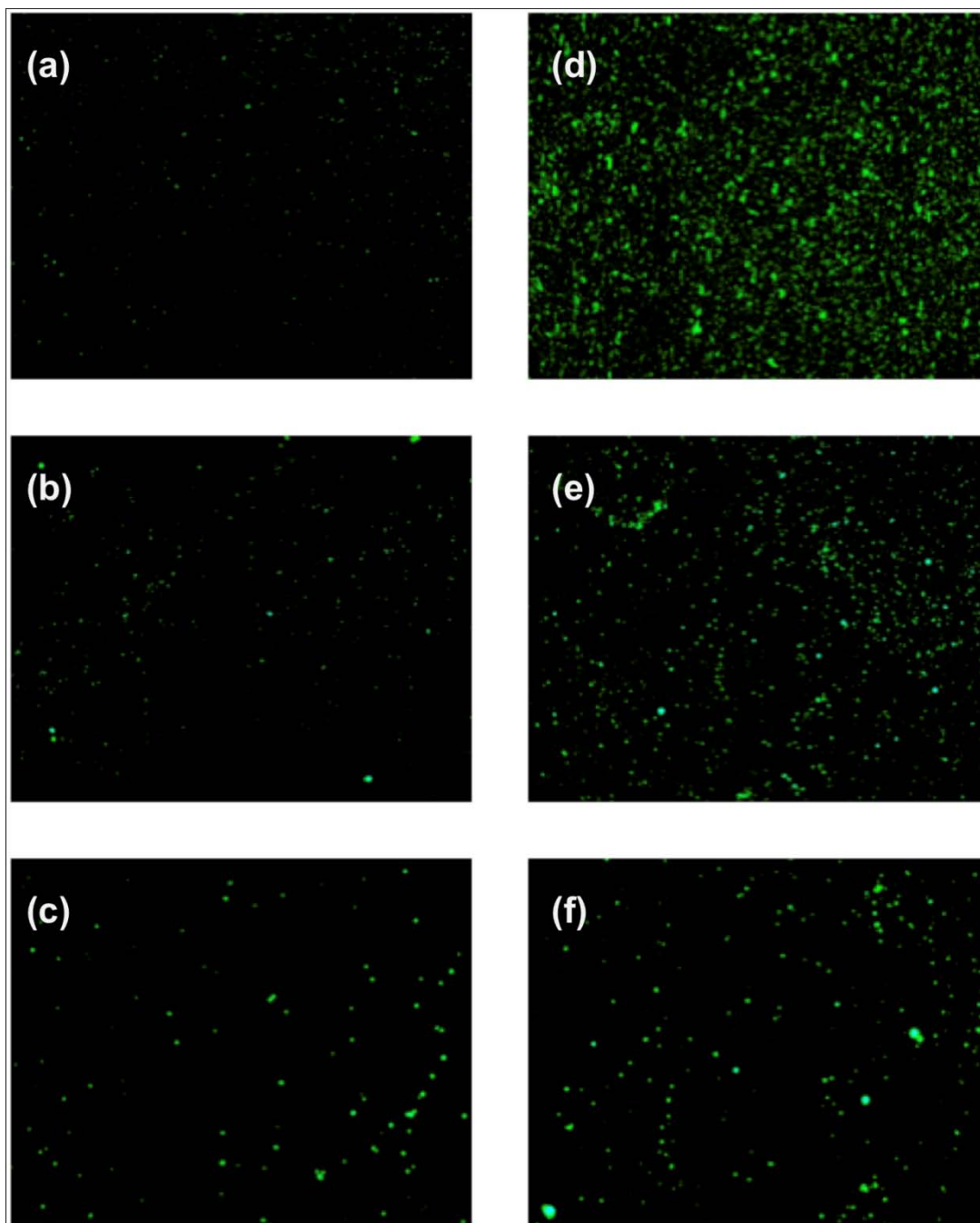


Figure 4.5 Representative fluorescence microscopy images of adhered platelets stained with calcein-AM on biomedical grade titanium [(a) 4 $\times$ , (b) 10 $\times$  and (c) 20 $\times$ ] and titania nanotube arrays [(d) 4 $\times$ , (e) 10 $\times$  and (f) 20 $\times$ ].

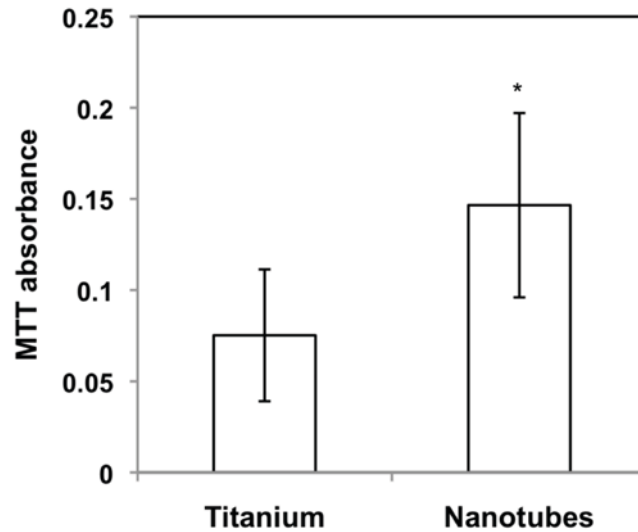


Figure 4.6 Cell viability measured using MTT assay for adhered platelets on titania nanotube arrays and biomedical grade titanium. Platelets viability is significantly higher on titania nanotube arrays compared to biomedical grade titanium (\*→  $p < 0.05$ ).

and activation on titania nanotube arrays (See **Figure 4.7(a)**) as compared to biomedical grade titanium (See **Figure 4.7(d)**). Titania nanotube arrays have uniform nanoscale topography, thus resulting in uniform platelet adhesion consistent across the surface (See **Figure 4.7(d)**). Whereas, the biomedical grade titanium have localized regions that are inherently rough, thus resulting in localized platelet adhesion across the surface (See **Figure 4.7(a)**). Further, high-magnification SEM images show significant changes and drastic differences in platelet morphology on titania nanotube arrays (See **Figure 4.7(e)**) as compared to biomedical grade titanium (See **Figure 4.7(b)**). The platelets are exhibiting dendritic behavior on titania nanotubes indicating significant activation. The dramatic morphological changes are promoting platelet-platelet contact resulting in aggregation (See **Figure 4.7(f)**). Such behavior is absent on biomedical grade titanium

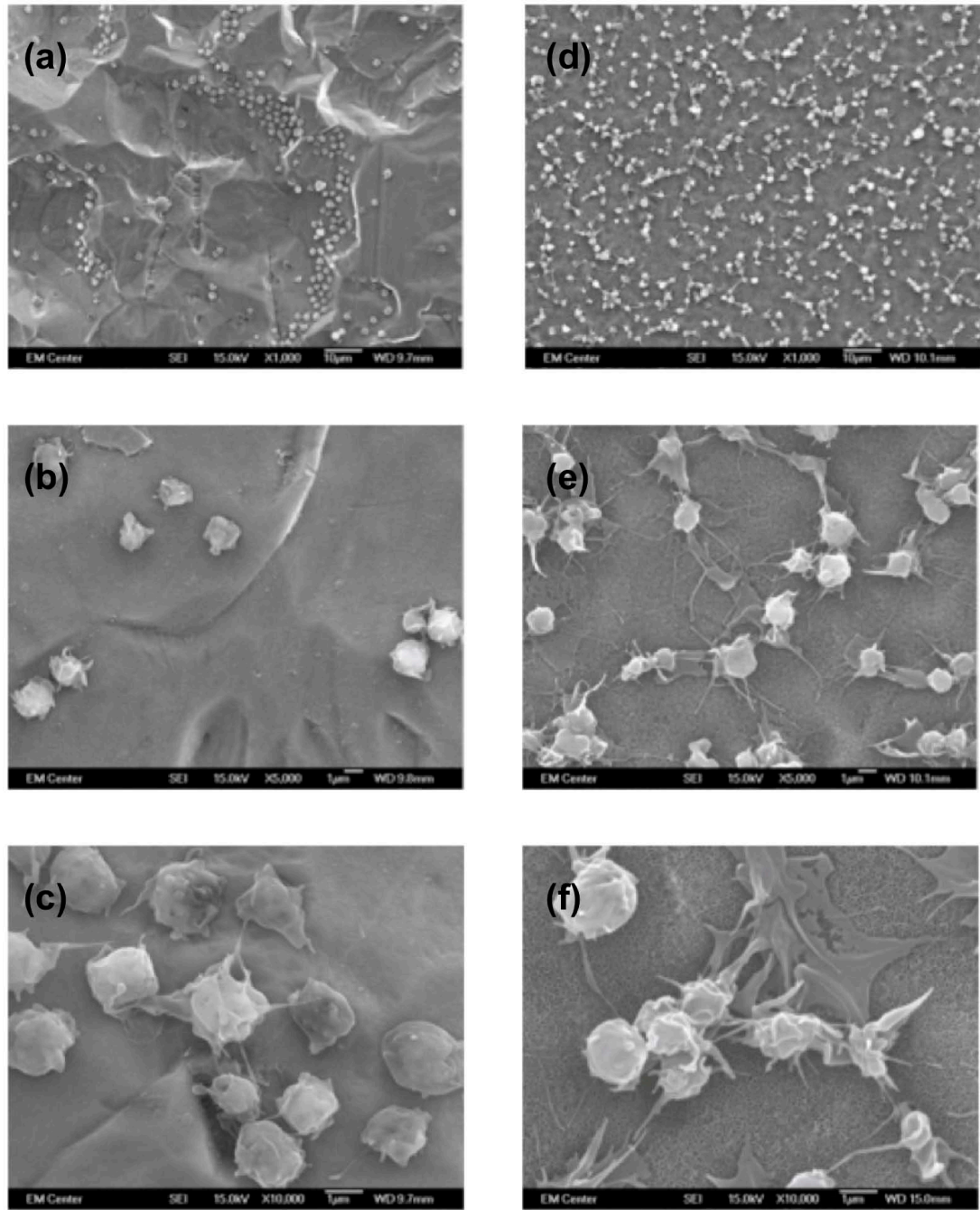


Figure 4.7 Representative SEM images of adhered and activated platelets on biomedical grade titanium [(a), (b) and (c)] and titania nanotube arrays [(d), (e) and (f)].

(See **Figure 4.7(c)**). Further, the SEM images were used to determine the percentage of the adhered platelets that were unactivated, or had a short-dendritic or long-dendritic morphology (See **Figure 4.8**). Our results indicate that all the platelets on titania nanotube arrays were activated. The majority of the platelets had a long-dendritic morphology (~ 75%), followed by fewer platelets with a short-dendritic morphology (~ 25%). In contrast, the majority of the platelets on biomedical grade titanium had a short dendritic morphology (~ 50%) suggesting incomplete activation, followed by platelets with a long-dendritic morphology (~ 40%) suggesting complete activation, and fewer unactivated platelets (~ 10%). These results suggest that there is significant platelet activation on titania nanotube arrays compared to smooth titanium surface. It is important to note that even though biomedical grade titanium does not support significant platelet adhesion, they could potentially activate platelets as the clotting cascade progresses.

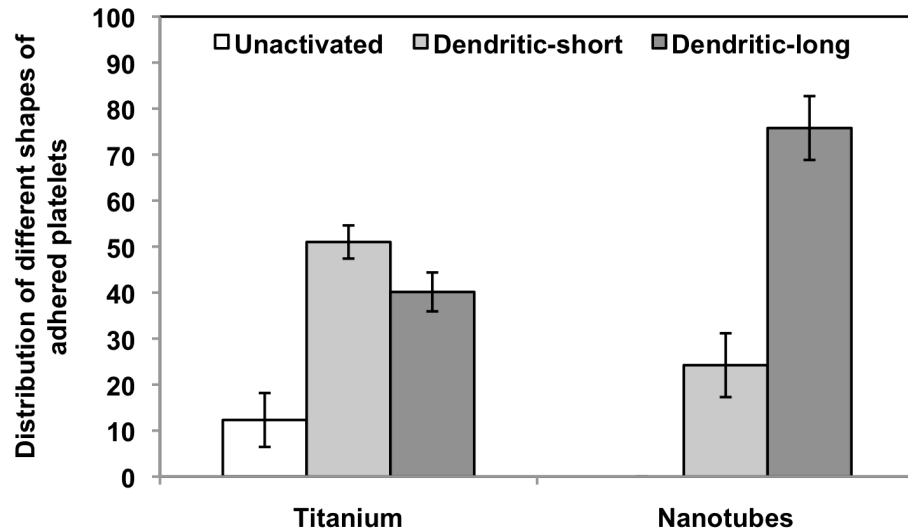


Figure 4.8 Distribution of different shapes of adhered platelets on biomedical grade titanium and titania nanotube arrays.

The presence of blood clots on implanted devices may lead to the formation of embolisms, slow wound healing, or adverse immune reactions. Thus, understanding the whole blood clotting kinetics of blood-contacting biomaterials will likely promote the long-term success of implantable biomedical devices. Our results indicated that the blood clotted on both titania nanotube arrays and biomedical grade titanium within 30 mins, however, the rate of clotting was higher for titania nanotube arrays (See **Figure 4.9**).

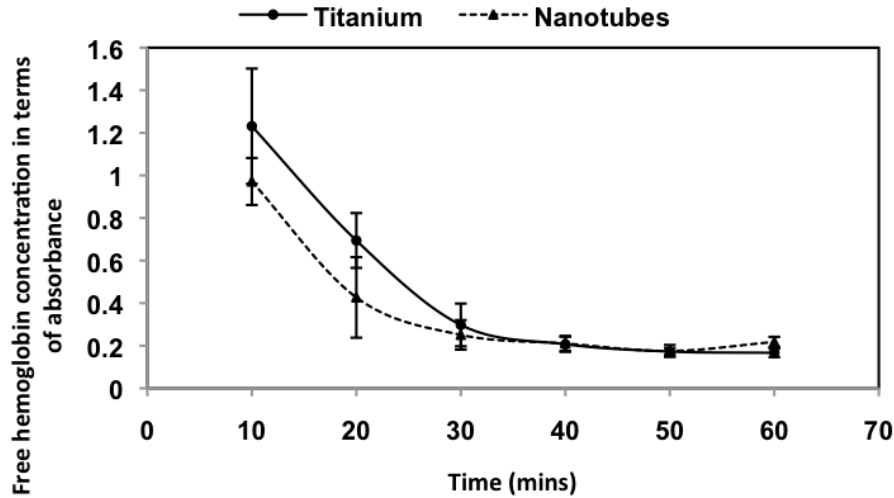


Figure 4.9 Free hemoglobin concentrations in terms of absorbance on titania nanotube arrays and biomedical grade titanium for up to 60 mins of clotting time.

Slightly decreased amounts of free hemoglobin were present on titania nanotube arrays as compared to biomedical grade titanium prior to complete blood clotting. However, no significant differences were observed for the free hemoglobin concentration on titania nanotube arrays after 30 mins of clotting. Further, the density of the fibrin network after

60 mins of clotting time on titania nanotube arrays and biomedical grade titanium was examined using SEM imaging. Visual inspection shows the presence of a fibrin matrix density on both titania nanotube arrays and biomedical grade titanium (See Figure 4.10), identifying the initial stages of clot formation. The clotting cascade in the blood is initiated by thrombin. It is an enzyme that transforms fibrinogen into fibrin monomers, which under normal conditions will form polymeric fibrin fibers to form a clot network. The clot is characterized by the strength of the fibrin mesh that entraps different components of the blood. Our results indicate that the titania nanotube arrays demonstrated a slightly more rapid formation of fibrin network by transforming fibrinogen into fibrin, thus reducing the clotting time while forming a dense fibrin network. The demonstrated decrease in clotting time is not completely understood and warrants further investigation.

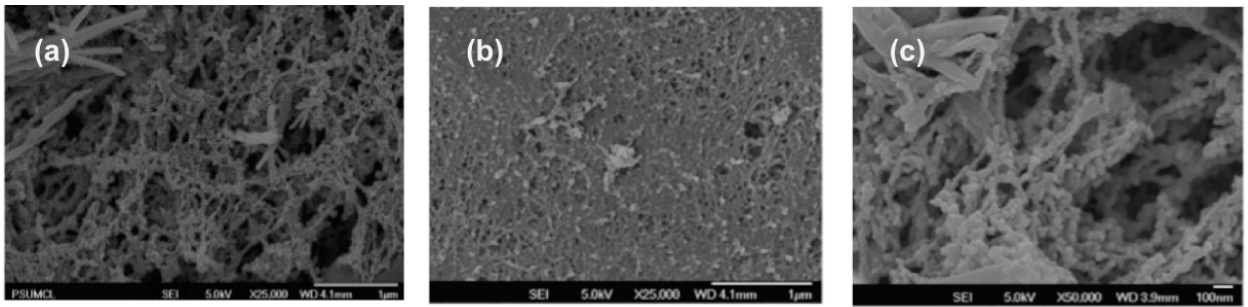


Figure 4.10 Representative SEM images of whole blood clotted on (a) biomedical grade titanium and (b)-(c) titania nanotube arrays.

#### 4.4 Conclusion

Biomaterial rejection remains a serious problem, eliciting a need for a more in-depth look at the mechanisms behind material-tissue interactions. Recently, there has

been an increased interest in exploring nanoscale surface topographies as biomimetic interfaces for implantable devices. Several studies have reported favorable cellular response on such nanoscale topographies. However, very few studies report the hemocompatibility of nano-biomaterials. In this work, we have evaluated the hemocompatibility of titania nanotube arrays fabricated by anodization technique. Our results indicate increased blood serum protein adsorption, platelet adhesion and activation, and whole blood clotting kinetics on titania nanotube arrays. However, the hemocompatibility can be altered by changing the size parameters of titania nanotube arrays. There is a precise correlation between the anodization voltage and nanotube pore size, thus by varying the voltage and anodization time, nanotubes with different diameters and lengths can be fabricated, thus resulting in an altered hemocompatible response. Further studies are now directed towards understanding and evaluating the effects of different size nanotubes on hemocompatibility and evaluating specific components that initiate an immune response.

#### 4.6 References

1. Bhat, S. V., *Biomaterials*. Second ed.; Alpha Science International Ltd.: 2005.
2. Ratner, B. D.; Hench, L., Perspectives on biomaterials. *Current Opinion in Solid State and Materials Science* **1999**, *4* (4), 379.
3. Langer, R., Biomaterials and biomedical engineering. *Chemical Engineering Science* **1995**, *50* (24), 4109.
4. Jones, F. H., Teeth and bones: applications of surface science to dental materials and related biomaterials. *Surface Science Reports* **2001**, *42* (3-5), 75-205.
5. Healy, K. E.; Thomas, C. H.; Reznia, A.; Kim, J. E.; McKeown, P. J.; Lom, B.; Hockberger, P. E., Kinetics of bone cell organization and mineralization on materials with patterned surface chemistry. *Biomaterials* **1996**, *17* (2), 195-208.
6. Stevens, M. M., Biomaterials for bone tissue engineering. *Materials Today* **2008**, *11* (5), 18.
7. Bonzani, I. C.; George, J. H.; Stevens, M. M., Novel materials for bone and cartilage regeneration. *Current Opinion in Chemical Biology* **2006**, *10* (6), 568.
8. Charest, J. L.; Garcia, A. J.; King, W. P., Myoblast alignment and differentiation on cell culture substrates with microscale topography and model chemistries. *Biomaterials* **2007**, *28* (13), 2202-10.
9. Mata, A.; Kim, E. J.; Boehm, C. A.; Fleischman, A. J.; Muschler, G. F.; Roy, S., A three-dimensional scaffold with precise micro-architecture and surface micro-textures. *Biomaterials* **2009**, *30* (27), 4610-7.
10. Hersel, U.; Dahmen, C.; Kessler, H., RGD modified polymers: biomaterials for stimulated cell adhesion and beyond. *Biomaterials* **2003**, *24* (24), 4385-4415.
11. Tang, C. J.; Wang, G. X.; Shen, Y.; Wan, L. J.; Xiao, L.; Zhang, Q.; Yu, Q. S.; Liu, L. S.; Wen, G. B., A study on surface endothelialization of plasma coated intravascular stents. *Surface and Coatings Technology* **2004** (9-10), 1487.
12. Adelow, C.; Segura, T.; Hubbell, J. A.; Frey, P., The effect of enzymatically degradable poly(ethylene glycol) hydrogels on smooth muscle cell phenotype. *Biomaterials* **2008**, *29* (3), 314-26.
13. Beamish, J. A.; Geyer, L. C.; Haq-Siddiqi, N. A.; Kottke-Marchant, K.; Marchant, R. E., The effects of heparin releasing hydrogels on vascular smooth muscle cell phenotype. *Biomaterials* **2009**, *30* (31), 6286-94.
14. Fairbanks, B. D.; Schwartz, M. P.; Bowman, C. N.; Anseth, K. S., Photoinitiated polymerization of PEG-diacrylate with lithium phenyl-2,4,6-trimethylbenzoylphosphinate: polymerization rate and cytocompatibility. *Biomaterials* **2009**, *30* (35), 6702-7.
15. Klouda, L.; Hacker, M. C.; Kretlow, J. D.; Mikos, A. G., Cytocompatibility evaluation of amphiphilic, thermally responsive and chemically crosslinkable macromers for in situ forming hydrogels. *Biomaterials* **2009**, *30* (27), 4558-66.

16. Cole, M. A.; Voelcker, N. H.; Thissen, H.; Griesser, H. J., Stimuli-responsive interfaces and systems for the control of protein-surface and cell-surface interactions. *Biomaterials* **2009**, *30* (9), 1827-50.
17. Xu, L. C.; Siedlecki, C. A., Effects of surface wettability and contact time on protein adhesion to biomaterial surfaces. *Biomaterials* **2007**, *28* (22), 3273-83.
18. Kouvrakoglou, S.; Dee, K. C.; Bizios, R.; McIntire, L. V.; Zygourakis, K., Endothelial cell migration on surfaces modified with immobilized adhesive peptides. *Biomaterials* **2000**, *21* (17), 1725.
19. Leary Swan, E. E.; Popat, K. C.; Desai, T. A., Peptide-immobilized nanoporous alumina membranes for enhanced osteoblast adhesion. *Biomaterials* **2005**, *26* (14), 1969-1976.
20. Meyers, S. R.; Khoo, X.; Huang, X.; Walsh, E. B.; Grinstaff, M. W.; Kenan, D. J., The development of peptide-based interfacial biomaterials for generating biological functionality on the surface of bioinert materials. *Biomaterials* **2009**, *30* (3), 277-86.
21. Zhang, H.; Lin, C. Y.; Hollister, S. J., The interaction between bone marrow stromal cells and RGD-modified three-dimensional porous polycaprolactone scaffolds. *Biomaterials* **2009**, *30* (25), 4063-9.
22. Oezyuerek, Z.; Franke, K.; Nitschke, M.; Schulze, R.; Simon, F.; Eichhorn, K.-J.; Pompe, T.; Werner, C.; Voit, B., Sulfated glyco-block copolymers with specific receptor and growth factor binding to support cell adhesion and proliferation. *Biomaterials* **2009**, *30* (6), 1026.
23. Luginbuehl, V.; Meinel, L.; Merkle, H. P.; Gander, B., Localized delivery of growth factors for bone repair. *European Journal of Pharmaceutics and Biopharmaceutics* **2004**, *58* (2), 197.
24. Boyan, B. D.; Hummert, T. W.; Dean, D. D.; Schwartz, Z., Role of material surfaces in regulating bone and cartilage cell response. *Biomaterials* **1996**, *17* (2), 137-46.
25. Gao, L.; Feng, B.; Wang, J.; Lu, X.; Liu, D.; Qu, S.; Weng, J., Micro/nanostructural porous surface on titanium and bioactivity. *J Biomed Mater Res B Appl Biomater* **2009**, *89B* (2), 335-41.
26. Berry, C. C.; Campbell, G.; Spadicino, A.; Robertson, M.; Curtis, A. S. G. A. S. G., The influence of microscale topography on fibroblast attachment and motility. *Biomaterials* **2004**, *25* (26), 5781-5788.
27. Popat, K. C.; Leoni, L.; Grimes, C. A.; Desai, T. A., Influence of engineered titania nanotubular surfaces on bone cells. *Biomaterials* **2007**, *28* (21), 3188-97.
28. Shi, X.; Sitharaman, B.; Pham, Q. P.; Liang, F.; Wu, K.; Edward Billups, W.; Wilson, L. J.; Mikos, A. G., Fabrication of porous ultra-short single-walled carbon nanotube nanocomposite scaffolds for bone tissue engineering. *Biomaterials* **2007**, *28* (28), 4078-90.

29. Lee, J.; Chu, B. H.; Chen, K. H.; Ren, F.; Lele, T. P., Randomly oriented, upright SiO<sub>2</sub> coated nanorods for reduced adhesion of mammalian cells. *Biomaterials* **2009**, *30* (27), 4488-93.
30. Popat, K. C.; Daniels, R. H.; Dubrow, R. S.; Hardev, V.; Desai, T. A., Nanostructured surfaces for bone biotemplating applications. *J Orthop Res* **2006**, *24* (4), 619-27.
31. Porter, J. R.; Henson, A.; Ryan, S.; Popat, K. C., Biocompatibility and mesenchymal stem cell response to poly(epsilon-caprolactone) nanowire surfaces for orthopedic tissue engineering. *Tissue Eng Part A* **2009**, *15* (9), 2547-59.
32. Lopez, C. A.; Fleischman, A. J.; Roy, S.; Desai, T. A., Evaluation of silicon nanoporous membranes and ECM-based microenvironments on neurosecretory cells. *Biomaterials* **2006**, *27* (16), 3075-83.
33. Popat, K. C.; Leary Swan, E. E.; Mukhatyar, V.; Chatvanichkul, K. I.; Mor, G. K.; Grimes, C. A.; Desai, T. A., Influence of nanoporous alumina membranes on long-term osteoblast response. *Biomaterials* **2005**, *26* (22), 4516-22.
34. Fiore, V. F.; Lofton, M. C.; Roser-Page, S.; Yang, S. C.; Roman, J.; Murthy, N.; Barker, T. H., Polyketal microparticles for therapeutic delivery to the lung. *Biomaterials* *31* (5), 810-7.
35. Gupta, A. K.; Gupta, M., Synthesis and surface engineering of iron oxide nanoparticles for biomedical applications. *Biomaterials* **2005**, *26* (18), 3995-4021.
36. Bhattarai, N.; Edmondson, D.; Veiseh, O.; Matsen, F. A.; Zhang, M., Electrospun chitosan-based nanofibers and their cellular compatibility. *Biomaterials* **2005**, *26* (31), 6176-84.
37. Lee, J. Y.; Bashur, C. A.; Goldstein, A. S.; Schmidt, C. E., Polypyrrole-coated electrospun PLGA nanofibers for neural tissue applications. *Biomaterials* **2009**, *30* (26), 4325-35.
38. Sargeant, T. D.; Rao, M. S.; Koh, C. Y.; Stupp, S. I., Covalent functionalization of NiTi surfaces with bioactive peptide amphiphile nanofibers. *Biomaterials* **2008**, *29* (8), 1085-98.
39. Boyan, B. D., The changing face of dental research: blurring the boundaries between industry and academia. *J Dent Res* **1996**, *75* (6), 1426-7.
40. Mendonca, G.; Mendonca, D. B.; Aragao, F. J.; Cooper, L. F., Advancing dental implant surface technology--from micron- to nanotopography. *Biomaterials* **2008**, *29* (28), 3822-35.
41. Werner, S.; Huck, O.; Frisch, B.; Vautier, D.; Elkaim, R.; Voegel, J. C.; Brunel, G.; Tenenbaum, H., The effect of microstructured surfaces and laminin-derived peptide coatings on soft tissue interactions with titanium dental implants. *Biomaterials* **2009**, *30* (12), 2291-301.
42. Naidu, S. H.; Kulkarni, N.; Saunders, M., Titanium Basal Joint Arthroplasty: A Finite Element Analysis and Clinical Study. *The Journal of Hand Surgery* **2006**, *31* (5), 760.

43. Semlitsch, M. F.; Weber, H.; Streicher, R. M.; Schön, R., Joint replacement components made of hot-forged and surface-treated Ti-6Al-7Nb alloy. *Biomaterials* **1992**, *13* (11), 781.
44. Wang, K., The use of titanium for medical applications in the USA. *Materials Science and Engineering: A* **1996**, *213* (1-2), 134-137.
45. Heissler, E.; Fischer, F. S.; Boiouri, S.; Lehrmann, T.; Mathar, W.; Gebhardt, A.; Lanksch, W.; Bler, J., Custom-made cast titanium implants produced with CAD/CAM for the reconstruction of cranium defects. *International Journal of Oral and Maxillofacial Surgery* **1998**, *27* (5), 334.
46. Blake, G. B.; MacFarlane, M. R.; Hinton, J. W., Titanium in reconstructive surgery of the skull and face. *British Journal of Plastic Surgery* **1990**, *43* (5), 528.
47. Peng, L.; Eltgroth, M. L.; LaTempa, T. J.; Grimes, C. A.; Desai, T. A., The effect of TiO<sub>2</sub> nanotubes on endothelial function and smooth muscle proliferation. *Biomaterials* **2009**, *30* (7), 1268-72.
48. Fine, E.; Zhang, L.; Fenniri, H.; Webster, T. J., Enhanced endothelial cell functions on rosette nanotube-coated titanium vascular stents. *Int J Nanomedicine* **2009**, *4*, 91-7.
49. Liu, X.; Chu, P. K.; Ding, C., Surface modification of titanium, titanium alloys, and related materials for biomedical applications. *Materials Science and Engineering: R: Reports* **2004**, *47* (3-4), 49-121.
50. Sul, Y.-T., The significance of the surface properties of oxidized titanium to the bone response: special emphasis on potential biochemical bonding of oxidized titanium implant. *Biomaterials* **2003**, *24* (22), 3893.
51. Huang, N.; Yang, P.; Leng, Y. X.; Chen, J. Y.; Sun, H.; Wang, J.; Wang, G. J.; Ding, P. D.; Xi, T. F.; Leng, Y., Hemocompatibility of titanium oxide films. *Biomaterials* **2003**, *24* (13), 2177-2187.
52. Motlagh, D.; Yang, J.; Lui, K. Y.; Webb, A. R.; Ameer, G. A., Hemocompatibility evaluation of poly(glycerol-sebacate) in vitro for vascular tissue engineering. *Biomaterials* **2006**, *27* (24), 4315-24.
53. Miller, R.; Guo, Z.; Vogler, E. A.; Siedlecki, C. A., Plasma coagulation response to surfaces with nanoscale chemical heterogeneity. *Biomaterials* **2006**, *27* (2), 208-15.
54. Roy, S. C.; Paulose, M.; Grimes, C. A., The effect of TiO<sub>2</sub> nanotubes in the enhancement of blood clotting for the control of hemorrhage. *Biomaterials* **2007**, *28* (31), 4667-72.
55. Tang, L.; Eaton, J. W., Natural responses to unnatural materials: A molecular mechanism for foreign body reactions. *Mol Med* **1999**, *5* (6), 351-8.
56. Mor, G. K.; Varghese, O. K.; Paulose, M.; Shankar, K.; Grimes, C. A., A review on highly ordered, vertically oriented TiO<sub>2</sub> nanotube arrays: Fabrication, material properties, and solar energy applications. *Solar Energy Materials and Solar Cells* **2006**, *90* (14), 2011-2075.

57. Mor, G. K.; Carvalho, M. A.; Varghese, O. K.; M.V., P.; Grimes, C. A., A room temperature TiO<sub>2</sub> nanotube hydrogen sensor able to self-clean photoactively from environmental contamination. *Journal of Materials Research* **2004**, *19* (2), 628-34.
58. Mor, G. K.; Varghese, O. K.; Paulose, M.; Grimes, C. A., Transparent highly ordered TiO<sub>2</sub> nanotube arrays via anodization of titanium thin films. *Advanced Functional Materials* **2005**, *15*, 1291-96.
59. Popat, K. C.; Eltgroth, M.; LaTempa, T. J.; Grimes, C. A.; Desai, T. A., Titania nanotubes: a novel platform for drug-eluting coatings for medical implants? *Small* **2007**, *3* (11), 1878-81.
60. Ruan, C.; Paulose, M.; Varghese, O. K.; Mor, G. K.; Grimes, C. A., Fabrication of highly ordered TiO<sub>2</sub> nanotube arrays using an organic electrolyte. *J Phys Chem B* **2005**, *109* (33), 15754-9.
61. Woo, K. M.; Chen, V. J.; Ma, P. X., Nano-fibrous scaffolding architecture selectively enhances protein adsorption contributing to cell attachment. *J Biomed Mater Res A* **2003**, *67* (2), 531-7.
62. Sheppard, J. I.; McClung, W. G.; Feuerstein, I. A., Adherent platelet morphology on adsorbed fibrinogen: Effects of protein incubation time and albumin addition. *Journal of Biomedical Materials Research* **1994**, *28* (10), 1175-1186.
63. Mor, G. K.; Varghese, O. K.; Paulose, M.; Mukherjee, N.; Grimes, C. A., Fabrication of tapered, conical-shaped titania nanotubes. *Journal of Materials Research* **2003**, *18* (11), 2588-93.
64. Popat, K.; Leoni, L.; Grimes, C.; Desai, T., *Biomaterials* **2007**, *28* (null), 3188.
65. Gong, D.; Grimes, C. A.; Varghese, O. K.; Hu, W.; Singh, R. S.; Chen, Z.; Dickey, E. C., Titanium oxide nanotube arrays prepared by anodic oxidation. *Journal of Materials Research* **2001**, *16* (12), 3331-34.

## CHAPTER 5

### REDUCED THROMBOGENICITY ON TITANIA NANOTUBE ARRAYS

#### 5.1 Introduction

Titanium and titanium-based alloys are the most widely used materials for implantable biomedical devices such as dental <sup>1-3</sup>, prosthetic <sup>4-7</sup> and craniofacial implants <sup>8,9</sup>. Titanium reacts with atmospheric oxygen to form a passivating oxide layer of titania, which exhibits enhanced biocompatibility when implanted *in vivo* <sup>4, 10</sup>. Further, this oxide layer enables a hard and scratch resistant material surface with improved corrosion and wear resistance, and a low coefficient of friction <sup>11, 12</sup>. Titanium-based materials are widely used in blood-contacting devices such as intra-osseous implants <sup>13, 14</sup>, cardiovascular stents <sup>15, 16</sup>, and hard and soft tissue grafts <sup>17</sup>. The constant exposure of these materials introduces serious and ongoing concerns regarding poor blood-biomaterial interactions. To date, all blood-contacting materials have been shown to initiate immunological events in the form of inflammation, thrombosis, fibrosis and/or infection <sup>18, 19</sup>; potentially leading to complete implant failure <sup>20, 21</sup>. This foreign body response has been proven to be a major hindrance to the integration of the material with the natural tissue. Thus, the ability to modulate thrombogenicity of titanium surfaces is critical for the long-term success of blood-contacting devices. Whole blood plasma elicits four main events capable of a thrombogenic response *in vivo*: platelet adhesion/activation, leukocyte recruitment, and further activation of complement and coagulation <sup>21</sup>. Several key processes are initiated on the biomaterial surface the moment it comes in contact with the blood. Within seconds to minutes, key blood serum proteins

are adsorbed and undergo conformational changes on the surface<sup>18</sup>. This layer of adsorbed proteins will allow subsequent adhesion and activation of a-nuclear platelets, which play an essential role in both the formation of the fibrin clot as well as the recruitment of leukocytes (including monocytes and neutrophils). The platelets then initiate an inflammatory immune response and promote a virtually unstoppable cascade of events resulting in thrombosis and/or fibrous encapsulation of the implant. Within the body resides a multitude of topographical and biochemical cues that influence the cellular functionality. Therefore, material surfaces with topographical or biomolecular cues that mimic the natural tissue hierarchy provide possible solutions for enhancing blood-compatibility, further preventing biomaterial rejection<sup>22-28</sup>. Recently there has been an increased interest in exploring nanoscale surface topographies on implant surfaces for their potential in eliciting physiological cellular responses. Since the cells *in vivo* are in constant interaction with their surroundings (comprised of pits, protrusion and pores including additional subcellular structures on the nano-meter size scale), surface nanoarchitectures similar to that of the natural *in vivo* environment often elicit enhanced cellular responses. State of the art advances in technology have enabled the fabrication of unique nanostructures on biomaterial surfaces that better mimic the natural tissue hierarchy (e.g. nanoparticles<sup>29, 30</sup>, nanofibers<sup>31-33</sup>, nanopores<sup>34, 35</sup>, nanowires<sup>36, 37</sup>, nanostructured hydrogels<sup>38</sup>, and nanotube arrays<sup>39-42</sup>). Studies have shown that nanoscale architectures promote a multitude of cellular responses including improved osseo-integration<sup>31, 38, 43, 44</sup>, augmented mesenchymal stem cell differentiation<sup>37, 45, 46</sup>, enhanced neuronal activation<sup>36, 47</sup>, and increased growth rate of endothelial cells<sup>48-51</sup>. These studies point out the importance of nanoscale architectures on implant surfaces,

suggesting a possible correlation with the cellular functionality<sup>52</sup>. Recent studies have evaluated the hemocompatibility and immunogenicity of nanomaterials with respect to the effects of size, charge and pore ordering<sup>53-57</sup>; however, limited information exists in literature about the thrombogenicity of these nanoscale interfaces<sup>58-61</sup>, thus eliciting a need for a more in-depth look at the mechanisms behind blood-nanomaterial interactions..

In this study, we have evaluated the potential of titania nanotube arrays as interfaces for blood-contacting implants by investigating the thrombogenic effects of the nanotube architecture on the components of whole blood plasma. Titania nanotube arrays (diameter: approx. 100 nm, length: 1-1.5  $\mu\text{m}$ ) were fabricated using a simple anodization process, as previously described<sup>62,63</sup>. The effect of nanotube architecture on populations of platelets isolated in a buffer was presented in chapter IV. The results indicated an increase in platelet adhesion and activation on titania nanotube arrays<sup>61</sup>. However, no studies have reported the interaction of whole blood plasma components with these nanotube arrays. Thus, in this study, the effect of the nanotube architecture on whole human blood plasma was investigated to better understand a physiologically relevant thrombogenic response. The functionality of platelets and leukocytes were investigated on titania nanotube arrays after 2 hours of contact with whole blood plasma using fluorescence microscopy, a cell cytotoxicity assay, and scanning electron microscopy (SEM). Contact activation was characterized by a chromogenic analysis to determine the amount of kallikrein deposited on titania nanotube arrays. Complement activation and platelet factor 4 (PF-4) microparticles were evaluated using commercially available enzyme immunoassay (EIA) and enzyme-linked immunosorbant assay (ELISA)

kits respectively. Further, a human fibrinogen antigen assay was used to determine the degree of protein adsorption and aggregation on titania nanotube arrays. This work evaluates the blood-compatibility of titania nanotube arrays which is critical for long-term success of blood-contacting devices.

## **5.2 Experimental Methods**

### **5.2.1 *Fabrication and Characterization of Titania Nanotube Arrays***

Titania nanotube arrays were fabricated using a simple anodization process, described in detail in chapter 2<sup>62-64</sup>. Biomedical grade titanium (as-received, non-polished) surfaces were used as controls. The nanotube architecture was examined for uniformity and repeatability using SEM imaging.

### **5.2.2 *Plasma Isolation from Whole Blood***

Whole blood from healthy individuals, acquired through venopuncture, was drawn into standard 6 ml vacuum tubes coated with the anti-coagulant, ethylenediaminetetraacetic acid (EDTA). The first tube was discarded to account for the skin plug and locally activated platelets resulting from the needle insertion. The blood vials were centrifuged at 150 g for 15 min to separate the plasma from the red blood cells (erythrocytes) (**See Figure 5.1**). The plasma was then pooled into fresh tubes, and used within 2 hours of removal from the body.

### **5.2.3 *Plasma Incubation on Titania Nanotube Arrays***

Titania nanotube arrays and as-received, non-polished biomedical grade titanium (control), both 0.5 cm × 0.5 cm, were incubated with pooled plasma. Prior to incubation,

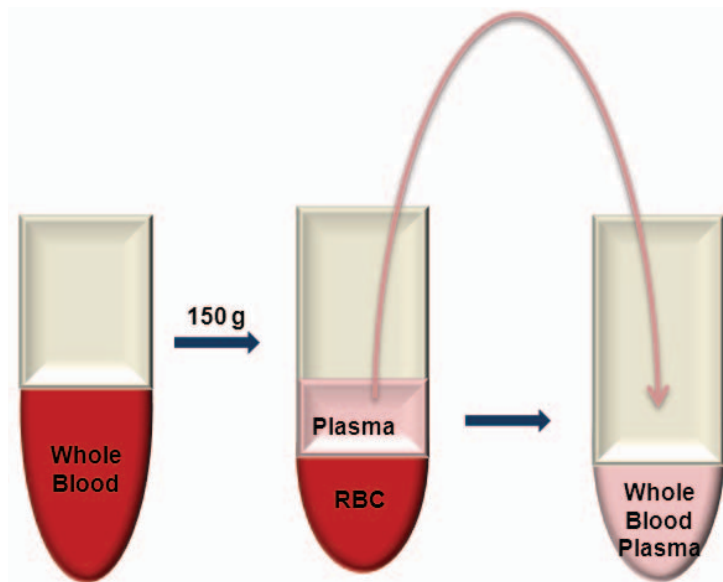


Figure 5.1 Schematic of the isolation of whole blood plasma, following removal from healthy individuals.

all substrates were sterilized in 70% ethanol for 30 min, followed by washing (2×) with PBS. They were air dried and further sterilized by *uv* exposure for 30 min. The substrates were then incubated in a 24-well plate with 500  $\mu$ l of pooled plasma at 37°C and 5% CO<sub>2</sub> on a horizontal shaker plate (100rpm) for 2 hours. The effects of the surface architecture of titania nanotube arrays on plasma components (platelets and leukocytes) were investigated and compared to that on the control substrates after 2 hours of contact with whole blood plasma.

#### 5.2.4 Platelet/Leukocyte Adhesion

Cellular adhesion was investigated by fluorescence microscope imaging using calcein-AM live stain. Prior to staining, the un-adhered cells were removed by aspirating the supernatant plasma from the substrates followed by gently rinsing (2×) with PBS.

The substrates were then transferred to a new 24-well plate and incubated with 500  $\mu$ l of 5  $\mu$ M calcein-AM solution in PBS for 20 min at room temperature. They were rinsed with PBS and further imaged using a fluorescence microscope with filter set 62 HE BP 474/28 (green) (Zeiss). The cell coverage was determined using the fluorescence microscope images and the ImageJ software.

### **5.2.5 Cytotoxicity Assay**

The material cytotoxicity was characterized using a commercially available lactate dehydrogenase (LDH) cytotoxicity assay kit (Cayman Chemical). The protocol provided by the manufacturer was followed. In brief, the substrates were rapidly shaken on a horizontal shaker plate (1000 rpm) for 5 min at room temperature. The manufacturer-provided standards along with the substrate-exposed plasma samples were transferred to a 96 well plate. A reaction solution (96% v/v assay buffer, 1% v/v NAD<sup>+</sup>, 1% v/v Lactic Acid, 1% v/v INT, and 1% v/v LDH Diaphorase) was added in the amounts equal (1:1) to all standards and samples, and further incubated with gentle shaking on an orbital shaker for 30 min at room temperature. The absorbance of the solution was measured at a wavelength of 490 nm to determine the cytotoxic effects of the substrates.

### **5.2.6 Platelet/Leukocyte Detection by Direct Immunofluorescence**

The substrates were concurrently stained with 4',6-diamidino-2-phenylindole-dihydrochloride (DAPI) nucleus stain to identify adherent leukocytes, and F-actin cytoskeletal stain to identify adherent platelets and leukocytes using direct

immunofluorescence microscope imaging. Prior to staining, the un-adhered cells were removed by aspirating the plasma from the substrates followed by gently rinsing (2×) with PBS, and transferred to a new 24-well plate. Adherent cells were fixed in 3.7wt % formaldehyde in PBS for 15 min at room temperature and washed (3×, 5 min per wash) in PBS. The cell membranes were permeabilized using 1% Triton-X in PBS at room temperature for 3 min. This was followed by rinsing with PBS and incubating in 10% bovine serum albumin (BSA) in PBS for 30 min at room temperature to block unspecific immune reactions. The substrates were washed (3×, 5 min per wash) in PBS and incubated in rhodamine-conjugated phalloidin (dilution 1:40) with 2% BSA in PBS for 20 min at room temperature to stain for F-actin on the cell membranes. The cell nuclei were then stained with 0.2 µg/ml DAPI in a solution of 2% BSA in PBS for 5 min, and washed (3×, 5 min per wash) in PBS. The substrates were imaged with a fluorescence microscope using a 49 DAPI BP 445/50 blue filter and filter set 62 HE BP 585/35 (red) (Zeiss). The number of adherent cells was determined using the fluorescence images and the ImageJ software.

### ***5.2.7 Platelet/Leukocyte - Complex Detection by Indirect Immunofluorescence***

Indirect immunofluorescence staining was used to determine the cellular expression through the presence of specific marker proteins on platelets and leukocytes. Prior to staining, the un-adhered cells were removed by aspirating the plasma from the substrates followed by gently rinsing (2×) with PBS, and transferred to a new 24-well plate. Adherent cells were fixed in 3.7wt % formaldehyde in PBS for 15 min at room temperature and washed (3×, 5 min per wash) in PBS. The cell membranes were

permeabilized using 1% Triton-X in PBS at room temperature for 3 min. This was followed by washing with PBS and incubating in 10% BSA in PBS for 30 min at room temperature to block unspecific immune reactions. The substrates were washed (3×, 5 min per wash) in PBS and incubated in primary antibodies (dilution 1:50, Santa Cruz Biotechnology) in a solution of 2% BSA in PBS for 1 hour at room temperature. The primary antibodies (**See Table 5.1**) included: P-Selectin (platelet-specific) and CD45 (leukocyte-specific).

Table 5.1 Blocking agents, primary antibodies and secondary antibodies used for immunofluorescence identification of membrane specific marker proteins on platelets and leukocytes.

	<b>Platelet</b>	<b>Leukocyte</b>	<b>Monocyte/Macrophage</b>	<b>Neutrophil</b>
	<b>P-Selectin</b>	<b>CD45</b>	<b>CD14</b>	<b>CD16</b>
<b>Blocking</b>	Normal Bovine Serum	Normal Bovine Serum	Normal Bovine Serum	Normal Bovine Serum
<b>Primary Antibody</b>	Goat anti-P-Selectin	Mouse anti-CD45	Goat anti-CD14	Mouse anti-CD16
<b>Secondary Antibody</b>	Texas red (TR)-conjugated donkey anti-goat IgG	Fluorescein isothiocyanate (FITC)-conjugated chicken anti-Mouse IgG	Texas red (TR)-conjugated donkey anti-goat IgG	Fluorescein isothiocyanate (FITC)-conjugated chicken anti-Mouse IgG

The substrates were then washed (3×, 5 min per wash) in PBS, and incubated with fluorescently-labeled secondary antibodies (dilution 1:100, Santa Cruz Biotechnology) in a solution of 2% BSA in PBS for 1 hour at room temperature. The secondary antibodies included: donkey anti-goat conjugated with Texas Red (for P-Selectin) and chicken anti-mouse conjugated with FITC (for CD45). The substrates were washed (3×, 5 min per

wash) in PBS, and imaged with a fluorescence microscope using filter set 62 HE BP 585/35 (red) and BP 474/28 (green) (Zeiss). All images were processed using the ImageJ Software. Cellular expression was determined by presence, increased fluorescence, and altered cellular size and structure.

### **5.2.8 *Monocyte/Neutrophil Detection by Indirect Immunofluorescence***

Indirect immunofluorescence staining was used to determine the cellular expression through the presence of leukocyte-specific marker proteins on monocytes/macrophages and neutrophils. Prior to staining, the unadhered cells were removed by aspirating the plasma from the substrates followed by gently rinsing (2×) with PBS, and transferred to a new 24-well plate. Adherent cells were fixed in 3.7wt % formaldehyde in PBS for 15 min at room temperature and washed (3×, 5 min per wash) in PBS. The cell membranes were permeabilized using 1% Triton-X in PBS at room temperature for 3 min. This was followed by washing with PBS and incubating in 10% BSA in PBS for 30 min at room temperature to block unspecific immune reactions. The substrates were washed (3×, 5 min per wash) in PBS and incubated in primary antibodies (dilution 1:50, Santa Cruz Biotechnology) in a solution of 2% BSA in PBS for 1 hour at room temperature. The primary antibodies included: CD14 (monocyte-specific) and CD16 (neutrophil-specific). The substrates were then washed (3×, 5 min per wash) in PBS, and incubated with fluorescently-labeled secondary antibodies (dilution 1:100, Santa Cruz Biotechnology, Santa Cruz, CA) in a solution of 2% BSA in PBS for 1 hour at room temperature. The secondary antibodies included: donkey anti-goat conjugated with Texas Red (for CD14) and chicken anti-mouse conjugated with FITC (for CD16).

The substrates were washed (3×, 5 min per wash) in PBS, and imaged with a fluorescence microscope using filter set 62 HE BP 585/35 (red) and BP 474/28 (green) (Zeiss). All images were processed using the ImageJ Software. Cellular expression was determined by presence, increased fluorescence, and altered cellular size and structure.

### **5.2.9 Platelet/Leukocyte Morphology**

The platelet-leukocyte morphology was investigated using SEM imaging to visualize the platelet-leukocyte interaction with the nanotube architecture. The unadhered cells were removed by aspirating the plasma from the substrates followed by gently rinsing (2×) with PBS. The substrates were then transferred to a petri-dish and the adherent cells were fixed by incubation in a solution of primary fixative (6% glutaraldehyde (Sigma), 0.1 M sodium cacodylate (Polysciences), and 0.1 M sucrose (Sigma)) for 45 min. This was followed by incubation in a solution of secondary fixative (primary fixative without glutaraldehyde) for 10 min; and consecutive solutions of ethanol (35%, 50%, 70% and 100%) for 10 min each. For further dehydration, the substrates were placed into a solution of hexamethyldisilazane (HMDS, Sigma) for 10 min. The substrates were then air dried and stored in a desiccator until further imaging by SEM. Prior to imaging, the substrates were coated with a 10 nm layer of gold and imaged at 15kV.

### **5.2.10 Complement Activation**

Complement activation was assessed using an enzyme immunoassay (EIA, Quidel) to evaluate the degree of SC5b-9 complement activation. The protocol provided

by the manufacturer was followed. In brief, the microassay wells were rehydrated by incubation in a wash solution provided by the manufacturer for 2 min. The SC5b-9 standards, controls, and diluted substrate-exposed plasma samples (1:10 in assay diluent) were transferred into microassay wells and incubated for 60 min at room temperature. The wells were gently washed (5×) with the wash buffer, followed by incubation with SC5b-9 conjugate for 30 min at room temperature. This was followed by gently washing (5×) the wells with the wash buffer. The tetramethyl benzidine buffer (TMB) was immediately added to each well and incubated for 15 min at room temperature in a dark environment. The reaction was stopped and the optical density was immediately measured using a spectrophotometer at 450 nm to determine the amount of SC5b-9 complement activation present in each sample.

#### **5.2.11 *Contact Activation***

Contact activation was assessed to evaluate the degree of plasma kallikrein (Chromogenix) present on the substrate-exposed plasma using an acid stop method. The protocol provided by the manufacturer was followed. In brief, the substrate-exposed plasma samples were diluted 10-fold in Tris Buffer (pH 7.5) and incubated at 37°C and 5% CO<sub>2</sub> for 3-4 min. Pre-warmed (37°C) chromogenic solution was added in equal amounts (1:1) to all of the samples, and further incubated at 37°C and 5% CO<sub>2</sub> for 10 min. The reaction was stopped by adding 20% acetic acid in equal amounts (1:1) to all of the samples. The plasma blanks were prepared by adding the reagents in reverse order without incubation. The optical density was immediately measured using a

spectrophotometer at 405 nm to determine the amount of contact activation on the substrates.

#### **5.2.12 PF-4 Expression**

PF-4 expression was assessed using a commercially available enzyme linked immunosorbant assay (ELISA, RayBio) kit to evaluate the degree of platelet activation. The protocol provided by the manufacturer was followed. In brief, PF-4 standards and diluted substrate-exposed plasma samples (1:200 in assay diluent) were transferred into microassay wells and incubated for 2.5 hours on a horizontal shaker plate (100 rpm) at room temperature. The wells were gently washed (4×) with the wash buffer, followed by incubation with the biotinylated antibody for 1 hour on a horizontal shaker plate (100 rpm) at room temperature. This was followed by gently washing (4×) the wells to remove unbound biotinylated antibody. A horseradish peroxidase (HRP)-streptavidin solution (1:25,000 in assay diluent) was then added to each well and allowed to react with the biotinylated antibody bound to the captured PF-4. The microassay wells were incubated for 45 min on a horizontal shaker plate (100 rpm) at room temperature. This was followed by gently washing (4×) the wells with the wash buffer. The TMB solution was immediately added to each well, and incubated for 30 min on a horizontal shaker plate (100 rpm) at room temperature in a dark environment. The reaction was stopped and the optical density was immediately measured using a spectrophotometer at 450 nm to determine the amount of PF-4 released by platelets on each of the substrates.

### **5.2.13 Fibrinogen Expression**

The fibrinogen expression by platelets was assessed using an enzyme immunoassay (EIA, Innovative Research). The protocol provided by the manufacturer was followed. In brief, human fibrinogen antigen standards and diluted substrate-exposed plasma samples (1:100,000 in assay diluent) were transferred into microassay wells and incubated for 30 min on a horizontal shaker plate (300 rpm) at room temperature. The wells were gently washed (3×) with the wash buffer, followed by incubation with the anti-human fibrinogen primary antibody for 30 min on a horizontal shaker plate (300 rpm) at room temperature. This was followed by gently washing (3×) the wells to remove unbound primary antibodies. Peroxidase secondary antibody was diluted (1:1 in assay diluent), added to each well and allowed to react with the anti-fibrinogen primary antibody bound to the captured fibrinogen. The wells were incubated for 30 min on a horizontal shaker plate (300 rpm) at room temperature followed by gently washing (3×) to remove unbound secondary antibodies. The TMB solution was immediately added to each well and incubated for 8 min on a horizontal shaker plate (300 rpm) at room temperature in a dark environment. The reaction was stopped and the optical density was immediately measured using a spectrophotometer at 450 nm to determine the amount of anti-fibrinogen on each of the substrates.

### **5.2.14 Statistical Analysis**

Each experiment was reconfirmed on at least three different substrates from at least three different whole blood plasma populations ( $n_{\min} = 9$ ). Further, all of the quantitative results were evaluated using an analysis of variance (ANOVA). Statistical

significance was considered at  $p < 0.05$ . During the analysis, variances among each group were not assumed to be equal and a two sample t-test approach was used to test the significance between the control substrate and titania nanotube arrays. This analysis was conducted using the Microsoft Office Excel data analysis software.

### **5.3 Results and Discussion**

The exposure of implantable devices to blood introduces serious and ongoing concerns regarding poor blood-biomaterial interactions such as platelet adhesion/activation, leukocyte recruitment and further immune response, potentially leading to complete implant failure. This foreign body reaction has been proven to be a major hindrance to the long-term success of blood-contacting devices such as intra-osseous implants, stent grafts, etc. eliciting a need for a more in-depth look at the mechanisms behind blood-nanomaterial interactions. Whole blood plasma contains four main components: platelets, leukocytes, complement and coagulation which may play an important role in implant failure *in vivo*. Thus, in this study we have evaluated the thrombogenicity of titania nanotube arrays after 2 hours of incubation in whole blood plasma. Previous studies have shown that the 2 hour time point used here is optimal for microparticle release, selectin expression, platelet aggregation and leukocyte recruitment<sup>65, 66</sup>. Thrombogenicity is a key consideration for the long-term success of blood-contacting implants resulting in a need to better understand the mechanisms behind blood/nano-biomaterial interactions.

Vertically oriented, immobilized, high aspect ratio titania nanotube arrays utilized in this study were fabricated using a simple anodization process as described

previously<sup>42, 62, 63</sup>. The nanotube architecture was examined for uniformity and repeatability using SEM imaging (See **Figure 5.2**). The results indicate that the nanotubes have an approximate diameter of 100 nm and length of 1-1.5  $\mu\text{m}$ . Previous studies have demonstrated enhanced cellular functionality on nanotube arrays with similar size<sup>46</sup>.

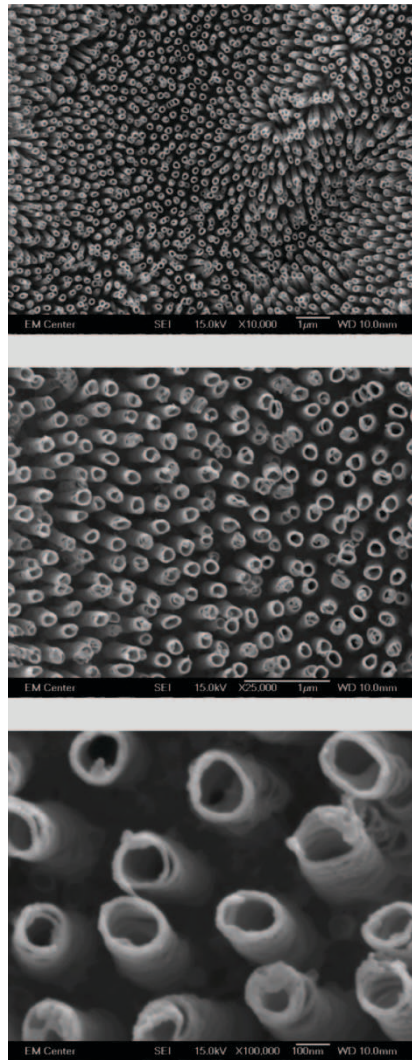
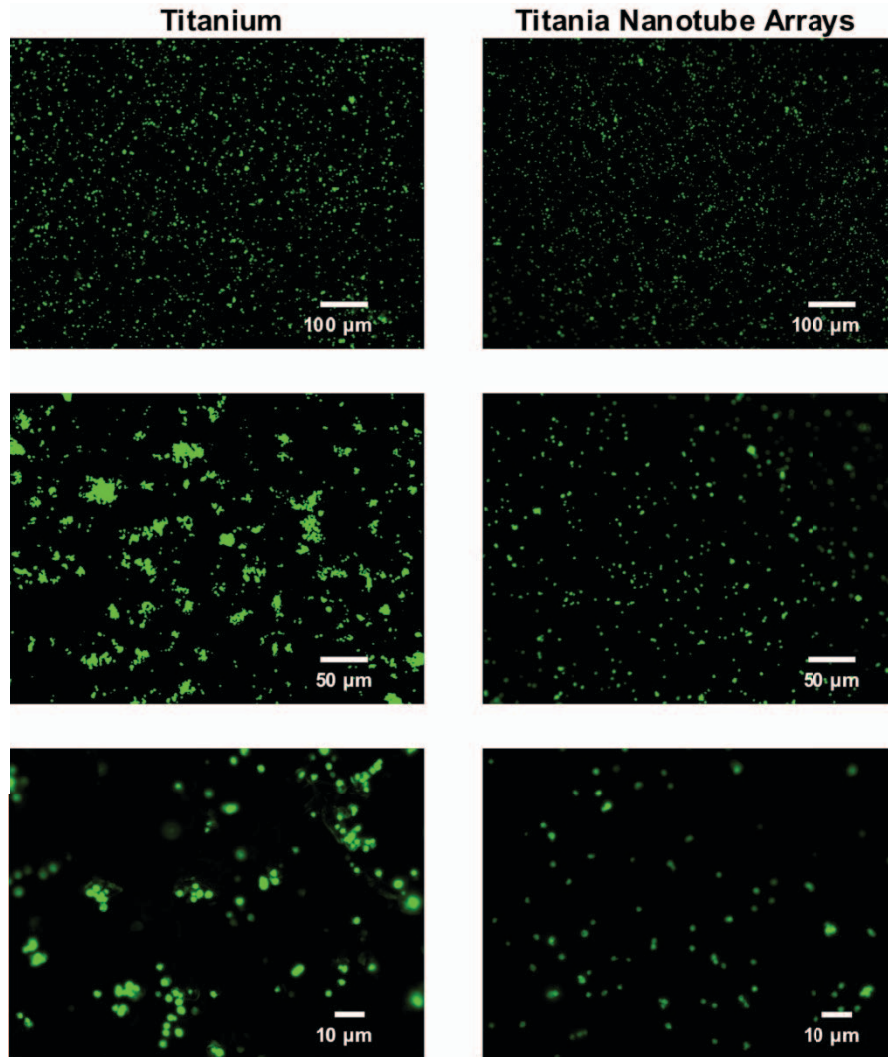


Figure 5.2 Representative SEM images (10000 $\times$ , 25000 $\times$ , 100000 $\times$  magnification) showing the nanoarchitecture of titania nanotube arrays fabricated using an anodization technique. Titania nanotube arrays were coated with a 10 nm layer of gold and imaged at 15kV.

Platelet and leukocyte adhesion were investigated after 2 hours of incubation in whole blood plasma using fluorescence microscope imaging by staining the cells with calcein-AM live stain (See **Figure 5.3**). Calcein-AM is a cell-permeate stain that labels viable cells by converting the non- fluorescent calcein-AM into a green-fluorescent



**Figure 5.3** Representative fluorescence microscopy images of adhered platelets and leukocytes stained with calcein-AM on the control substrate and titania nanotube arrays after 2 hours of incubation in whole blood plasma. The images indicate a decrease in platelet and leukocyte adhesion on titania nanotube arrays.

calcein. This conversion is accomplished through the hydrolyzation of intracellular acetoxymethyl esterases. The fluorescence microscope images were processed using the ImageJ software. These results indicate a decrease in the cell adhesion on titania nanotube arrays as compared to the control substrate. This is likely due to the altered surface topography, resulting in fewer adhesion and activation sites for the cells. High magnification images indicate minimal cellular aggregation on titania nanotube arrays as compared to that on the control substrate (See Figure 5.3). The fluorescence microscope images were further analyzed for cell coverage using the ImageJ software (See Figure 5.4). The results indicate an approximate 75% decrease in cell coverage on titania nanotube arrays as compared to the control substrate ( $p < 0.05$ ). This identifies a potential reduction in platelet and leukocyte adhesion on titania nanotube arrays that may be beneficial in controlling thrombogenic effects of the material surfaces.

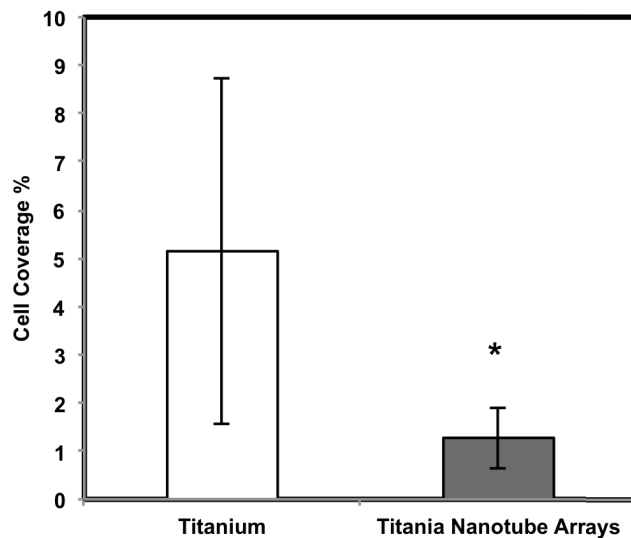


Figure 5.4 Cell coverage calculated using the fluorescence microscope images and the ImageJ software. The results indicate a significant 75% decrease in cell coverage on titania nanotube arrays compared to the control substrate (\*  $\rightarrow p < 0.05$ ).

The material cytotoxicity was characterized after 2 hours of incubation in whole blood plasma using a commercially available lactate dehydrogenase (LDH) assay kit. LDH is an enzyme located inside the cytoplasm of cells that is released upon cell death, thus this enzyme acts as a good indicator of cytotoxicity. This assay measures the amount of formazan following a two-step reduction, where LDH catalyzes  $\text{NAD}^+$  to NADH and  $\text{H}^+$  by oxidation and a subsequent catalyst reaction by diaphorase converting tetrazolium salt to a colored formazan. Spectrophotometric measurements determine the concentration of LDH released into the culture medium, therefore indicating the level of cytotoxicity and the concentration of dead cells on the substrates. These results show that the adhered platelets and leukocytes on titania nanotube arrays displayed a comparable cytotoxicity on titania nanotube arrays and the control substrate (**See Figure 5.5**). Thus, neither substrate promotes short-term cytotoxic effects on the components of whole blood plasma.

The cell cytoskeleton is composed of microfilaments, microtubules and intermediate filaments. When activated, these components play integral roles in assisting cell-cell and cell-ECM communication as well as mediating fundamental cellular events such as division, motility, protein trafficking and secretion. Therefore, cellular interaction with titania nanotube arrays may result in altered platelet-leukocyte communication. After 2 hours of incubation in whole blood plasma, titania nanotube arrays and the control substrates were stained with rhodamine-conjugated phalloidin (F-actin stain) and DAPI (nucleus stain), and imaged using a fluorescence microscope to identify the cell-material and platelet-leukocyte interactions (**See Figure 5.6**). Actin, a subunit of the microfilaments that participate in the formation of the cell cytoskeleton,

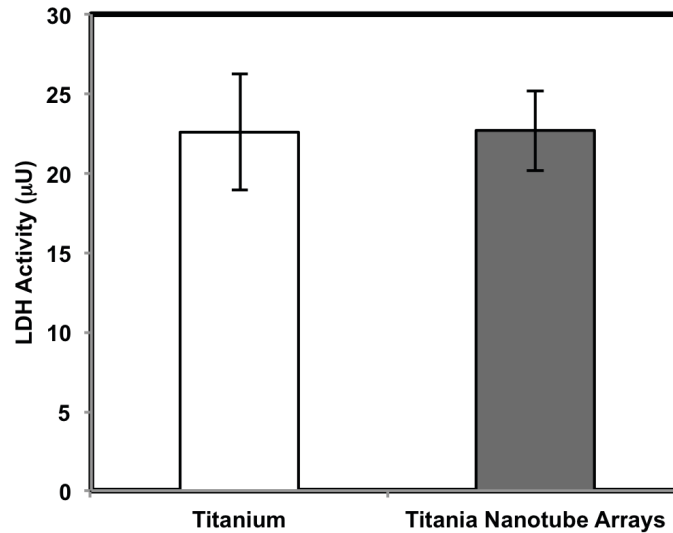


Figure 5.5 Cell cytotoxicity measured using an LDH Assay on the control substrate and titania nanotube arrays after 2 hours of incubation in whole blood plasma. The results indicate no significant difference in LDH activation on titania nanotube arrays compared to the control substrate.

acts as a key component for a multitude of cellular processes including motility, signaling and shape. In physiological conditions where ATP is present, actin obtains directionality in its conversion into long filamentous polymers termed F-actin; a transformation necessary for cytokinesis and chemotaxis. Further, leukocyte-specific identification was accomplished by fluorescence microscope imaging using a DAPI nucleus stain. The DAPI nucleic acid stain passes through intact membranes and preferentially stains dsDNA with a blue-fluorescence label. DAPI stains selectively for leukocytes present on the substrate surface since platelets do not possess nuclei. The images indicate limited platelet-leukocyte interaction on titania nanotube arrays as compared to the control substrate, further identifying a slight decrease in cell-cell communication on titania nanotube arrays. The reduced platelet-leukocyte interaction exhibited on the titania

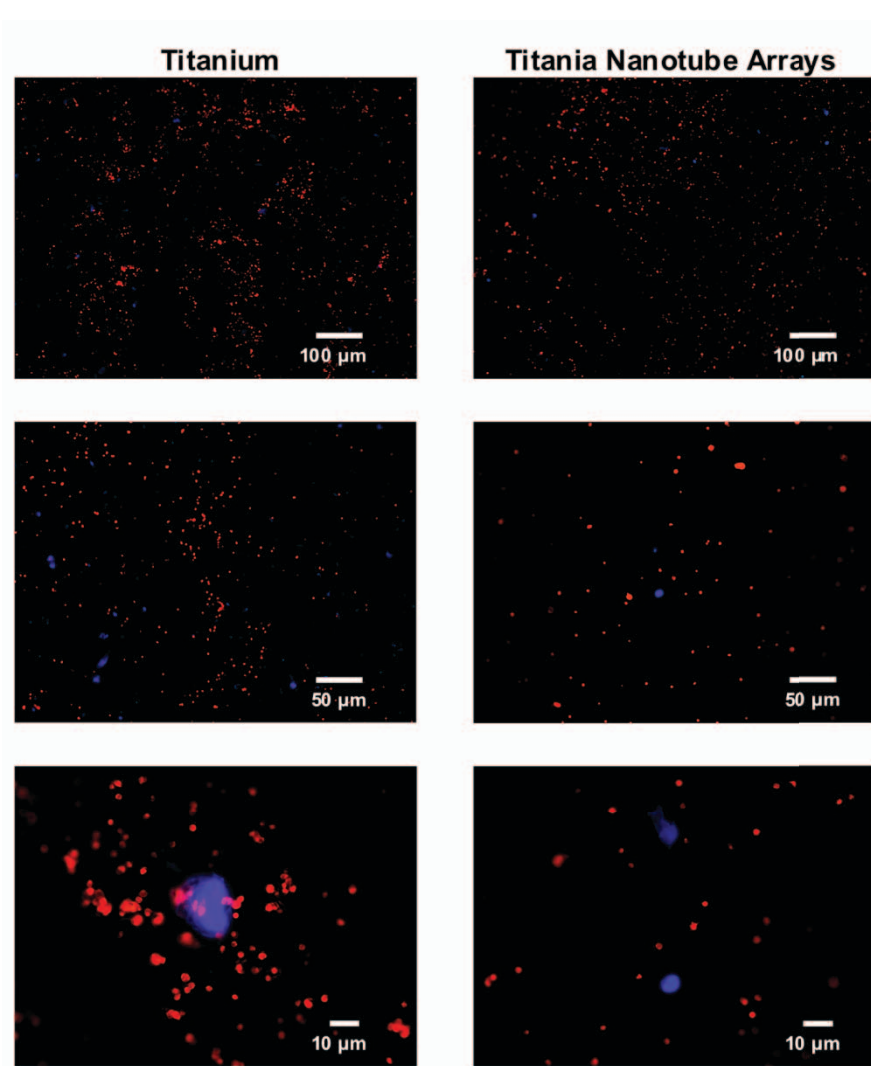


Figure 5.6 Representative fluorescence microscope images of adhered platelets and leukocytes stained with DAPI (nucleus) and rhodamine-conjugated phalloidin (actin) on the control substrate and titania nanotube arrays after 2 hours of incubation in whole blood plasma. The images indicate a decrease in platelet-leukocyte adhesion and aggregation on titania nanotube arrays.

nanotube arrays will likely lead to a reduction in platelet-leukocyte co-stimulation, thus playing a role in the inhibition of thrombogenic effects. Further, the fluorescence microscope images were processed and analyzed using the ImageJ software to determine

the total number of adhered cells followed by the number of adhered platelets and leukocytes on the surface (See **Figure 5.7**).

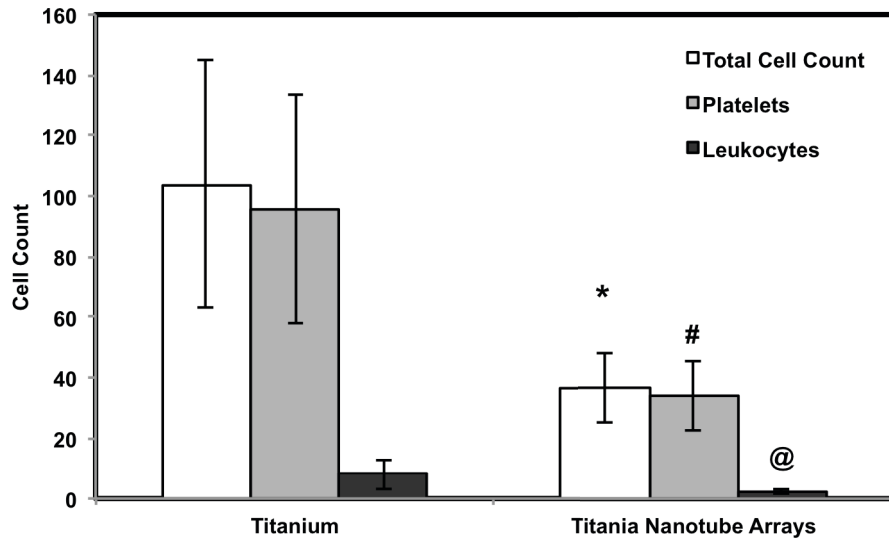


Figure 5.7 Cell count calculated using the fluorescence images and the ImageJ software. The results indicate a significant 69% decrease in total cell count on titania nanotube arrays compared to the control substrate (\*, #, @  $\rightarrow p < 0.05$ ).

The results indicate an approximate 65% reduction in the total number of cells on titania nanotube arrays as compared to the control substrate ( $p < 0.05$ ). Further, the results show an approximate 65% reduction in the number of platelets and 69% reduction in the number of leukocytes on titania nanotube arrays as compared to the control substrate ( $p < 0.05$ ). The results presented here identify significantly reduced platelet and leukocyte adhesion on titania nanotube arrays as compared to the control substrate.

Cellular activation and differentiation are highly prevalent in both cell-cell and cell-material interactions. In each of these instances, proteins are expressed and/or

released for local environmental adaptations. Platelet activation has been shown to occur as a result of protein adsorption on the material surface followed by leukocyte recruitment <sup>18</sup>. The presence of leukocytes often promotes additional stimulation to platelets and increases localized thrombogenicity <sup>21</sup>. In this study, platelet-leukocyte complexes were investigated after 2 hours of incubation in whole blood plasma by the indirect immunofluorescence staining (**See Figure 5.8**) of specific marker proteins that are known to be released and/or expressed in activated platelets (P-selectin) and leukocytes (CD45). Following platelet activation, P-selectin is expressed on the surface of platelets by attaching to the actin filaments through anchor proteins. P-selectin plays an essential role in the recruitment of leukocytes, further promoting fibrin deposition. Leukocytes express a common antigen, CD45, which functions as a regulator of cytokine receptor signaling. This transmembrane protein acts to guide cellular processes such as cell growth and differentiation, and directs several pathways in immune cells. However, CD45 has not been found to be present in platelets. The fluorescence microscope images were processed using the ImageJ software. The images indicate a decrease in both P-selectin and CD45 expression on titania nanotube arrays as compared to the control substrates. Higher magnification fluorescence images identified a lack of platelet-leukocyte complex interaction on titania nanotube arrays. These interactions were present on the control substrate (**See Figure 5.8**). Thus, the nanotube architecture and the variation in surface topography elicit a reduction in the expression of marker proteins in platelets and leukocytes. Leukocytes, also known as white blood cells (WBCs), are drawn to the surface of an implantable device following platelet adhesion, further contributing to localized thrombogenicity. These specialized cells play a major role in

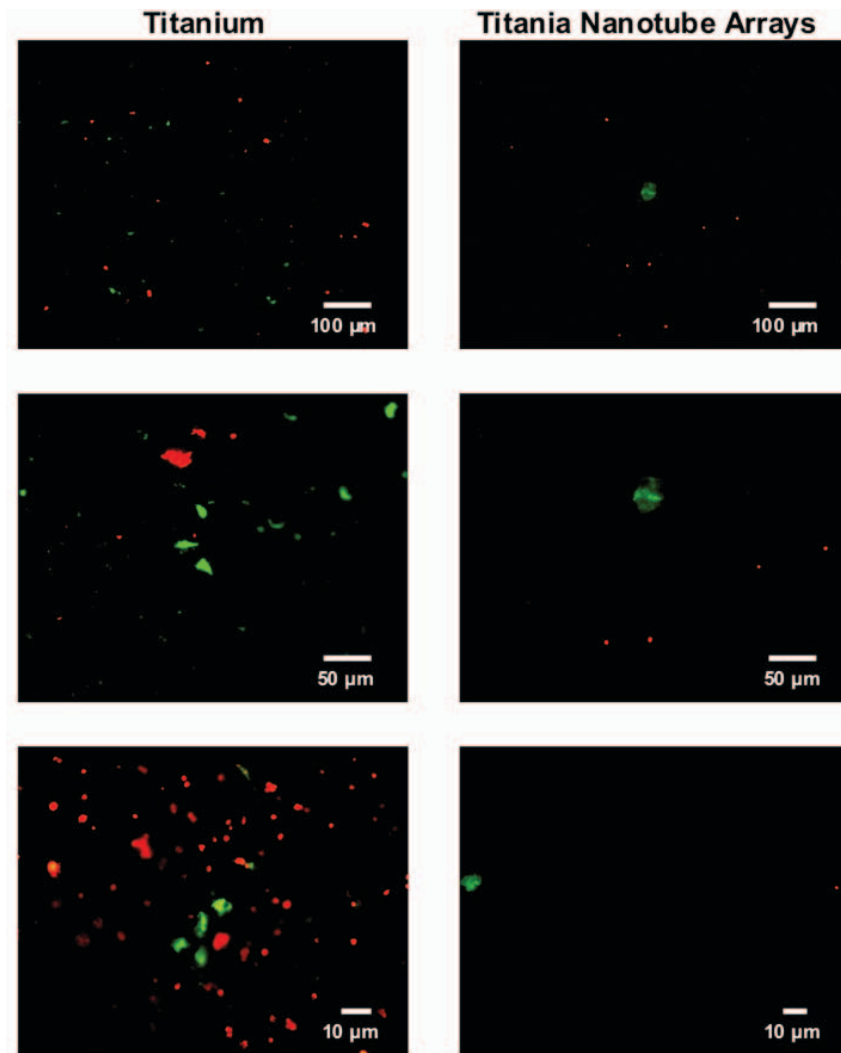


Figure 5.8 Representative fluorescence microscope images of platelets immuno-stained for P-Selectin and leukocytes immuno-stained for CD45 on titania nanotube arrays and the control substrate after 2 hours of incubation in whole blood plasma. The images indicate a considerable reduction in P-Selectin (TR-conjugated) and CD45 (FITC-conjugated) expression on titania nanotube arrays.

the immune system by defending the body against foreign infiltration, either due to infection or biomaterial insertion. The most prevalent among the leukocytes are neutrophils, accounting for 50-70% of all leukocytes. These granulocytes are generally

the first responders to platelet activation, playing a large part in fighting infection and the acute inflammatory response by phagocytosis. Although much less prevalent, monocytes (3-9% of leukocytes) are phagocytic cells capable of leaving the blood stream (diapedesis) to enter the tissue, where they differentiate into macrophages. Monocytes act as antigen presenting cells with an added ability to secrete cytokines and attract inflammatory cells such as fibroblasts, making them substantial components in chronic inflammation. In this study, the interaction and subsequent activation of neutrophils and monocytes were investigated after 2 hours of incubation in whole blood plasma by the indirect immunofluorescence staining of specific marker proteins that are known to be expressed in neutrophils (CD16) or monocytes (CD14) (**See Figure 5.9**). Neutrophils, also known as polymorphonuclear (PMN) leukocytes, express CD16 receptors that bind to immunoglobulin-G antibodies having a regulatory role in cytolytic function. Primarily expressed by monocytes/macrophages as a surface antigen, CD14 is able to detect pathogen associated molecular patterns including bacterial lipopolysaccharide (LPS), further mediating the innate immune response. The fluorescence microscope images were processed using the ImageJ software. The images indicate an obvious decrease in individual expressions of CD16 and CD14 as well as a decrease in the co-localization on titania nanotube arrays as compared to the control substrates (**See Figure 5.9**). The reduced platelet-leukocyte interaction exhibited on the titania nanotube arrays may lead to limited platelet-leukocyte co-stimulation, further playing a role in the inhibition of thrombogenic effects.

The morphological changes of a cell are often attributed to cell-cell and cell-extracellular (e.g. biomaterial) stimulation. Thus, the degree of cellular functionality is

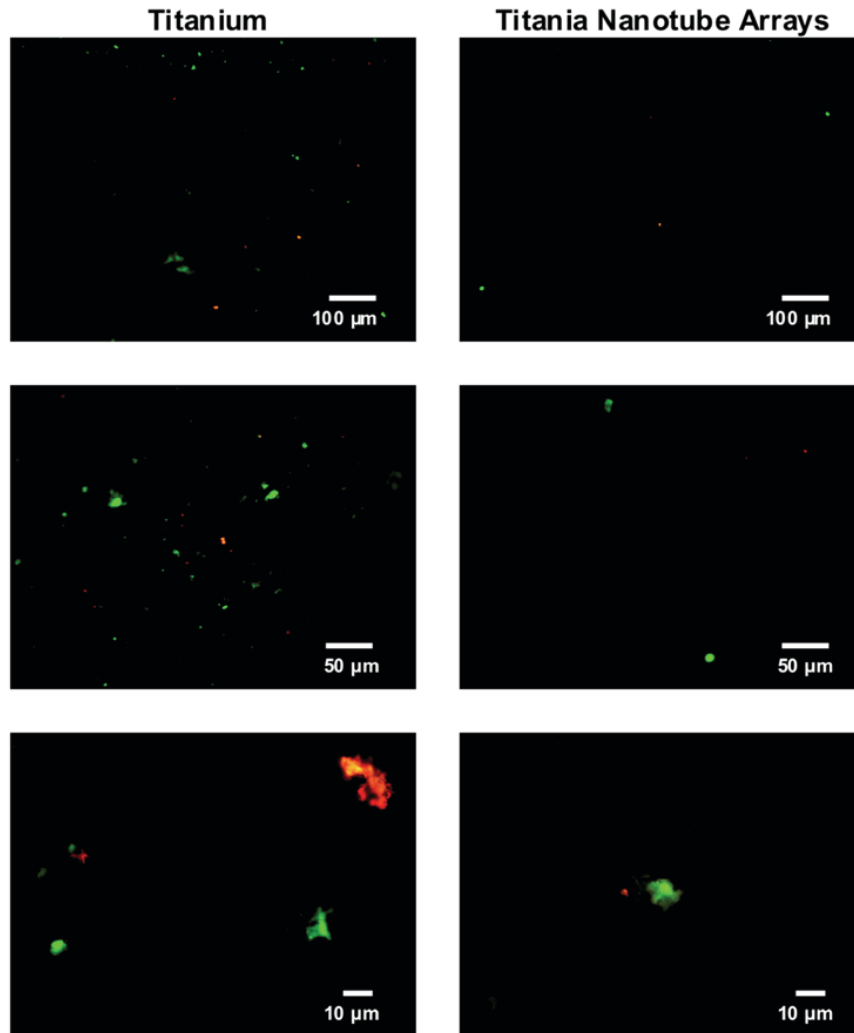


Figure 5.9 Representative fluorescence microscope images of monocytes/macrophages immuno-stained for CD14 and neutrophils immuno-stained CD16 on titania nanotube arrays and the control substrate after 2 hours of incubation in whole blood plasma. The images indicate a decrease in CD14 (TR-conjugated) and CD16 (FITC-conjugated) expression on titania nanotube arrays.

often derived from cellular interactions with their environment, and can be visualized by SEM imaging. Platelet and leukocyte adhesion, aggregation, morphology and subsequent interactions with the nanotube architecture were investigated after 2 hours of incubation

in whole blood plasma (See Figure 5.10). Low-magnification SEM images show a lesser degree of adhesion and aggregation of platelets and leukocytes on titania nanotube arrays

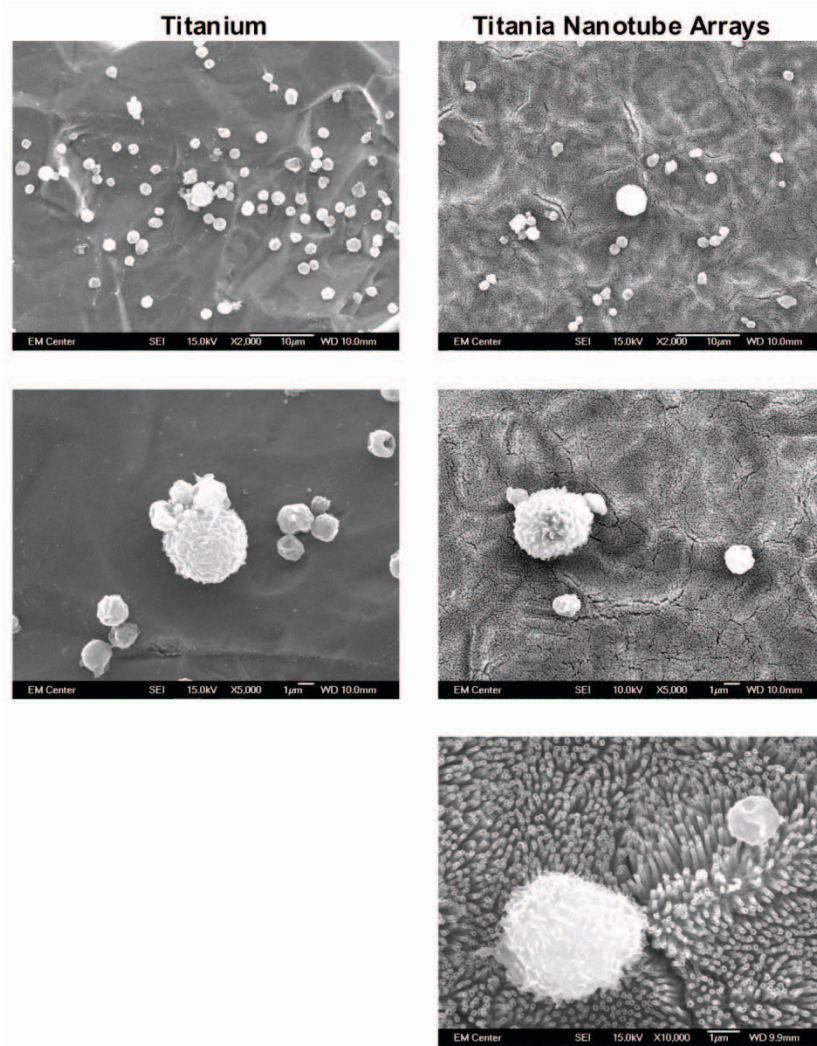


Figure 5.10 Representative SEM images of adhered platelets and leukocytes on titania nanotube arrays and the control substrate after 2 hours of incubation in whole blood plasma. The substrates were coated with a 10 nm layer of gold and imaged at 15kV. Images show a lower degree of platelet-leukocyte interaction and cellular aggregation on titania nanotube arrays. Neither titania nanotube arrays nor the control substrate showed increased platelet activation as a result of the material surface.

as compared to the control substrate. Higher magnification SEM images confirm previous immunofluorescence microscope images, indicating a reduction in platelet-leukocyte

complex formation on titania nanotube arrays as compared to the control substrate. These results show regions of localized platelet-leukocyte adhesion and aggregation on the control substrate. Surface-specific activation is not shown to be present in either platelets or leukocytes as a result of the surface architecture. However, the platelet-leukocyte interaction appears to promote increased platelet activation as indicated by the altered morphology and dendritic extensions on the control substrate. These results identify a reduction in cellular adhesion and aggregation on titania nanotube arrays as compared to the control substrate, indicating a lower propensity for thrombogenic effects on titania nanotube arrays.

The complement pathway enhances opsonization by antigen phagocytosis, which further attracts neutrophils and macrophages through chemotaxis, lyses foreign cells, clumps antigen and alters the molecular structures of viruses <sup>21</sup>. Overall, this pathway supports the innate immune system. The biocompatibility of implantable devices is directly related to the effect of complement activation on inflammatory reactions, specifically granulocyte (including neutrophils) and monocyte activation. The final complement pathway, often identified by the SC5b-9 complex, provides an accurate account of the amount of complement activation occurring on the biomaterial. In this study, a quantitative SC5b-9 EIA analysis was performed after 2 hours of incubation of titania nanotube arrays and the control substrates with whole blood plasma (**See Figure 5.11**). The results identify a nominal decrease in the degree of complement activation on titania nanotube arrays as compared to the control substrates. Thus, indicating a slightly reduced inflammatory response on titania nanotube arrays. These results are likely due to a combination of factors including the use of more physiologically relevant whole blood

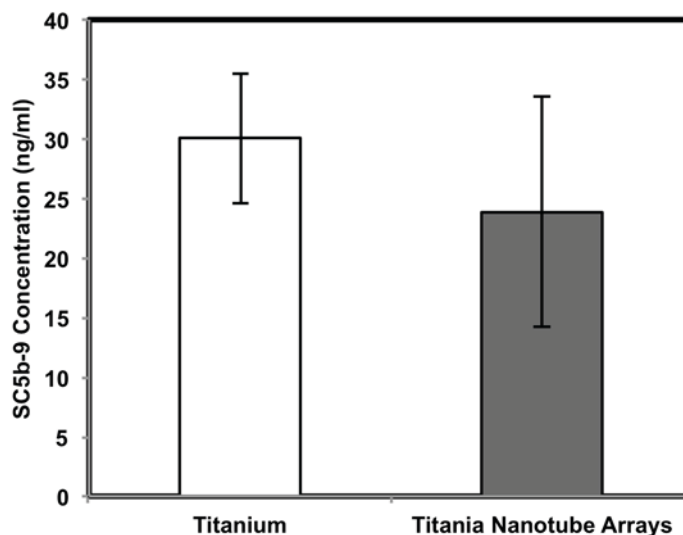


Figure 5.11 Complement activation measured by the amount of SC5b-9 activation on titania nanotube arrays and the control substrate after 2 hours of incubation in human plasma. The results indicate no significant difference in the level of complement activation on titania nanotube arrays as compared to the control substrate.

plasma rather than isolated platelets as shown in chapter 4.

A series of interactions are immediately triggered following implantation of a material that comes in contact with blood. The first stages of the clotting cascade and further blood coagulation is initiated upon primary contact between blood and a negatively charged surface. This interaction induces the intrinsic clotting pathway, involving factor XI, prekallikrein and high molecular weight kininogen (HMWK). The degree of contact activation on the titania nanotube arrays and the control substrate after 2 hours of incubation in whole blood plasma was determined colorimetrically by identifying the chromogenic kallikrein and further calculating the p-nitroaniline (pNA) release rate. Our results show a significant increase in contact activation on titania

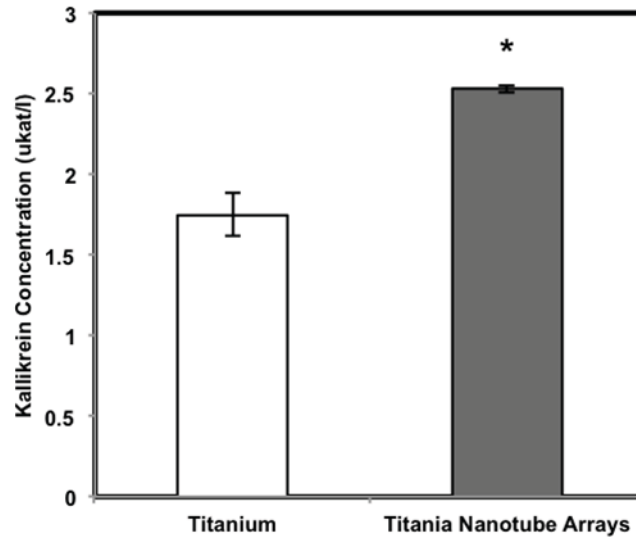


Figure 5.12 Contact activation measured by the amount of kallikrein on titania nanotube arrays and the control substrate after 2 hours of incubation in whole plasma. The results indicate a significant increase in contact activation on titania nanotube arrays compared to the control substrate (\*  $\rightarrow p < 0.05$ )

nanotube arrays as compared to the control substrate (See Figure 5.12). The amounts of kallikrein inhibition on titania nanotube arrays are statistically different than that on the control substrate ( $p < 0.05$ ). Since contact activation is a surface-mediated event, the rate of contact activation is proportional to the surface area contacted. In addition, the degree of contact activation has been shown to be related to the surface charge, with increased activation on negatively charged surfaces<sup>21</sup>. Therefore, the increase in contact activation shown on titania nanotube arrays is likely due to the increased surface area of nanotube architecture and altered surface charge. However, the contact activation may be directed for a specific application by adjusting the charge of the material surface, and precisely tuning the pore size, wall-thickness, and nanotube length by modifying the anodization parameters.

Following receptor initiated platelet stimulation and further activation, substances stored in platelet granules are released, often termed a platelet release reaction. Of these, PF-4 has been widely studied as an indicator of platelet activation. In order to quantify the amount of PF-4 released by alpha-granules in activated platelets, a commercially available human PF-4 ELISA kit was evaluated after 2 hours of incubation in whole blood plasma. The results showed no significant difference in the amount of PF-4 released on titania nanotube arrays as compared to the control substrate (**See Figure 5.13**), thus identifying a comparable degree of platelet release reaction on both substrates. Platelet activation and the subsequent release of biologically active compounds such as PF-4 have been shown to be influenced by the presence of leukocytes<sup>21</sup>. Therefore, the low degree of leukocyte adhesion is likely contributing to the low PF-4 expression on both substrates. A further reduction in PF-4 expression may be obtained by precisely tuning the nanotube dimensions.

The clotting cascade in blood is initiated by thrombin, a key protein responsible for platelet activation. Thrombin is an enzyme that transforms fibrinogen into fibrin monomers, which under normal conditions will form polymeric fibrin fibers to form a clot (thrombus) network. A clot is characterized by the strength of the fibrin mesh that entraps different components of the blood. Thus, in order to evaluate the pro-coagulant activity, fibrinogen adsorption was evaluated after 2 hours of incubation in whole blood plasma using commercially available human fibrinogen antigen assay. The substrates were incubated with whole blood plasma to allow for fibrinogen adhesion on the material surface. After 2 hours of incubation, the substrate-exposed plasma was assayed to determine the amount of fibrinogen that was not adsorbed on the material surface

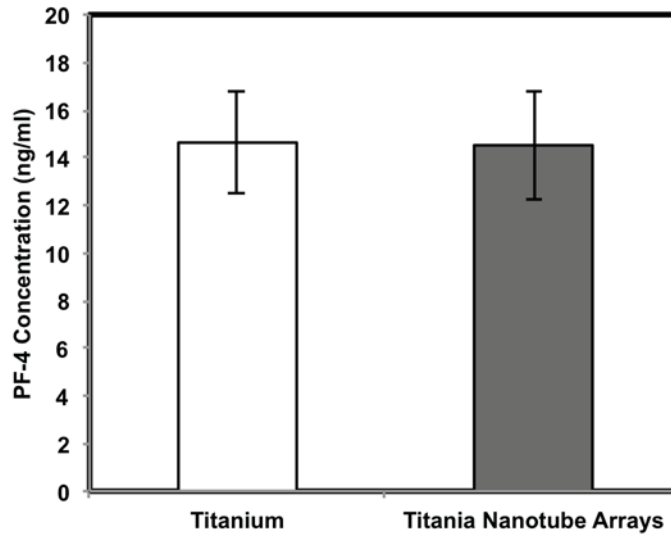


Figure 5.13 Platelet release reaction measured by the amount of PF-4 released from  $\alpha$ -granules within the platelets on titania nanotube arrays and the control substrate after 2 hours of incubation in whole blood plasma. The results indicate no significant difference in PF-4 concentration on titania nanotube arrays compared to the control substrate.

(See Figure 5.14). The results indicate a slight increase in the amount of fibrinogen in the substrate-exposed plasma on the titania nanotube arrays as compared to the control substrate. Thus, identifying a slightly lower amount of adsorbed fibrinogen on the titania nanotube arrays as compared to the control substrate. These results identify the nanotube architecture as a surface which reduces fibrin clot formation, further promoting biomaterial compatibility.

#### 5.4 Conclusion

In this study, the thrombogenic effects of titania nanotube arrays have been evaluated for their use as interfaces in blood-contacting implants. The ability to modulate the thrombogenicity of titanium surfaces may prove beneficial towards the long-term

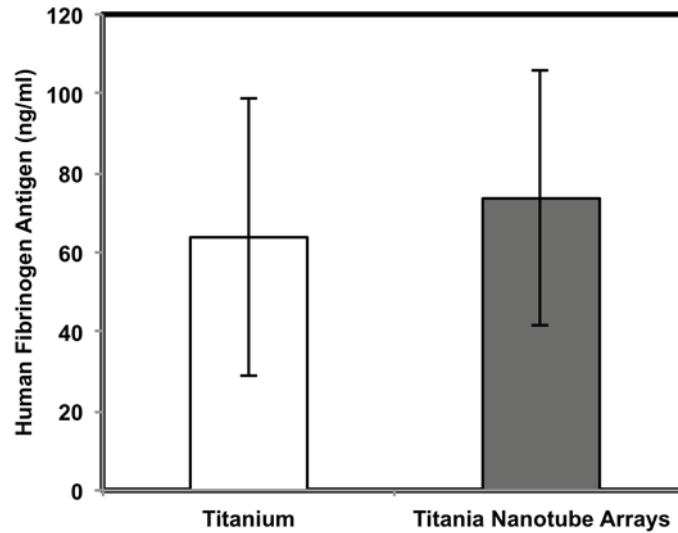


Figure 5.14 Human fibrinogen antigen concentration measured on titania nanotube arrays and the control substrate after 2 hours of incubation in whole blood plasma. The results indicate a slight increase in fibrinogen concentration in the substrate-exposed whole blood plasma on titania nanotube arrays compared to the control substrate.

Table 5.2 Summary of results identifying a decrease in thrombogenic effects on titania nanotube arrays as compared to biomedical grade titanium after 2 hours of contact with whole blood plasma.

Comparison between surfaces	Titanium	Titania Nanotube Arrays
Cell adhesion	↑	↓
Cytotoxicity		Similar
Platelet-leukocyte interaction	↑	↓
Complement activation	↑	↓
Contact activation	↓	↑
Platelet release reaction		Similar
Free fibrinogen		Similar

success of these implantable devices. The results presented here indicate a decrease in thrombogenic effects on titania nanotube arrays as compared to biomedical grade titanium after 2 hours of contact with whole blood plasma (See Table 5.2). Platelet/leukocyte adhesion, evaluated using fluorescence microscope images and the ImageJ software, indicate a significant decrease in the total number of platelets and leukocytes as well as the total cellular coverage on titania nanotube arrays as compared to the control substrate. In addition, SEM images and enzyme immunoassays show limited surface-induced activation and morphology on both substrates, however identifying the leukocyte-induced activation of platelets present only on the control substrates. A significant increase in contact activation was further identified on titania nanotube arrays, likely resulting from their increased surface area. Enzyme immunoassays indicate slightly decreased levels of complement activation and a slightly increased degree of free fibrinogen expressed on titania nanotube arrays showing a decrease in surface induced fibrin clot formation. These results suggest improved blood-compatibility of titania nanotube arrays, identifying this nanoarchitecture as a potential interface for promoting the long-term success of blood-contacting implants. The results presented here identify a physiologically relevant representation of the thrombogenic effects of titania nanotube arrays, as whole blood plasma was used rather than platelet rich plasma. Future studies are now directed towards understanding the effect of nanotube size on the immune response.

## 5.6 References

1. Jones, F. H., Teeth and bones: applications of surface science to dental materials and related biomaterials. *Surface Science Reports* **2001**, *42* (3-5), 75.
2. Rossi, S.; Tirri, T.; Paldan, H.; Kuntsi-Vaattovaara, H.; Tulamo, R.; Närhi, T., Peri-implant tissue response to TiO<sub>2</sub> surface modified implants. *Clinical Oral Implants Research* **2008**, *19* (4), 348-355.
3. Lin, Y.; Gallucci, G. O.; Buser, D.; Bosshardt, D.; Belser, U. C.; Yelick, P. C., Bioengineered Periodontal Tissue Formed on Titanium Dental Implants. *Journal of Dental Research* **2011**, *90* (2), 251-256.
4. Long, M.; Rack, H. J., Titanium alloys in total joint replacement--a materials science perspective. *Biomaterials* **1998**, *19* (18), 1621-1639.
5. Messinger, S. D., Incorporating the prosthetic: Traumatic, limb-loss, rehabilitation and refigured military bodies. *Disability & Rehabilitation* **2009**, *31* (25), 2130-2134.
6. Pezzin, L. E.; Dillingham, T. R.; MacKenzie, E. J.; Ephraim, P.; Rossbach, P., Use and satisfaction with prosthetic limb devices and related services. *Archives of Physical Medicine and Rehabilitation* **2004**, *85* (5), 723-729.
7. Wang, K., The use of titanium for medical applications in the USA. *Materials Science and Engineering: A* **1996**, *213* (1-2), 134.
8. Bhargava, D.; Bartlett, P.; Russell, J.; Liddington, M.; Tyagi, A.; Chumas, P., Construction of titanium cranioplasty plate using craniectomy bone flap as template. *Acta Neurochirurgica* **2010**, *152* (1), 173-176.
9. Eufinger, H.; Wehmöller, M., Individual Prefabricated Titanium Implants in Reconstructive Craniofacial Surgery: Clinical and Technical Aspects of the First 22 Cases. *Plastic and Reconstructive Surgery* **1998**, *102* (2), 300-308.
10. Wang, R.; Fenton, A., Titanium for prosthodontic applications: a review of the literature. *Quintessence Int* **1996**, *27* (6), 401-408.
11. Cáceres, D.; Munuera, C.; Ocal, C.; Jiménez, J. A.; Gutiérrez, A.; López, M. F., Nanomechanical properties of surface-modified titanium alloys for biomedical applications. *Acta Biomaterialia* **2008**, *4* (5), 1545-1552.
12. Niinomi, M., Mechanical biocompatibilities of titanium alloys for biomedical applications. *Journal of the Mechanical Behavior of Biomedical Materials* **2008**, *1* (1), 30-42.
13. Kang, N. V.; Pendegrass, C.; Marks, L.; Blunn, G., Osseocutaneous Integration of an Intraosseous Transcutaneous Amputation Prosthesis Implant Used for Reconstruction of a Transhumeral Amputee: Case Report. *The Journal of Hand Surgery* **2010**, *35* (7), 1130-1134.
14. Smith, C. M.; Roy, T. D.; Bhalkikar, A.; Li, B.; Hickman, J. J.; Church, K. H., Engineering a Titanium and Polycaprolactone Construct for a Biocompatible

- Interface Between the Body and Artificial Limb. *Tissue Engineering Part A* **2010**, *16* (2), 717-724.
15. Karjalainen, P. P.; Ylitalo, A.; Airaksinen, J. K.; Nammas, W., Five-Year Clinical Outcome of Titanium-Nitride-Oxide-Coated Bioactive Stent Implantation in a Real-World Population: A Comparison with Paclitaxel-eluting Stents: The PORI Registry. *Journal of Interventional Cardiology* **2011**, *24* (1), 1-8.
  16. Nammas, W., Titanium-nitride-oxide-coated bioactive stents: A novel evolution of stent technology. *International Journal of Cardiology* **2011**, *146* (3), 456-456.
  17. Speroni, S.; Briguglio, F.; Maridat, i. P.; Beretta, M.; Maiorana, C., Hard and soft tissue augmentation in implant surgery: a case report. *Minerva Stomatologica* **2011**, *60* (3), 123-31
  18. Anderson, J. M.; Rodriguez, A.; Chang, D. T., Foreign body reaction to biomaterials. *Seminars in Immunology* **2008**, *20* (2), 86.
  19. Jackson, C. M.; Nemerson, Y., Blood Coagulation. *Annual Review of Biochemistry* **1980**, *49* (1), 765-811.
  20. McGuigan, A. P.; Sefton, M. V., The influence of biomaterials on endothelial cell thrombogenicity. *Biomaterials* **2007**, *28* (16), 2547-2571.
  21. Gorbet, M. B.; Sefton, M. V. M. V., Biomaterial-associated thrombosis: roles of coagulation factors, complement, platelets and leukocytes. *Biomaterials* **2004**, *25* (26), 5681-5703.
  22. Curtis, A.; Wilkinson, C., Topographical control of cells. *Biomaterials* **1997**, *18* (24), 1573-1583.
  23. Das, K.; Bose, S.; Bandyopadhyay, A., Surface modifications and cell-materials interactions with anodized Ti. *Acta Biomaterialia* **2007**, *3* (4), 573-585.
  24. Decuzzi, P.; Ferrari, M., Modulating cellular adhesion through nanotopography. *Biomaterials* **2010**, *31* (1), 173-179.
  25. Hersel, U.; Dahmen, C.; Kessler, H., RGD modified polymers: biomaterials for stimulated cell adhesion and beyond. *Biomaterials* **2003**, *24* (24), 4385.
  26. Kasemo, B.; Lausmaa, J., Material-Tissue Interfaces: The Role of Surface Properties and Processes. *Environmental Health Perspectives* **1994**, *102* (ArticleType: primary\_article / Issue Title: Supplement 5: Biopersistence of Respirable Synthetic Fibers and Minerals / Full publication date: Oct., 1994 / Copyright © 1994 The National Institute of Environmental Health Sciences (NIEHS)), 41-45.
  27. Riehle, M., Biocompatibility: Nanomaterials for cell- and tissue engineering. *NanoBioTechnology* **2005**, *1* (3), 308-309.
  28. Vogel, V.; Sheetz, M. P., Cell fate regulation by coupling mechanical cycles to biochemical signaling pathways. *Current Opinion in Cell Biology* **2009**, *21* (1), 38-46.

29. Kunzler, T. P.; Huwiler, C.; Drobek, T.; Vörös, J.; Spencer, N. D., Systematic study of osteoblast response to nanotopography by means of nanoparticle-density gradients. *Biomaterials* **2007**, *28* (33), 5000-5006.
30. Liu, X.; Lee, P. y.; Ho, C. m.; Lui, V.; Chen, Y.; Che, C. m.; Tam, P.; Wong, K., Silver Nanoparticles Mediate Differential Responses in Keratinocytes and Fibroblasts during Skin Wound Healing. *ChemMedChem* **2010**, *5* (3), 468-475.
31. Khang, D.; Sato, M.; Price, R. L.; Ribbe, A. E.; Webster, T. J., Selective adhesion and mineral deposition by osteoblasts on carbon nanofiber patterns. Dove Medical Press: 2006; Vol. 1, pp 65-72.
32. Ramakrishna, F. Y. C. Y. X. M. K. S. W. S., Characterization of neural stem cells on electrospun poly(L-lactic acid) nanofibrous scaffold. *Journal of Biomaterials Science, Polymer Edition* **2004**, *15*, 1483-1497.
33. Ruckh, T. T.; Kumar, K.; Kipper, M. J.; Popat, K. C., Osteogenic differentiation of bone marrow stromal cells on poly(epsilon-caprolactone) nanofiber scaffolds. *Acta Biomater* **2010**, *6* (8), 2949-59.
34. La Flamme, K. E.; Popat, K. C.; Leoni, L.; Markiewicz, E.; La Tempa, T. J.; Roman, B. B.; Grimes, C. A.; Desai, T. A., Biocompatibility of nanoporous alumina membranes for immunoisolation. *Biomaterials* **2007**, *28* (16), 2638-2645.
35. Popat, K. C.; Leary Swan, E. E.; Mukhatyar, V.; Chatvanichkul, K.-I.; Mor, G. K.; Grimes, C. A.; Desai, T. A., Influence of nanoporous alumina membranes on long-term osteoblast response. *Biomaterials* **2005**, *26* (22), 4516-4522.
36. Bechara, S. L.; Judson, A.; Popat, K. C., Template synthesized poly([var epsilon]-caprolactone) nanowire surfaces for neural tissue engineering. *Biomaterials* **2010**, *31* (13), 3492-3501.
37. Porter, J. R.; Henson, A.; Ryan, S.; Popat, K. C., Biocompatibility and mesenchymal stem cell response to poly(epsilon-caprolactone) nanowire surfaces for orthopedic tissue engineering. *Tissue Eng Part A* **2009**, *15* (9), 2547-59.
38. Zhang, L.; Ramsaywack, S.; Fenniri, H.; Webster, T. J., Enhanced osteoblast adhesion on self-assembled nanostructured hydrogel scaffolds. *Tissue Eng Part A* **2008**, *14* (8), 1353-64.
39. Brammer, K. S.; Oh, S.; Gallagher, J. O.; Jin, S., Enhanced Cellular Mobility Guided by TiO<sub>2</sub> Nanotube Surfaces. *Nano Letters* **2008**, *8* (3), 786-793.
40. Martin, C. R.; Kohli, P., The emerging field of nanotube biotechnology. *Nat Rev Drug Discov* **2003**, *2* (1), 29-37.
41. Park, J.; Bauer, S.; von der Mark, K.; Schmuki, P., Nanosize and Vitality: TiO<sub>2</sub> Nanotube Diameter Directs Cell Fate. *Nano Letters* **2007**, *7* (6), 1686-1691.
42. Popat, K. C.; Leoni, L.; Grimes, C. A.; Desai, T. A., Influence of engineered titania nanotubular surfaces on bone cells. *Biomaterials* **2007**, *28* (21), 3188-3197.

43. Brammer, K. S.; Oh, S.; Cobb, C. J.; Bjursten, L. M.; Heyde, H. v. d.; Jin, S., Improved bone-forming functionality on diameter-controlled TiO<sub>2</sub> nanotube surface. *Acta Biomaterialia* **2009**, *5* (8), 3215.
44. Porter, J. R.; Henson, A.; Popat, K. C., Biodegradable poly(epsilon-caprolactone) nanowires for bone tissue engineering applications. *Biomaterials* **2009**, *30* (5), 780-8.
45. Bauer, S.; Park, J.; Faltenbacher, J.; Berger, S.; von der Mark, K.; Schmuki, P., Size selective behavior of mesenchymal stem cells on ZrO<sub>2</sub> and TiO<sub>2</sub> nanotube arrays. *Integrative Biology* **2009**, *1* (8-9), 525-532.
46. Oh, S.; Brammer, K. S.; Li, Y. S. J.; Teng, D.; Engler, A. J.; Chien, S.; Jin, S., Stem cell fate dictated solely by altered nanotube dimension. *Proceedings of the National Academy of Sciences* **2009**, *106* (7), 2130-2135.
47. Brunetti, V.; Maiorano, G.; Rizzello, L.; Sorce, B.; Sabella, S.; Cingolani, R.; Pompa, P. P., Neurons sense nanoscale roughness with nanometer sensitivity. *Proceedings of the National Academy of Sciences* **2010**, *107* (14), 6264-6269.
48. Buttiglieri, S.; Pasqui, D.; Migliori, M.; Johnstone, H.; Affrossman, S.; Sereni, L.; Wratten, M. L.; Barbucci, R.; Tetta, C.; Camussi, G., Endothelization and adherence of leucocytes to nanostructured surfaces. *Biomaterials* **2003**, *24* (16), 2731-2738.
49. Miller, D. C.; Thapa, A.; Haberstroh, K. M.; Webster, T. J., Endothelial and vascular smooth muscle cell function on poly(lactic-co-glycolic acid) with nanostructured surface features. *Biomaterials* **2004**, *25* (1), 53.
50. Park, J.; Bauer, S.; Schmuki, P.; von der Mark, K., Narrow Window in Nanoscale Dependent Activation of Endothelial Cell Growth and Differentiation on TiO<sub>2</sub> Nanotube Surfaces. *Nano Letters* **2009**, *9* (9), 3157-3164.
51. Peng, L.; Eltgroth, M. L.; LaTempa, T. J.; Grimes, C. A.; Desai, T. A., The effect of TiO<sub>2</sub> nanotubes on endothelial function and smooth muscle proliferation. *Biomaterials* **2009**, *30* (7), 1268-1272.
52. Curtis, A. S. G.; Gadegaard, N.; Dalby, M. J.; Riehle, M. O.; Wilkinson, C. D. W.; Aitchison, G., Cells react to nanoscale order and symmetry in their surroundings. *IEEE Trans Nanobioscience* **2004**, *3* (1), 61-5.
53. Mayer, A.; Vadon, M.; Rinner, B.; Novak, A.; Wintersteiger, R.; Fröhlich, E., The role of nanoparticle size in hemocompatibility. *Toxicology* **2009**, *258* (2-3), 139-147.
54. Fillion, T. M.; Xu, J.; Prasad, M. L.; Song, J., In vivo tissue responses to thermal-responsive shape memory polymer nanocomposites. *Biomaterials* **2011**, *32* (4), 985-991.
55. Barshtein, G.; Arbell, D.; Yedgar, S., Hemolytic Effect of Polymeric Nanoparticles: Role of Albumin. *NanoBioscience, IEEE Transactions on* **2011**, *PP* (99), 1-1.

56. Dash, B. C.; Réthoré, G.; Monaghan, M.; Fitzgerald, K.; Gallagher, W.; Pandit, A., The influence of size and charge of chitosan/polyglutamic acid hollow spheres on cellular internalization, viability and blood compatibility. *Biomaterials* **2010**, *31* (32), 8188-8197.
57. Lin, Y. S.; Haynes, C. L., Impacts of mesoporous silica nanoparticle size, pore ordering, and pore integrity on hemolytic activity. *J Am Chem Soc* **2010**, *132* (13), 4834-42.
58. Park, J. Y.; Gemmell, C. H.; Davies, J. E., Platelet interactions with titanium: modulation of platelet activity by surface topography. *Biomaterials* **2001**, *22* (19), 2671-2682.
59. Ainslie, K. M.; Tao, S. L.; Popat, K. C.; Daniels, H.; Hardev, V.; Grimes, C. A.; Desai, T. A., In vitro inflammatory response of nanostructured titania, silicon oxide, and polycaprolactone. *Journal of Biomedical Materials Research Part A* **2009**, *91A* (3), 647-655.
60. Ainslie, K. M.; Tao, S. L.; Popat, K. C.; Desai, T. A., In vitro Immunogenicity of Silicon-Based Micro- and Nanostructured Surfaces. *ACS Nano* **2008**, *2* (5), 1076-1084.
61. Smith, B. S.; Yoriya, S.; Grissom, L.; Grimes, C. A.; Popat, K. C., Hemocompatibility of titania nanotube arrays. *Journal of Biomedical Materials Research Part A* **2010**, *95A* (2), 350-360.
62. Ruan, C.; Paulose, M.; Varghese, O. K.; Mor, G. K.; Grimes, C. A., Fabrication of Highly Ordered TiO<sub>2</sub> Nanotube Arrays Using an Organic Electrolyte. *The Journal of Physical Chemistry B* **2005**, *109* (33), 15754-15759.
63. Smith, B. S.; Yoriya, S.; Johnson, T.; Popat, K. C., Dermal fibroblast and epidermal keratinocyte functionality on titania nanotube arrays. *Acta Biomaterialia* **2011**, *7* (6), 2686-2696.
64. Roy, P.; Berger, S.; Schmuki, P., TiO<sub>2</sub> Nanotubes: Synthesis and Applications. *Angewandte Chemie International Edition* **2011**, *50* (13), 2904-2939.
65. Sperling, C.; Schweiss, R. B.; Steller, U.; Werner, C., In vitro hemocompatibility of self-assembled monolayers displaying various functional groups. *Biomaterials* **2005**, *26* (33), 6547-6557.
66. Gorbet, M. B.; Sefton, M. V., Leukocyte activation and leukocyte procoagulant activities after blood contact with polystyrene and polyethylene glycol-immobilized polystyrene beads. *Journal of Laboratory and Clinical Medicine* **2001**, *137* (5), 345-355.

## CHAPTER 6

### MODULATING IMMUNE RESPONSES ON TITANIA NANOTUBE ARRAYS

#### 6.1 Introduction

For the 8-10% (20-25 million people) of Americans that have implanted biomedical devices, biomaterial failure and the need for revision surgery is a critical concern<sup>1,2</sup>. In fact, the biggest shortcoming has been the lack of complete biointegration of materials<sup>3,4</sup>. Biocompatibility can be defined as the ability of a material to coexist with natural tissue or organs without initiating harm. The degree of biocompatibility may therefore be determined by characterizing the extent of an inflammatory reaction acting to neutralize or sequester the implanted biomedical device<sup>5</sup>. The physiological response to implanted biomaterials has been well documented, identifying a complex cascade of events, which often result in a foreign body reaction on the surface of the biomaterial and in the surrounding tissue<sup>1</sup>. The successful integration of long-term implantable devices is highly dependent on the early events of tissue/material interaction, either promoting fibrosis (foreign body reaction) or a wound healing response (extracellular matrix production and vasculature)<sup>6</sup>. Immediately following implantation, biomaterials initiate immunological events in the form of protein adsorption, followed by platelet adhesion/activation, which recruits immune cells (monocytes and neutrophils) to the site of injury through biochemical cues. This inflammatory cell infiltration subsequently leads to acute and chronic inflammation, promoting additional cellular activation (monocyte differentiation into macrophages), apoptosis and intercellular communication (cytokine/chemokine). This cascade of events perpetuates cellular infiltration and

activation (lymphocytes and fibroblasts) initiating granulocyte recruitment. The resulting foreign body reaction (foreign body giant cells, FBGC) and fibrosis potentially leads to fibrous encapsulation and complete implant rejection<sup>3,4</sup>. The cells required for healthy tissue regeneration are compromised through this adverse immune response, thus hindering the natural wound healing response and the long-term success of implantable biomedical devices such as intra-osseous implants<sup>7,8</sup> and stent grafts<sup>9,10</sup>. In order to better understand this critical stage in biomaterial integration, a great need exists for a more in-depth look at the mechanisms behind immune-biomaterial interactions.

Titanium and titanium-based alloys have been the most widely utilized materials for use in implantable biomedical devices since the mid-1900s, when titanium was found to possess tissue-compatible properties<sup>11,12</sup>. Clinical applications for these materials include dental<sup>13,14</sup>, craniofacial and prosthetic implants<sup>15-18</sup>, cardiovascular stents<sup>19</sup> and hard and soft tissue grafts<sup>20</sup>. The two main factors contributing to the widespread use of titanium in biomedical implants include their impressive mechanical and biocompatible properties<sup>12,21</sup>. In addition, titanium reacts naturally with atmospheric oxygen to produce a passivating oxide layer on its surface, termed titania. Protecting the non-toxic metal from environmental factors, titania creates a hard and scratch-resistant material surface, improves corrosion and wear resistance, enables a low coefficient of friction and provides a favorable biocompatible interface for tissue integration<sup>17,22</sup>. Although titanium and titanium-based alloys are among the better choices for biomedical implants, to date, all long-term implanted biomaterials have the potential of initiating physiological events shown to promote poor tissue/material integration<sup>3,4</sup>.

The human body is composed of a hierarchy of biological structures from the smallest molecule to the largest tissue. Therefore, when micro-scale cells interact with their macro-scale environment, they do so through countless nano-scale topographies, biochemical cues and protein interactions. In fact, cells are in constant interaction with their surroundings, comprised of nano-scale subcellular structures including fibers, pits, pores and protrusions. Thus, identifying a need for better understanding the effect of topographical (micro- and nano-scale)<sup>23-26</sup> or biochemical cues (biofunctional)<sup>27, 28</sup> on cellular functionality. Recent technological advances have enabled the fabrication of nano-engineered biomaterial surfaces with the goal of providing relevant nanoscale cues. Studies have identified enhanced integration of various cell types on nanoparticles<sup>29</sup>, nanofibers<sup>30, 31</sup>, nanopores<sup>32, 33</sup>, nanowires<sup>34, 35</sup>, nanostructured hydrogels<sup>36</sup> and nanotube arrays<sup>37, 38</sup>. Of these nanotopographical fabrications, current research has correlated favorable cellular functionality with nanotube array interfaces. Previous studies on titania nanotube arrays have demonstrated enhanced osseointegration<sup>39, 40</sup>, improved endothelialization<sup>41</sup>, altered hemocompatibility and thrombogenicity<sup>42</sup>, preferential fibroblast orientation<sup>43</sup>, increased dermal matrix deposition<sup>43, 44</sup> and selective behavioral responses of stem cells<sup>45, 46</sup>. In addition, the nanotube arrays can be filled with drugs such as antibiotics or growth factors to thwart infection and encourage tissue integration respectively, through a localized delivery of drugs<sup>47, 48</sup>. However, prior to the application of this promising nano-architecture in implantable devices, it is imperative to obtain a better understanding of the effect of the nanotube interface on the immune reaction.

The ability to modulate the immune reaction at the tissue/biomaterial interface is critical for the long-term success of implantable devices. An evaluation of the immune response *in vitro* can be accurately represented through whole blood lysate, present in less than 1% of whole human blood. This immune-rich portion of blood is mainly comprised of white blood cells (leukocytes) and platelets (thrombocytes), which play a fundamental role in the human immune response and the foreign body reaction (FBR), potentially leading to poor implant integration *in vivo*. However, limited studies exist on interaction of immune cells with titania nanotube arrays. Thus, in this study we have evaluated the effect of titania nanotube arrays (diameter: 170 nm, length: 1  $\mu\text{m}$ ) on the physiologically relevant whole human blood lysate, in order to better understand the mechanisms behind immune/nano-biomaterial interactions. Immune cell viability, adhesion, proliferation, morphology, nitric oxide release and cytokine/chemokine expression were investigated after 2 hours, 2 and 7 days of culture using a cell viability assay, fluorescence microscope imaging, scanning electron microscopy (SEM), a Griess reagent kit and cytokine bead assays (CBA) on titania nanotube arrays as compared to biomedical grade titanium (control). In order to promote the long-term health of tissue-biomaterial integration, a reduction in adverse immune reactions is imperative.

## **6.2 Experimental Methods**

### **6.2.1 *Fabrication and Characterization of Titania Nanotube Arrays***

Titania nanotube arrays were fabricated using a simple anodization process, described in detail in chapter 2<sup>49, 50</sup>. Biomedical grade titanium (as-received, non-

polished) surfaces were used as controls. The nanotube architecture was examined for uniformity and repeatability using SEM imaging.

### **6.2.2 Whole Human Blood Lysate Isolation**

Whole human blood was acquired through venopuncture from healthy individuals. Blood was drawn into standard 6 ml vacuum tubes coated with ethylenediaminetetraacetic acid (EDTA) for its anti-coagulant properties. The first tube was discarded to account for the skin plug and locally activated platelets, resulting from the needle insertion. Whole human blood was mixed with Gey's balanced salt solution (150 mM of  $\text{NH}_4\text{Cl}$  and 10 mM of  $\text{KHCO}_3$ ) at a ratio of 1:2 and placed into a 15 ml conical tube (See Figure 6.1). The blood: Gey's mixture was set onto a rocker plate for 5-10 min at RT, to allow for the red blood cells (RBCs) to isotonicly lyse. The mixed vials were centrifuged at 300 g's for 5 min at 4 °C, and the supernatant was discarded. The cell pellet was resuspended in 5 ml of Gey's solution and immediately centrifuged at 300 g's for 5 min at 4 °C to lyse all remaining RBCs. The supernatant was discarded. This was followed by washing the cell pellet (2×) by resuspension in Hanks Buffered Salt Solution (without Ca and Mg, Sigma) and centrifuged at 300 g's for 5 min at 4 °C. The supernatant was discarded after each wash. The cell pellets from 3 vials were combined by resuspension in cold RPMI medium (Sigma) supplemented with 10% FBS and 1% penicillin/streptomycin. The cell density was determined by trypan blue dye exclusion, using a hemocytometer. Cell suspensions were further diluted in RPMI medium to obtain a concentration of  $2 \times 10^6$  cells/ml. Isolated cells were seeded within 4 hours of removal from the body.

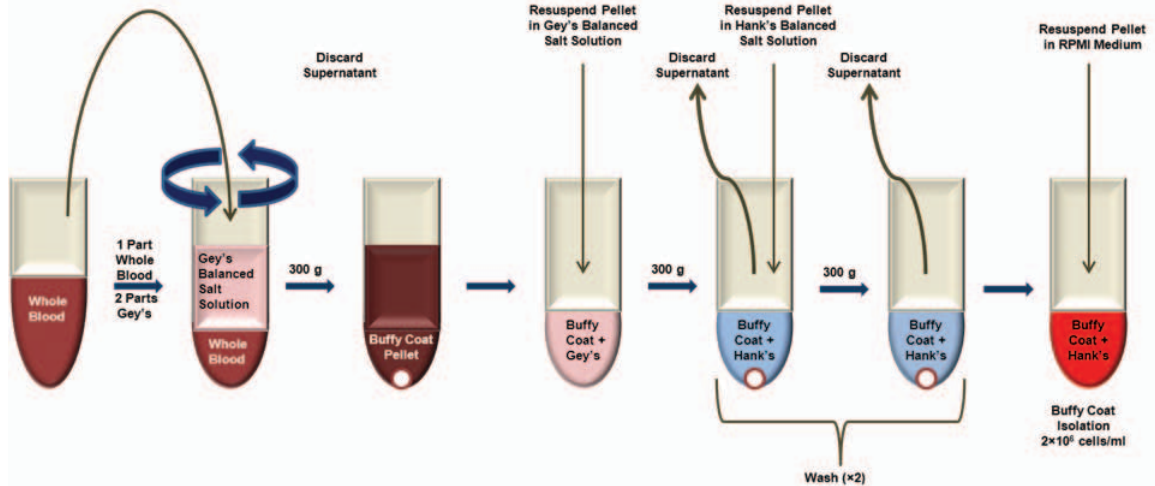


Figure 6.1 Schematic of the isolation of whole human blood lysate.

### 6.2.3 Incubation of Whole Blood Lysate on Titania Nanotube Arrays

In order to evaluate the immune response *in vivo*, the cells were seeded on titania nanotube arrays and biomedical grade titanium (0.5 cm × 0.5 cm) in a 24-well plate. Prior to seeding, all substrates were sterilized by incubation in 70% ethanol for 30 min, washed (2×) with PBS, air dried and subjected to 30 min of *uv* exposure. Immune cells were seeded at a density of  $2 \times 10^6$  cells/ml. The substrates were incubated at 37°C and 5% CO<sub>2</sub> in 500 μL of cell-rich media and investigated for viability, adhesion, proliferation, morphology, NO release, morphology and cytokine/chemokine expression after 2 hours, 2 and 7 days of culture. Additional substrates were incubated with 2 μg/ml lipopolysaccharide (LPS from *E. coli*, Sigma) in cell-rich media, as a positive cellular control, in order to evaluate the effect of LPS on cell/nano-biomaterial interaction. The substrates incubated in LPS enriched media were investigated for cytokine/chemokine production using CBA assays, performed by flow cytometry after 2 hours, 2 and 7 days of culture.

#### **6.2.4 Viability of Whole Blood Lysate on Titania Nanotube Arrays**

Cellular viability was characterized using a commercially available Methylthiazol Tetrazolium (MTT) assay kit (Sigma) after 2 hours, 2 and 7 days of culture. Prior to measuring the MTT activity, un-adhered cells were removed by aspirating the cell rich media from the substrates followed by two gentle rinses with PBS. The substrates were then transferred to a new 24-well plate and the standard manufacturer protocol was followed. In brief, the substrates were incubated in 10% MTT solution in PBS for 3 hours and 45 min at 37°C and 5% CO<sub>2</sub>. The resulting formazon crystals were disrupted by adding a mixture of 10% Triton-X in MTT solvent to each substrate in the amount equal to the incubated MTT solution in PBS. The absorbance of the solution was measured at a wavelength of 570 nm using a plate reader (BMG Labtech). The net absorbance was calculated by subtracting the background absorbance at a wavelength of 690 nm to measure the amount of viable cells adhered on the substrates.

#### **6.2.5 Adhesion and Proliferation of Whole Blood Lysate on Titania Nanotube Arrays**

Cellular adhesion and proliferation was characterized by fluorescently staining adhered cells with 5-chloromethylfluorescein diacetate (CellTracker green CMFDA, Invitrogen) live stain and 4'6-diamidino-2-phenylindole-dihydrochloride (DAPI, Invitrogen) nucleus stain after 2 hours, 2 and 7 days of culture. Prior to staining, un-adhered cells were removed by aspirating the cell rich media from the substrates followed by two gentle rinses with PBS. The substrates were then transferred to a new 24-well plate and incubated with 3 μM CMFDA in PBS for 40 min at 37°C and 5% CO<sub>2</sub>. They were then placed into warm RPMI medium and incubated for 30 min at 37°C and 5%

CO<sub>2</sub>. The substrates were fixed in 3.7wt% formaldehyde in PBS for 15 min at RT, followed by 3 washes (5 min per wash) in PBS at RT. Adhered cells were further permeabilized by incubation in 1% Triton-X in PBS for 3 min and rinsed in PBS. The substrates were incubated in DAPI nuclear stain (300 nM) for 5 min at RT, rinsed in PBS and imaged with a fluorescence microscope (Zeiss) using 62 HE BP 474/28 green filter and 49 DAPI BP 445/50 blue filter. The number of cells adhered on the substrates was determined by counting the number of stained nuclei from the DAPI fluorescence images.

#### ***6.2.6 Cytoskeletal Organization of Whole Blood Lysate on Titania Nanotube Arrays***

Cytoskeletal organization was evaluated using fluorescence microscope imaging after 2 hours and 7 days of culture. The same samples that were stained for DAPI were concurrently stained for F-actin with rhodamine-conjugated phalloidin (70 nM, Cytoskeleton Inc.). Following permeabilization and prior to DAPI staining, substrates were incubated in rhodamine-conjugated phalloidin (70 nM) in PBS for 20 min at RT. The substrates were imaged with a fluorescence microscope using 62 HE BP 585/35 red filter.

#### ***6.2.7 Morphology of Whole Blood Lysate on Titania Nanotube Arrays***

Cellular morphology was investigated using SEM imaging after 2 hours, 2 and 7 days of culture. Prior to imaging, un-adhered cells were removed by aspirating the cell rich media from the substrates followed by two gentle rinses with PBS. The substrates were then transferred to a new well plate where the adhered cells were fixed and further

dehydrated on the substrate surface. The cells were incubated in a solution of primary fixative (3% glutaraldehyde (Sigma), 0.1 M sodium cacodylate (Polysciences) and 0.1 M sucrose (Sigma)) for 45 min. The substrates were then incubated in a secondary fixative (primary fixative without glutaraldehyde) for 10 min. They were subsequently dehydrated by incubation in consecutive solutions of increasing ethanol concentrations (35%, 50%, 70% and 100%) for 10 min each. Further dehydration was accomplished by incubating the substrates in hexamethyldisilazane (HMDS, Sigma) for 10 min. They were then air dried and stored in a desiccator until further imaging with SEM. The substrates were coated with a 10 nm layer of gold prior to imaging at 15 kV.

#### **6.2.8 *Nitric Oxide Release on Titania Nanotube Arrays***

The cell-released nitric oxide (NO) was detected using a commercially available Griess reagent kit (Biotium Inc.) after 2 hours, 2 and 7 days of culture. The standard manufacturer protocol was followed. In brief, substrate-exposed supernatant was incubated in a mixture of Griess reagent and DI water for 30 min at RT. The samples were photometrically measured at a wavelength of 548 nm using a plate reader (BMG Labtech). The absorbance values quantified the effect of titania nanotube arrays on the degree of NO release.

#### **6.2.9 *Cytokine and Chemokine Expression***

Human inflammatory cytokines/chemokines were detected using commercially available cytometric bead array (CBA, BD Biosciences) human plex flex sets after 2 hours, 2 and 7 days of culture. Human inflammatory cytokine/chemokine expression was

identified through the presence of TNF, IFN- $\gamma$ , TGF- $\beta$ 1, MIP-1 $\beta$ , MCP-1, IL-1 $\beta$ , IL-6, IL-8, IL-10 and IL-12p70 on the substrates with and without LPS. All immunoassays were run together. The standard manufacturer protocol was followed. In brief, substrate-exposed supernatant was removed at the designated time points and stored at -80 °C until further testing by CBA analysis using flow cytometry. Human flex set standards ( $\times 10$ ), human soluble protein flex set capture beads ( $\times 100$ ) and PE detection reagents ( $\times 100$ ) were prepared as directed, such that each analyte was added as 1/10<sup>th</sup> of the final calculation. The procedure was initiated by adding the standards and samples (100  $\mu$ l) to capture beads (50  $\mu$ l) in a 96-well plate. The mixture was gently vortexed for 15 sec and incubated for 1 hour at RT. Following incubation, PE detection reagent (50  $\mu$ l) was added to each well. The mixture was gently vortexed for 15 sec and incubated in a dark environment for 2 hours at RT. The samples were washed by adding the manufacturer provided wash buffer (100  $\mu$ l). The well plates were centrifuged at 1040 rpm for 3 min to pelletize the cell/bead population in the supernatant. The supernatant (200  $\mu$ l) was gently discarded by aspiration, making sure not to disrupt the cell/bead pellet on the bottom of the wells. Immediately following the resuspension of the cell/bead pellet in wash buffer (150  $\mu$ l), the cell/bead-rich samples were transferred to flow tubes (VWR 83009-678) and further tested by flow cytometry. Data was acquired on a FACS Auto II bioanalyzer. The standard samples were used to establish gated regions for the identification of each cytokine/chemokine. The results were analyzed using FCAP Array Software and Microsoft Office Excel Data Analysis Software.

### **6.2.10 Statistical Analysis**

Each experiment was reconfirmed on at least three different substrates from at least three different blood populations ( $n_{\min} = 9$ ). Further, all of the quantitative results were evaluated using an analysis of variance (ANOVA). Statistical significance was considered at  $p < 0.05$ . During the analysis, variances among each group were not assumed to be equal and a two sample t-test approach was utilized to test the significance between titania nanotube arrays and the control substrate. This analysis was conducted using the Microsoft Office Excel Data Analysis Software.

## **6.3 Results and Discussion**

Limited tissue-biomaterial integration and biomaterial failure often result from adverse immune responses in the form of a fibrous encapsulation, acting to wall off the implant from the natural tissue. Recent studies have identified titania nanotube arrays as potential biomimetic, biocompatible and non-biodegradable interfaces for implantable devices; making this specific nanoarchitecture appealing for use in implants. However, limited studies have investigated one of the most critical events in cell/nano-biomaterial integration, by evaluating the biomaterial generated immune response. After only 2 hours following implantation, monocytes and neutrophils adhere to the biomaterial surface and begin releasing factors of communication. By day 2 however, adverse immune reactions are visible through immune cell activation, differentiation (monocytes to macrophages) and cytokine and chemokine expression, promoting additional cellular infiltration. Between 7 and 10 days of incubation, the formation of fused cells (3+ nuclei) and FBGCs may be present on the biomaterial surface, leading to further fibrous

encapsulation and potential implant rejection. Thus, in this study we have evaluated the short- and long-term cellular immune response on titania nanotube arrays as compared to biomedical grade titanium.

Immobilized, vertically oriented and high aspect ratio nanotubes were fabricated after 24 hours of anodization at 60 V on titanium substrates, as described elsewhere<sup>39, 43, 50</sup>. The nanotube architecture was examined for uniformity and repeatability using SEM imaging (See **Figure 6.2**). The results indicate nanotube dimensions of approximately 170 nm in diameter and 1  $\mu\text{m}$  in length. Nanotube fabrication was performed using a simple anodization process, as previously described.

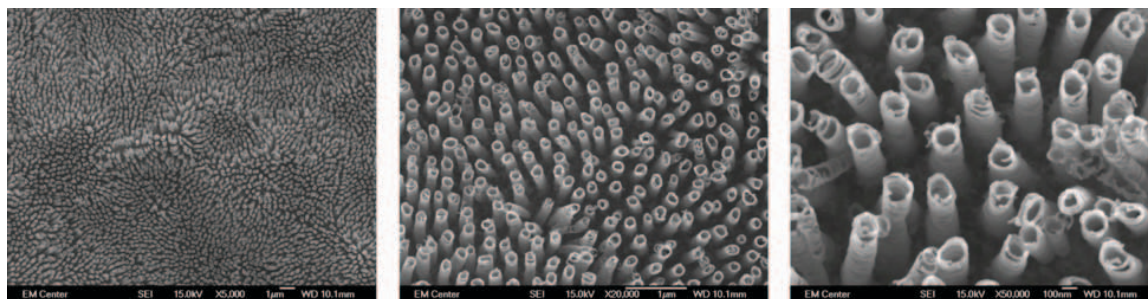


Figure 6.2 Representative SEM images (5,000 $\times$ , 20,000 $\times$ , 50,000 $\times$  magnification) showing the nanoarchitecture of titania nanotube arrays fabricated using an anodization technique. Titania nanotube arrays were coated with a 10 nm layer of gold and imaged at 15kV.

The cell viability was characterized using a commercially available MTT assay kit after 2 hours, 2 and 7 days of culture (See **Figure 6.3**). In this colorimetric assay, the mitochondrial succinate dehydrogenase, only present in metabolically active cells, convert methylthiazol tetrazolium into an insoluble form. Spectrophotometric

measurements of the net absorbance were calculated to determine the concentration of viable cells on the substrates. These results indicate a significant decrease in viable immune cells adhered on both substrates from 2 hours to 2 days of culture. In addition, a significantly reduced amount of immune cells are present on titania nanotube arrays as compared to the control substrate at all time-points. The results clearly indicate a significant decrease in both short- and long-term viability of immune cells on titania nanotube arrays as compared to the control substrate.

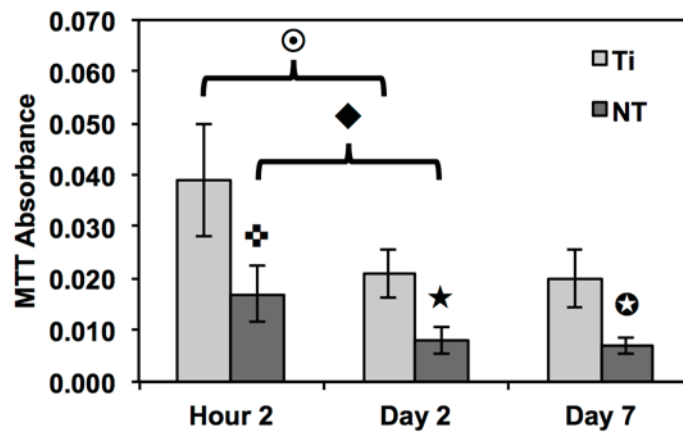


Figure 6.3 Cellular viability measured using an MTT assay to identify adhered immune cells. The results indicate a significant decrease in the number of adhered immune cells on titania nanotube arrays as compared to biomedical grade titanium. (□, □, □, □, □, ◆ →  $p < 0.05$ )

The immune response, initiated immediately upon implantation of a biomaterial, is elicited by cellular interactions at the biomaterial interface. Thus, cellular adhesion and proliferation are key factors in determining the fate of a successful implant. In this study, we have investigated the short- and long-term adhesion and proliferation of

immune cells on titania nanotube arrays using fluorescence microscope imaging of CMFDA live stain and DAPI nucleus stain, in order to better understand the immune/nano-biomaterial interaction (See **Figure 6.4(a)**).

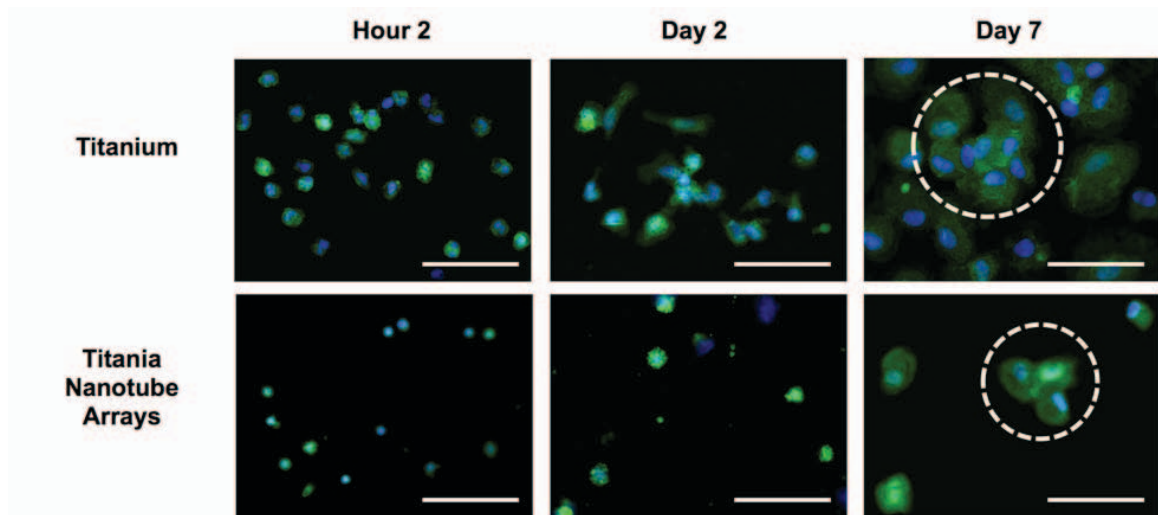


Figure 6.4 (a) Representative fluorescence microscope images of adhered monocytes, macrophages, neutrophils and foreign body giant cells (FBGC, 3 or more nuclei) stained with DAPI (nucleus) and CMFDA (cytoplasm) on titania nanotube arrays and biomedical grade titanium after 2 hours, 2 and 7 days of incubation in human whole blood lysate. The images show a decrease in cellular adhesion, fusion and the formation of FBGCs (indicated by the circled regions) on titania nanotube arrays. The scale bar represents 50  $\mu\text{m}$ .

After only 2 hours of culture, fluorescence images identify small and unactivated monocytes and neutrophils adhered on both substrates. Due to the lack of alteration in cell size and subsequent interaction with the material surface, it is immediately apparent that the adhered monocytes and neutrophils have not yet become activated or begun to differentiate. Thus, the results show a decrease in adhered cells on titania nanotube

arrays as compared to the control substrate. After 2 and 7 days of culture, results indicate a reduction in the number of adhered cells on both substrates. These findings are likely the result of either the short lifespan of monocytes or premature cell death due to *ex vivo* conditions. In addition, the adhered cells express heightened levels of activation after 2 and 7 days of culture, as shown by increases in size. However, when comparing the titania nanotube arrays and control substrates, a clear difference is apparent. The results indicate a reduction in immune cell adhesion on titania nanotube arrays as compared to the control substrate. This decrease in cell adhesion continues on titania nanotube arrays between days 2 and 7, further resulting in limited cell-cell interaction and minimal cellular elongation. In contrast, images of the control substrates identify a substantial increase in cell-cell interaction and cellular elongation after 2 and 7 days of culture. Therefore, the monocytes adhered on the control substrates after only 2 hours of culture clearly morph into their activated counterpart, macrophages which exhibit increased diameter, more expansive integration and altered structure. Images of the control substrates after 7 days of culture clearly identify cellular fusion and the production of foreign body giant cells (FBGCs). The formation of FBGCs has been associated with the inability of macrophages to remove or destroy a biomaterial, which leads them to fuse in a gesture of “frustrated phagocytosis.” Multiple nuclei are readily apparent within the cell conglomerates of FBGCs, identifying the first stages of fibrous encapsulation. Fluorescence images of titania nanotube arrays show a moderate initial adhesion followed by an extreme reduction in immune cell proliferation, while the control substrate promotes a strong immune cell adhesion early on, leading to FBGCs and an overall adverse immune response <sup>51</sup>. The total number of adhered cells was further

identified using the fluorescence images and the ImageJ software after 2 hours, 2 and 7 days of culture (See **Figure 6.4(b)**). The results show a significant reduction in cell count on titania nanotube arrays as compared to the control substrate after all time points. Thus, further identifying a vastly reduced short- and long-term immune response in terms of adhesion and proliferation on titania nanotube arrays as compared to the control substrate.

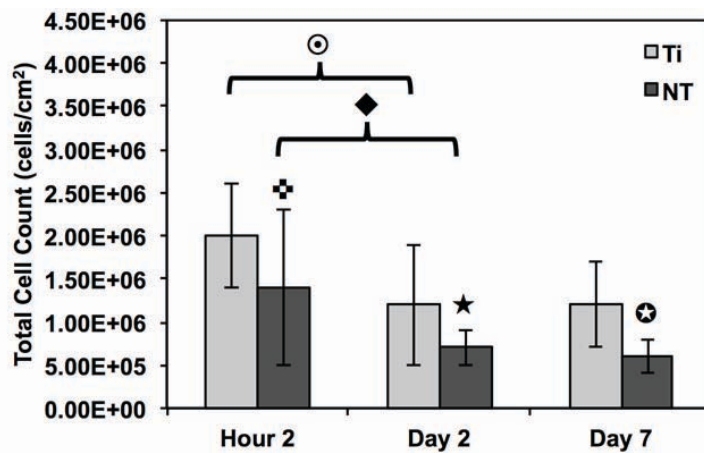


Figure 6.4 (b) Cell count calculated using the fluorescence images and the ImageJ software. The results indicate a significant decrease in the number of adhered immune cells on titania nanotube arrays as compared to biomedical grade titanium.

(□, □, □, □, ◆, ★ →  $p < 0.05$ )

Composed of microfilaments, microtubules and intermediate filaments, the cytoskeleton plays a quintessential role as the structural support within the cell membrane and acts as the barrier between the cellular components and the extracellular world. Cellular activation often perpetuates cytoskeletal reorganization, facilitating fundamental events such as cell division, motility, protein trafficking and secretion. In addition, this

essential component enables cell-cell and cell-ECM communication. Thus, the effect of titania nanotube arrays was characterized by cytoskeletal organization after 2 hours and 7 days of culture using fluorescence microscope imaging by evaluating substrates stained with rhodamine-conjugated phalloidin (F-actin stain) (See **Figure 6.5**).

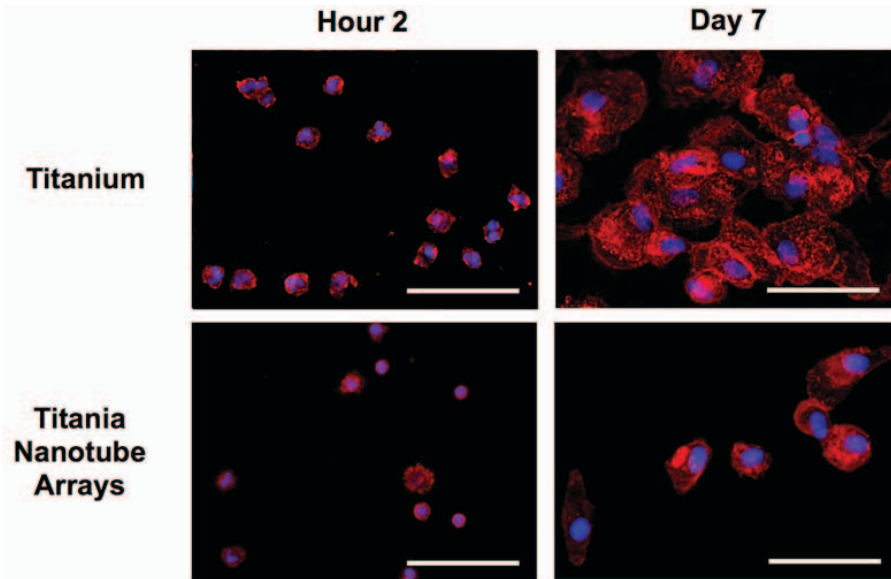


Figure 6.5 Representative fluorescence microscope images of adhered monocytes, macrophages, neutrophils and foreign body giant cells (3 or more nuclei) stained with DAPI (nucleus) and rhodamine-conjugated phalloidin (actin, cytoskeleton) on titania nanotube arrays and biomedical grade titanium after 2 hours, 2 and 7 day of incubation in human whole blood lysate. The images indicate a decrease in immune cell adhesion, activation and fusion on titania nanotube arrays. The scale bar represents 50  $\mu\text{m}$ .

The results clearly show limited cellular activation and cytoskeletal reorganization after 2 hours of culture on both substrates. After 7 days of culture, fluorescence images identify extremely reduced adhesion, activation and cell-cell interaction on titania nanotube arrays as compared to the control substrates. In addition, the cell-cell interaction occurring on

the control substrate shows immune cell fusion as seen by the interlinking of multiple cell cytoskeletons. The formation of FBGC's on the control substrates indicates the potentially adverse immune response elicited by biomedical grade titanium, unlike that seen on the titania nanotube arrays.

Cellular morphology is a strong indicator of cell/biomaterial integration, and has therefore been evaluated by SEM imaging to better understand the immune response elicited by titania nanotube arrays (See **Figure 6.6**).

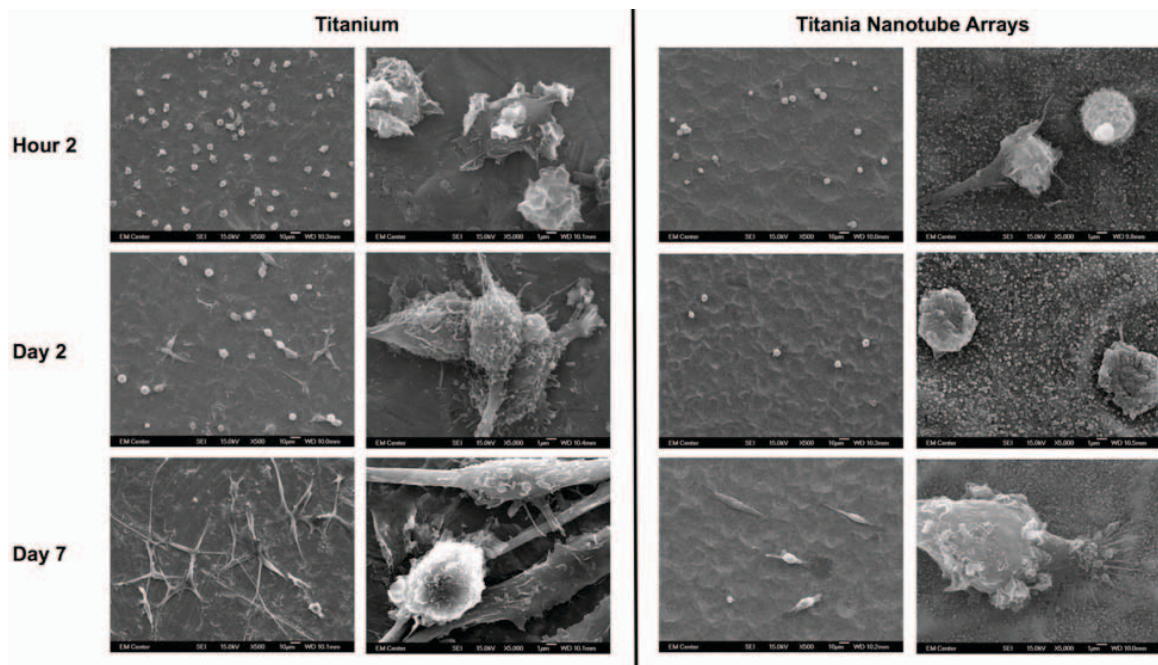


Figure 6.6 Representative SEM images of adhered immune cells on titania nanotube arrays and biomedical grade titanium after 2 hours, 2 and 7 days of incubation in human whole blood lysate. The substrates were coated with a 10 nm layer of gold and imaged at 15kV. The images indicate constrained cellular morphology on titania nanotube arrays, while showing increased cell-substrate integration and cell-cell interaction leading to the formation of foreign body giant cells on biomedical grade titanium.

The results show reduced short-term immune cell adhesion and morphology on titania nanotube arrays, clearly identifying a limited initial immune reaction. However, the high level of adhered immune cells on the control substrates show preliminary morphological changes of monocytes to macrophages, as seen by the cell structure from small round monocytes into the broader morphology of macrophages, by their greater cytoplasmic to nuclear area ratio. The increased activation of immune cells on the control substrates is likely due to substrate elicited immune cell activation, promoting additional cell-material and cell-cell activation. The results remain consistent after 2 and 7 days of culture where, even with the much reduced cell counts on both substrates, the trends of material interaction hold true. Titania nanotube arrays appear to facilitate a lack of immune cell adhesion, activation, morphological changes and overall integration, therefore reducing any possibility of cell-cell fusion. While the control substrates not only promote immune cell-biomaterial interaction, cellular activation (extreme morphological changes) and cell-cell fusion, but also result in the formation of FBGCs, showing preemptive signs of fibrous encapsulation. Thus, the specific nanotopography of the nanotube arrays directly correlates with a definitive reduction in initial immune cell adhesion and further cell-material integration. These traits are extremely promising for promoting the success of long-term implantable devices with a reduced immune response. Cellular differentiation and activation were determined by the presence of cell extensions, heightened cellular size and structure, and cellular fusion<sup>52</sup>.

In an attempt to degrade or phagocytose the biomaterial, adherent macrophages and neutrophils release degradative enzymes including nitric oxide synthase (iNOS) that plays a fundamental role in the immune response.. This small molecule mediates a

variety of physiological processes including vasodilation, inflammation, thrombosis, immunity and neurotransmission, hypotension, intercellular communication and toxic defense against infectious organisms, as well as regulating the functional activity, growth and death of many immune and inflammatory cell types<sup>53</sup>. Thus, the presence of this molecule determines the level of healthy integration of regions surrounding the implant. A commercially available Griess reagent kit was used in this study to detect the degree of nitrate present in the supernatant after 2 hours, 2 and 7 days of culture (See Figure 6.7).

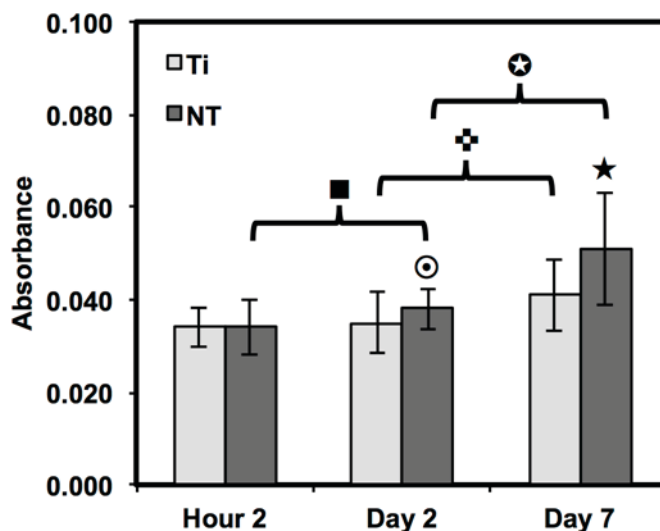


Figure 6.7 Nitric oxide release was measured by a Griess reagent. The results indicate a significant increase in long-term NO presence in substrate-exposed supernatant on titania nanotube arrays as compared to biomedical grade titanium. (□, □, □, ■, □ →  $p < 0.05$ )

The Griess diazotization reaction provides a quantitative analysis of nitrate, through a simple conversion of sulfanilic acid to a diazonium salt by nitrite interaction. Further

coupling of the diazonium salt to N-(1-naphthyl)ethylenediamine forms an azo dye, able to be spectrophotometrically detected at an absorbance of 548 nm. The results indicate a significant increase in NO between 2 hours and 7 days of culture on both substrates. In addition, the Griess reaction identifies a significant difference in NO released after 2 days of culture and a significant increase after 7 days of culture on titania nanotube arrays as compared to the control substrate. Studies have identified a connection between the activation of iNOS with IFN- $\gamma$  and TNF<sup>54</sup>. In addition, studies have shown that TGF- $\beta$ , IL-4 and IL-10 provide inhibitory signals to iNOS<sup>55,56</sup>. Due to the highly toxic effects of NO on cell functionality, the additional NO release seen on titania nanotube arrays may help to explain the reduced cellular proliferation and activation.

Inflammatory and wound healing cells such as lymphocytes, monocytes, macrophages, neutrophils and fibroblasts release inflammatory cytokines (small proteins) and chemokines (low molecule cytokines) following cellular adhesion and activation (See **Figure 6.8**)<sup>57</sup>.

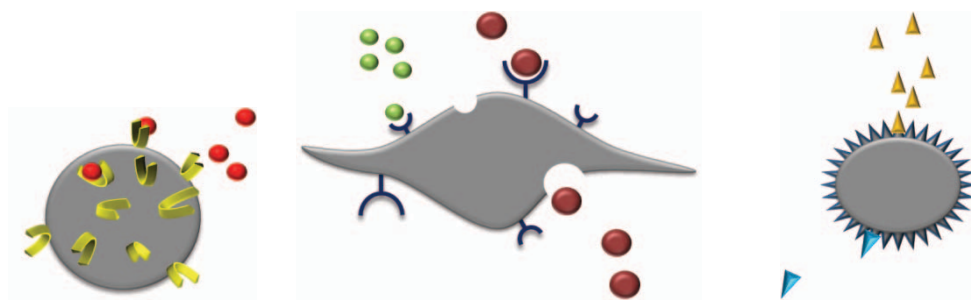


Figure 6.8 Schematic of various cell exocytosis and endocytosis of cytokine/chemokine processes.

This complex network of small proteins acts to modulate cellular interaction, infiltration, communication and behavior. In time, additional activation and matrix formation perpetuates inflammatory or wound healing responses. Cytokines bind to surface receptors, either promoting (pro-inflammatory) or impeding (anti-inflammatory) further intracellular function, intercellular communication and extracellular matrix (ECM) development. Pro-inflammatory cytokines including interleukins (IL-1 $\beta$ , IL-6, TNF $\alpha$ ) and interferons (IFN- $\gamma$ ) increase neutrophil production, stimulate lymphocyte proliferation and maturation, and promote inflammatory cytokine production. However, anti-inflammatory cytokines such as IL-4, IL-10 and IL-13 function as inhibitors for cytokine production, often by blocking cell receptor binding. Chemokines act to “chemo-attract” additional inflammatory and wound healing cells to the site of inflammation. Chemokine action is recognized and therefore moderated by two subgroups of receptors, CC receptors (CCRs) and CXC receptors (CXCRs) which recognize CC chemokines (MIP-1 $\beta$ , MCP-1) and CXC chemokines (IL-8) respectively. Through the presence of IL-8, for instance, neutrophils are drawn to the site of inflammation, while granule exocytosis is induced along with respiratory bursts that promote wound healing. Monocyte chemotactic proteins (MCP) and monocyte inflammatory proteins (MIP) attract immune cells including monocytes, leukocytes, basophils and/or eosinophils. Interferon (IFN- $\gamma$ ) and lipopolysaccharides (LPS) occur as the result of classically activated macrophages. These proteins act to produce NO, inhibit anti-inflammatory cytokines (IL-10), down-regulate mannose receptors and up-regulate pro-inflammatory cytokines (IL-1, IL-6, and TNF). In addition, an alternative path of macrophage activation by IL-4 and IL-13 cytokines plays a role in humoral immunity and repair. This

pathway acts to inhibit pro-inflammatory cytokines (IL-1, IL-6, and TNF), adjust chemokine expression, up-regulate mannose receptors and stimulate cytokine production (IL-10, IL-1ra). Thus, cytokines and chemokines are key factors in evaluating cellular activation and communication.

In this study, cellular expression was evaluated through the presence of cytokines and chemokines; known to affect specific functions within the inflammatory or wound healing processes including TNF, IFN- $\gamma$ , TGF- $\beta$ 1, MIP-1 $\beta$ , MCP-1, IL-1 $\beta$ , IL-6, IL-8, IL-10 and IL-12p70 after 2 hours, 2 and 7 days of culture (**See Figure 6.9**). The results identify cytokine activity of TNF, TGF- $\beta$ 1, MIP-1 $\beta$  and IL-8 after 2 hours of culture. Equivalent cytokine expression is shown on both substrates. The results show increased levels of cytokine expression of TNF, TGF- $\beta$ 1, MIP-1 $\beta$ , MCP-1, IL-1 $\beta$ , IL-6, IL-8 and IL-10 after 2 days of culture. Adhered immune cells show significant differences in the up regulation of TNF and IL-10 expression, while significantly deregulated of MIP-1 $\beta$ , MCP-1, IL-1 $\beta$ , IL-6 and IL-8 expression is present on titania nanotube arrays as compared to the control substrate. These findings identify the cellular attempt to reduce the immune response by the activation of the anti-inflammatory cytokine, IL-10 on both substrates. Further, the results identify the cytokine activity of TGF- $\beta$ 1, MIP-1 $\beta$ , MCP-1, IL-6 and IL-8 after 7 days of culture. TGF- $\beta$ 1, known for its profibrotic properties and its ability to actively suppress inflammation, is consistently expressed at all time points. This is likely due to the fact that TGF does not differentiate between its latent and active states. However, only in its active form does TGF bind to its receptor. Therefore, our results indicate the presence of TGF- $\beta$ 1 and do not determine its level of activation. In addition, TNF plays a large role in expanding the network of inflammatory cytokines.

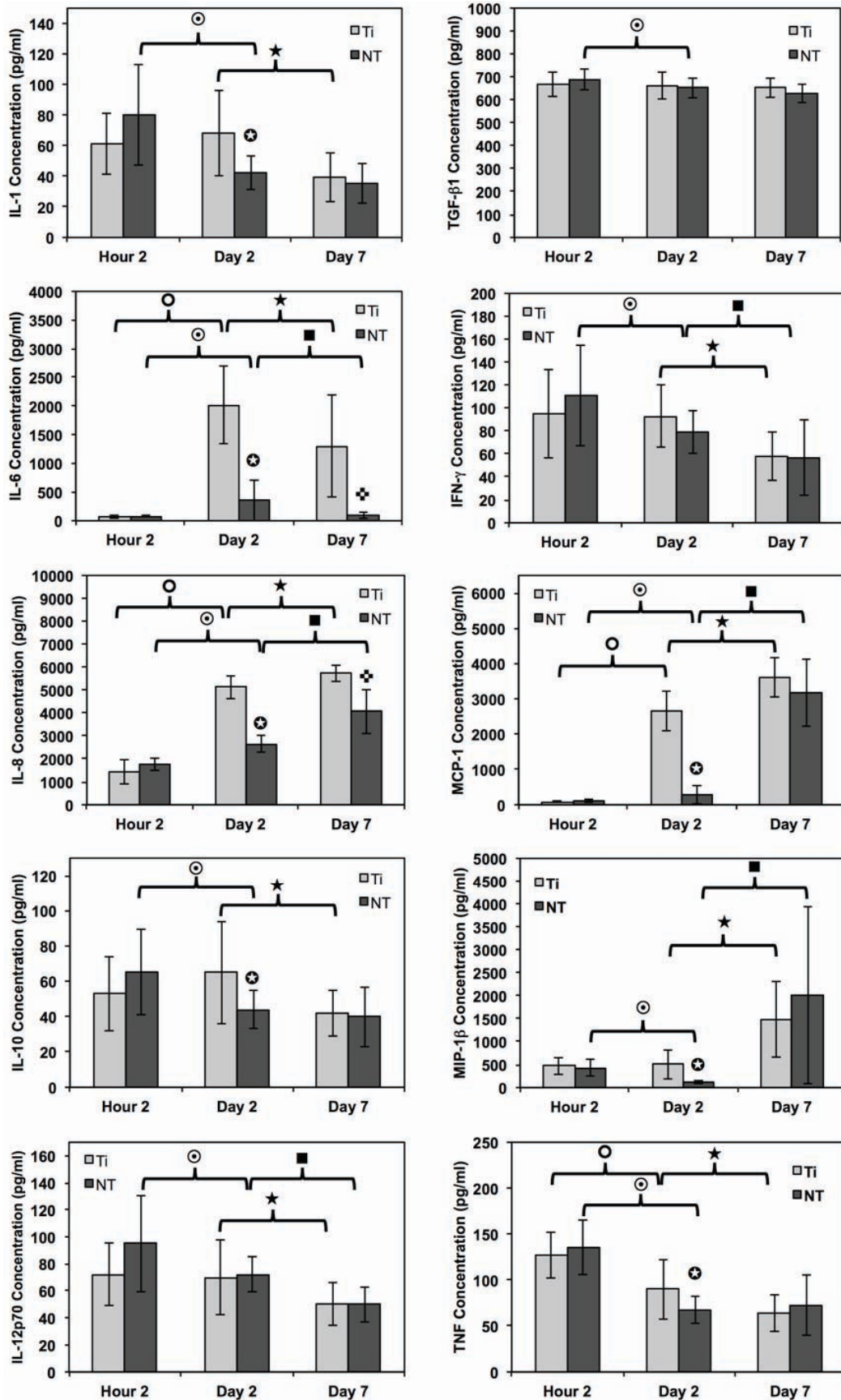


Figure 6.9 Cytokine/chemokine expression was identified using a CBA assay and flow cytometry. The results identify the presence of 10 different cytokines/chemokines including IL-1 $\beta$ , IL-6, IL-8, IL-10, IL-12p70, TNF, TGF- $\beta$ 1, IFN- $\gamma$ , MCP-1 and MIP-1 $\beta$ . The long-term results after 2 and 7 days of incubation in human whole blood lysate show significant reductions in protein expression on titania nanotube arrays as compared to biomedical grade titanium. (■,●,○,✚,★,⊕ → p < 0.05)

This cytokine shows a significantly decreased expression on both substrates between 2 hours and 2 days, indicating a reduced inflammatory response. The results show significant decreases in IL-6 and IL-8 expression on titania nanotube arrays as compared to the control substrate. Further indicating a significant reduction in the long-term expression of the pro-inflammatory cytokines and chemokines on titania nanotube arrays as compared to the control substrate. Thus, the results clearly confirm a reduction in immune responses on titania nanotube arrays (See Table 6.1(a) and (b)). Located on the outer membrane of gram-negative bacteria, LPS has been widely attributed to activating the immune response<sup>58,59</sup>. Thus, LPS was utilized as a positive control in determining its effect on immune cell activation in conjunction with titania nanotube arrays after 2 hours, 2 and 7 day of culture (See Figure 6.10). As expected, the results show an unmistakable increase in cytokine expression on titania nanotube arrays with the presence of LPS (See Table 6.2). Therefore, indicating that this factor contributes to increased immune cell functionality.

Table 6.1 (a and b) Summary of CBA results on titania nanotube arrays as compared to the control substrates after 2 hours, 2 and 7 days of culture. The results identify a decrease in long-term cytokine/chemokine expression on titania nanotube arrays as compared to the control substrates after 2 and 7 days of incubation in human whole blood lysate. (\* → p < 0.05)

(a)

Expression	Hour 2		Day 2		Day 7	
	Ti	NT	Ti	NT	Ti	NT
IL-1	=		* >		=	
IL-6	=		* >		* >	
IL-8	=		* >		* >	
IL-10	=		≠		=	
IL-12p70	=		=		=	
TGF-β1	=		=		=	
IFN-γ	=		=		=	
MCP-1	=		* >		=	
MIP-1β	=		* >		=	
TNF	=		≠		=	

(b)

Ti		NT		Expression	Ti		NT	
Hour 2	Day 2	Hour 2	Day 2		Day 2	Day 7	Day 2	Day 7
=		* >		IL-1	* >		=	
< *		< *		IL-6	* >		* >	
< *		< *		IL-8	< *		< *	
=		* >		IL-10	* >		=	
=		* >		IL-12p70	* >		* >	
=		* >		TGF-β1	=		=	
=		* >		IFN-γ	* >		* >	
< *		< *		MCP-1	< *		< *	
=		* >		MIP-1β	< *		< *	
* >		=		TNF	* >		< *	

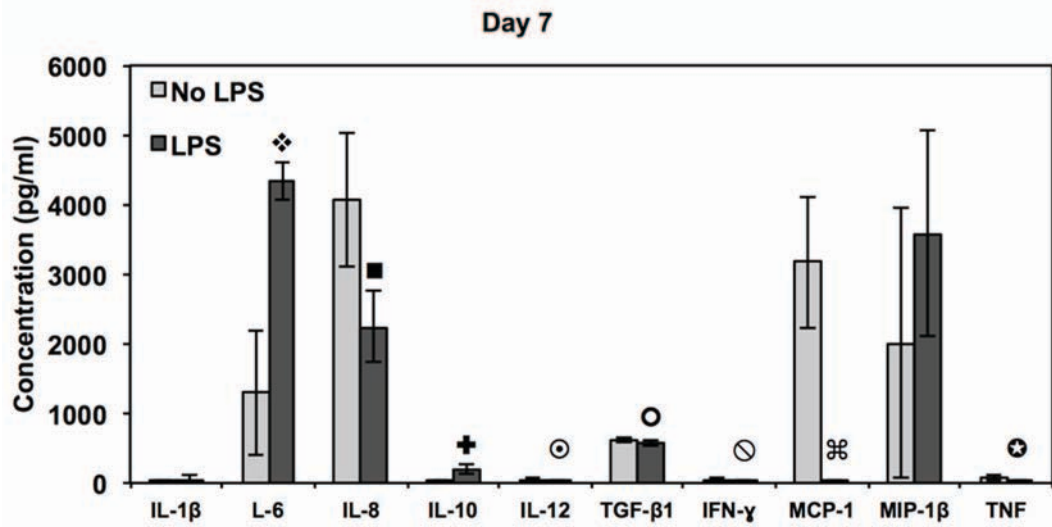
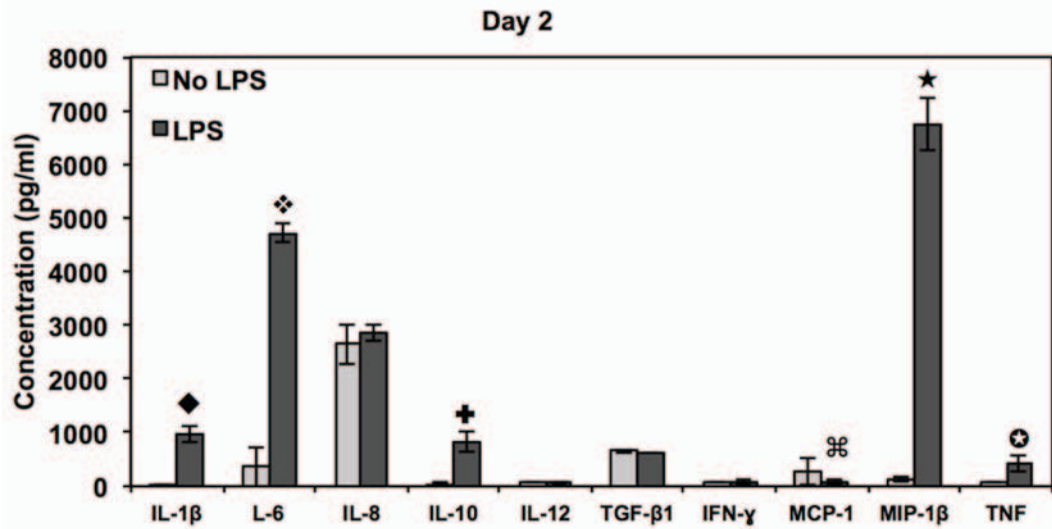
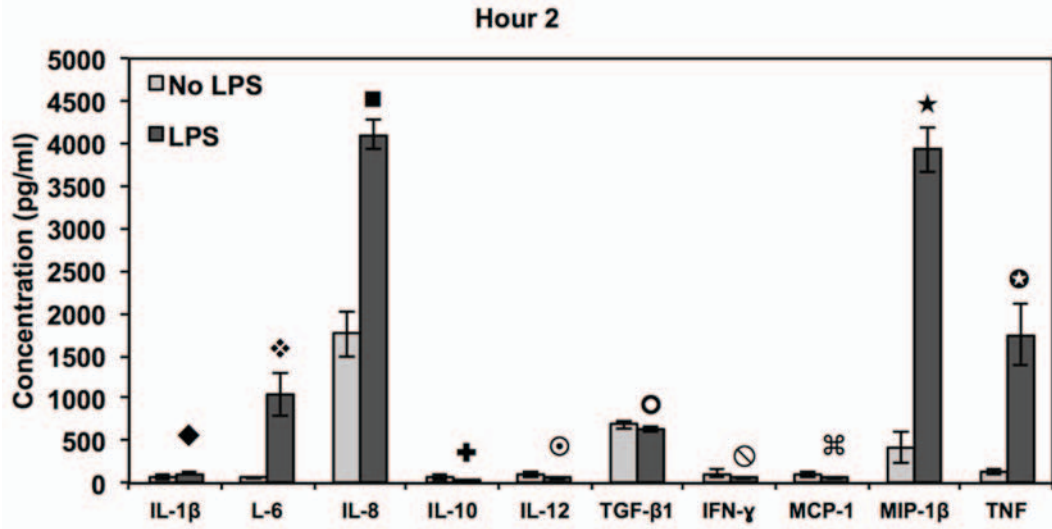


Figure 6.10 Cytokine/chemokine expression was identified using a CBA assay and flow cytometry. Human whole blood lysate incubated in RPMI medium with and without LPS tested for cytokine/chemokine expression after 2 hours, 2 and 7 days of incubation in human whole blood lysate on titania nanotube arrays as compared to the biomedical grade titanium. The results indicate altered short- and long-term cytokine/chemokine expression with the addition of LPS positive medium.  
 (◆, □, ■, □, ⊕, □, ⊕, □, □ → p < 0.05)

Table 6.2 Summary of CBA results for LPS positive samples on titania nanotube arrays as compared to the control substrate after 2 hours, 2 and 7 days of incubation in human whole blood lysate. (\* → p < 0.05)

Expression	Hour 2		Day 2		Day 7	
	NT + LPS	NT	NT + LPS	NT	NT + LPS	NT
IL-1	*	>	*	>	=	
IL-6	*	>	*	>	*	>
IL-8	*	>	=		<	*
IL-10	<	*	*	>	*	>
IL-12p70	<	*	=		<	*
TGF-β1	<	*	=		<	*
IFN-γ	<	*	=		<	*
MCP-1	<	*	<	*	<	*
MIP-1β	*	>	*	>	=	
TNF	*	>	*	>	<	*

## 6.4 Conclusion

The ability to modulate the adverse immune response of implantable biomedical devices will prove to be implemental in the success of long-term implants. The results presented here indicate a reduced immune reaction on titania nanotube arrays as compared to biomedical grade titanium after 2 hours, 2 and 7 days of culture with whole human blood lysate. MTT assays and fluorescence microscope images show significantly decreased cell viability and count after all time points on titania nanotube

arrays as compared to the control substrates. Short- and long-term monocyte, macrophage and neutrophil adhesion and proliferation evaluated by fluorescence microscope images indicate a reduction in cellular adhesion, proliferation and cytoskeletal reorganization on titania nanotube arrays. After 7 days of culture, fluorescence images identify extreme elongation and the formation of FBGCs on the control substrate, absent on titania nanotube arrays. In addition, SEM images identify a lack of cell-surface and cell-cell interaction on titania nanotube arrays, while prevalent on the control substrate. A Griess reaction kit shows significantly increased amounts of NO present on the nanotube arrays. Long-term cytokine and chemokine expression are shown to be significantly increased for MIP-1 $\beta$ , MCP-1, IL-6 and IL-8 on the control substrates, likely resulting from the cellular fusion and overall increased activation on the biomedical grade titanium substrates. These results suggest the improved biocompatibility of titania nanotube arrays, identifying this specific nanoarchitecture as a potential interface for promoting the short- and long-term success of implantable biomedical devices. The results presented here identify a physiologically relevant representation of the immune response on titania nanotube arrays, as whole human blood lysate includes a cell population similar to that of *in vivo* immune responses.

## 6.5 References

1. Jones, J. A. Biomaterials and the foreign body reaction: Surface chemistry dependent macrophage adhesion, fusion, apoptosis, and cytokine production. 3263192, Case Western Reserve University, United States -- Ohio, 2007.
2. Mooney, V.; Predecki, P. K.; Renning, J.; Gray, J., Skeletal extension of limb prosthetic attachments—problems in tissue reaction. *Journal of Biomedical Materials Research* **1971**, *5* (6), 143-159.
3. Anderson, J. M.; Rodriguez, A.; Chang, D. T., Foreign body reaction to biomaterials. *Seminars in Immunology* **2008**, *20* (2), 86-100.
4. Jackson, C. M.; Nemerson, Y., Blood Coagulation. *Annual Review of Biochemistry* **1980**, *49* (1), 765-811.
5. Luttkhuizen, D. T.; Harmsen, M. C.; Van Luyn, M. J., Cellular and molecular dynamics in the foreign body reaction. *Tissue Engineering* **2006**, *12* (7), 1955-70.
6. Remes, A.; Williams, D. F., Immune response in biocompatibility. *Biomaterials* **1992**, *13* (11), 731-743.
7. Cohen, J., Assay of Foreign-Body Reaction. *The Journal of Bone & Joint Surgery* **1959**, *41* (1), 152-166.
8. DiCarlo, E. F.; Bullough, P. G., The biologic responses to orthopedic implants and their wear debris. *Clinical Materials* **1992**, *9* (3-4), 235-260.
9. Mani, G.; Feldman, M. D.; Patel, D.; Agrawal, C. M., Coronary stents: A materials perspective. *Biomaterials* **2007**, *28* (9), 1689-1710.
10. Peuster, M.; Hesse, C.; Schloo, T.; Fink, C.; Beerbaum, P.; von Schnakenburg, C., Long-term biocompatibility of a corrodible peripheral iron stent in the porcine descending aorta. *Biomaterials* **2006**, *27* (28), 4955-4962.
11. John E, D., Bone bonding at natural and biomaterial surfaces. *Biomaterials* **2007**, *28* (34), 5058-5067.
12. Wang, K., The use of titanium for medical applications in the USA. *Materials Science and Engineering: A* **1996**, *213* (1-2), 134-137.
13. Jones, F. H., Teeth and bones: applications of surface science to dental materials and related biomaterials. *Surface Science Reports* **2001**, *42* (3-5), 75-205.
14. Lin, Y.; Gallucci, G. O.; Buser, D.; Bosshardt, D.; Belser, U. C.; Yelick, P. C., Bioengineered Periodontal Tissue Formed on Titanium Dental Implants. *Journal of Dental Research* **2011**, *90* (2), 251-256.
15. Bhargava, D.; Bartlett, P.; Russell, J.; Liddington, M.; Tyagi, A.; Chumas, P., Construction of titanium cranioplasty plate using craniectomy bone flap as template. *Acta Neurochirurgica* **2010**, *152* (1), 173-176.
16. Eufinger, H.; Wehmöller, M., Individual Prefabricated Titanium Implants in Reconstructive Craniofacial Surgery: Clinical and Technical Aspects of the First 22 Cases. *Plastic and Reconstructive Surgery* **1998**, *102* (2), 300-308.

17. Long, M.; Rack, H. J., Titanium alloys in total joint replacement--a materials science perspective. *Biomaterials* **1998**, *19* (18), 1621-1639.
18. Messinger, S. D., Incorporating the prosthetic: Traumatic, limb-loss, rehabilitation and refigured military bodies. *Disability & Rehabilitation* **2009**, *31* (25), 2130-2134.
19. Nammias, W., Titanium-nitride-oxide-coated bioactive stents: A novel evolution of stent technology. *International Journal of Cardiology* **2011**, *146* (3), 456-456.
20. Speroni, S.; Briguglio, F.; Maridat, i. P.; Beretta, M.; Maiorana, C., Hard and soft tissue augmentation in implant surgery: a case report. *Minerva Stomatologica* **2011**, *60* (3), 123-31
21. Niinomi, M., Mechanical biocompatibilities of titanium alloys for biomedical applications. *Journal of the Mechanical Behavior of Biomedical Materials* **2008**, *1* (1), 30-42.
22. Young-Taeg, S., The significance of the surface properties of oxidized titanium to the bone response: special emphasis on potential biochemical bonding of oxidized titanium implant. *Biomaterials* **2003**, *24* (22), 3893-3907.
23. Mendonça, G.; Mendonça, D. B. S.; Aragão, F. J. L.; Cooper, L. F., Advancing dental implant surface technology – From micron- to nanotopography. *Biomaterials* **2008**, *29* (28), 3822-3835.
24. Curtis, A.; Wilkinson, C., Topographical control of cells. *Biomaterials* **1997**, *18* (24), 1573-1583.
25. Decuzzi, P.; Ferrari, M., Modulating cellular adhesion through nanotopography. *Biomaterials* **2010**, *31* (1), 173-179.
26. Park, G. E. W., Thomas J., A Review of Nanotechnology for the Development of Better Orthopedic Implants. *Journal of Biomedical Nanotechnology* **2005**, *1*, 18-29.
27. Vogel, V.; Sheetz, M. P., Cell fate regulation by coupling mechanical cycles to biochemical signaling pathways. *Current Opinion in Cell Biology* **2009**, *21* (1), 38-46.
28. Dadsetan, M.; Jones, J. A.; Hiltner, A.; Anderson, J. M., Surface chemistry mediates adhesive structure, cytoskeletal organization, and fusion of macrophages. *Journal of Biomedical Materials Research Part A* **2004**, *71A* (3), 439-448.
29. Kunzler, T. P.; Huwiler, C.; Drobek, T.; Vörös, J.; Spencer, N. D., Systematic study of osteoblast response to nanotopography by means of nanoparticle-density gradients. *Biomaterials* **2007**, *28* (33), 5000-5006.
30. Khang, D.; Sato, M.; Price, R. L.; Ribbe, A. E.; Webster, T. J., Selective adhesion and mineral deposition by osteoblasts on carbon nanofiber patterns. Dove Medical Press: 2006; Vol. 1, pp 65-72.

31. Ruckh, T. T.; Kumar, K.; Kipper, M. J.; Popat, K. C., Osteogenic differentiation of bone marrow stromal cells on poly(epsilon-caprolactone) nanofiber scaffolds. *Acta Biomater* **2010**, *6* (8), 2949-59.
32. La Flamme, K. E.; Popat, K. C.; Leoni, L.; Markiewicz, E.; La Tempa, T. J.; Roman, B. B.; Grimes, C. A.; Desai, T. A., Biocompatibility of nanoporous alumina membranes for immunoisolation. *Biomaterials* **2007**, *28* (16), 2638-2645.
33. Popat, K. C.; Leary Swan, E. E.; Mukhatyar, V.; Chatvanichkul, K.-I.; Mor, G. K.; Grimes, C. A.; Desai, T. A., Influence of nanoporous alumina membranes on long-term osteoblast response. *Biomaterials* **2005**, *26* (22), 4516-4522.
34. Porter, J. R.; Henson, A.; Popat, K. C., Biodegradable poly(epsilon-caprolactone) nanowires for bone tissue engineering applications. *Biomaterials* **2009**, *30* (5), 780-8.
35. Bechara, S.; Wadman, L.; Popat, K. C., Electroconductive polymeric nanowire templates facilitates in vitro C17.2 neural stem cell line adhesion, proliferation and differentiation. *Acta Biomaterialia* **2011**, *7* (7), 2892-2901.
36. Jayawarna, V.; Ali, M.; Jowitt, T. A.; Miller, A. F.; Saiani, A.; Gough, J. E.; Ulijn, R. V., Nanostructured Hydrogels for Three-Dimensional Cell Culture Through Self-Assembly of Fluorenylmethoxycarbonyl-Dipeptides. *Advanced Materials* **2006**, *18* (5), 611-614.
37. Brammer, K. S.; Oh, S.; Cobb, C. J.; Bjursten, L. M.; Heyde, H. v. d.; Jin, S., Improved bone-forming functionality on diameter-controlled TiO<sub>2</sub> nanotube surface. *Acta Biomaterialia* **2009**, *5* (8), 3215-3223.
38. Park, J.; Bauer, S.; von der Mark, K.; Schmuki, P., Nanosize and Vitality: TiO<sub>2</sub> Nanotube Diameter Directs Cell Fate. *Nano Letters* **2007**, *7* (6), 1686-1691.
39. Popat, K. C.; Leoni, L.; Grimes, C. A.; Desai, T. A., Influence of engineered titania nanotubular surfaces on bone cells. *Biomaterials* **2007**, *28* (21), 3188-3197.
40. von Wilmowsky, C.; Bauer, S.; Roedl, S.; Neukam, F. W.; Schmuki, P.; Schlegel, K. A., The diameter of anodic TiO<sub>2</sub> nanotubes affects bone formation and correlates with the bone morphogenetic protein-2 expression in vivo. *Clinical Oral Implants Research* **2011**, *23* (3), 359-366.
41. Peng, L.; Eltgroth, M. L.; LaTempa, T. J.; Grimes, C. A.; Desai, T. A., The effect of TiO<sub>2</sub> nanotubes on endothelial function and smooth muscle proliferation. *Biomaterials* **2009**, *30* (7), 1268-1272.
42. Smith, B. S.; Yoriya, S.; Grissom, L.; Grimes, C. A.; Popat, K. C., Hemocompatibility of titania nanotube arrays. *Journal of Biomedical Materials Research Part A* **2010**, *95A* (2), 350-360.
43. Smith, B. S.; Yoriya, S.; Johnson, T.; Popat, K. C., Dermal fibroblast and epidermal keratinocyte functionality on titania nanotube arrays. *Acta Biomaterialia* **2011**, *7* (6), 2686-2696.

44. Puckett, S. D.; Lee, P. P.; Ciombor, D. M.; Aaron, R. K.; Webster, T. J., Nanotextured titanium surfaces for enhancing skin growth on transcutaneous osseointegrated devices. *Acta Biomaterialia* **2010**, *6* (6), 2352-2362.
45. von der Mark, K.; Bauer, S.; Park, J.; Schmuki, P., Another look at “Stem cell fate dictated solely by altered nanotube dimension”. *Proceedings of the National Academy of Sciences* **2009**, *106* (24), E60.
46. Bauer, S.; Park, J.; Faltenbacher, J.; Berger, S.; von der Mark, K.; Schmuki, P., Size selective behavior of mesenchymal stem cells on ZrO<sub>2</sub> and TiO<sub>2</sub> nanotube arrays. *Integrative Biology* **2009**, *1* (8-9), 525-532.
47. Kodama, A.; Bauer, S.; Komatsu, A.; Asoh, H.; Ono, S.; Schmuki, P., Bioactivation of titanium surfaces using coatings of TiO<sub>2</sub> nanotubes rapidly pre-loaded with synthetic hydroxyapatite. *Acta Biomaterialia* **2009**, *5* (6), 2322-2330.
48. Popat, K.; Eltgroth, M.; LaTempa, T.; Grimes, C.; Desai, T., Titania Nanotubes: A Novel Platform for Drug-Eluting Coatings for Medical Implants? *Small* **2007**, *3* (11), 1878-1881.
49. Roy, P.; Berger, S.; Schmuki, P., TiO<sub>2</sub> Nanotubes: Synthesis and Applications. *Angewandte Chemie International Edition* **2011**, *50* (13), 2904-2939.
50. Ruan, C.; Paulose, M.; Varghese, O. K.; Mor, G. K.; Grimes, C. A., Fabrication of Highly Ordered TiO<sub>2</sub> Nanotube Arrays Using an Organic Electrolyte. *The Journal of Physical Chemistry B* **2005**, *109* (33), 15754-15759.
51. Anderson, J. M., Chapter 4 Mechanisms of inflammation and infection with implanted devices. *Cardiovascular Pathology* **1993**, *2* (3, Supplement), 33-41.
52. Rhee, H. J.; Burgh-de Winter, C. P. M.; Daems, W. T., The differentiation of monocytes into macrophages, epithelioid cells, and multinucleated giant cells in subcutaneous granulomas. *Cell and Tissue Research* **1979**, *197* (3), 355-378.
53. Nathan, C., Nitric oxide as a secretory product of mammalian cells. *The FASEB journal : official publication of the Federation of American Societies for Experimental Biology* **1992**, *6* (12), 3051-64.
54. Munder, M.; Mallo, M.; Eichmann, K.; Modolell, M., Murine Macrophages Secrete Interferon  $\gamma$  upon Combined Stimulation with Interleukin (IL)-12 and IL-18: A Novel Pathway of Autocrine Macrophage Activation. *The Journal of Experimental Medicine* **1998**, *187* (12), 2103-2108.
55. Brodie, C.; Goldreich, N.; Haiman, T.; Kazimirsky, G., Functional IL-4 receptors on mouse astrocytes: IL-4 inhibits astrocyte activation and induces NGF secretion. *Journal of Neuroimmunology* **1998**, *81* (1-2), 20-30.
56. Bogdan, C., Nitric oxide and the immune response. *Nature immunology* **2001**, *2* (10), 907-16.
57. Higgins, D. M.; Basaraba, R. J.; Hohnbaum, A. C.; Lee, E. J.; Grainger, D. W.; Gonzalez-Juarrero, M., Localized Immunosuppressive Environment in the Foreign Body Response to Implanted Biomaterials. *The American journal of pathology* **2009**, *175* (1), 161-170.

58. Hoffmann, J. A., The immune response of *Drosophila*. *Nature* **2003**, 426 (6962), 33-38.
59. Moret, Y.; Schmid-Hempel, P., Survival for Immunity: The Price of Immune System Activation for Bumblebee Workers. *Science* **2000**, 290 (5494), 1166-1168.

## CHAPTER 7

### CONCLUSIONS AND DIRECTION OF FUTURE WORK

#### 7.1 Conclusions

The rejection of biomedical implants is a critical concern affecting up to 10% of these devices, resulting in the agony and cost of revision surgery. Transcutaneous intraosseous implantable devices (amputee prosthesis) are in constant interaction with the bone, blood and skin at the biomaterial (titanium and titanium alloys) interface. Poor implant integration and further failure of these devices often results from the lack of skin integration, unfavorable blood interactions, thrombosis and detrimental immune reactions. Thus, the ability to modulate the natural physiological response to titanium surfaces in terms of skin integration, optimal hemocompatibility, decreased thrombosis and immune reaction will contribute substantially to the long-term success of these implantable devices. Recently, there has been an increased interest in exploring nanoscale surface topographies as biomimetic interfaces for implantable devices. Several studies have reported favorable cellular response to such nanoscale topographies. However, very few studies document the skin, blood and immune response to nanoscale architectures. The simple fabrication, physiologically relevant nano-architecture, improved osseointegration and the capability for localized drug delivery identify titania nanotube arrays as promising interfaces for implantable biomedical devices.

In this study, titania nanotube arrays were specifically evaluated for their potential application as interfaces for transcutaneous implantable devices. This work reports on the effect of uniform, immobilized, vertically oriented and high aspect ratio titania

nanotube arrays (diameter 70-170 nm and length 1-1.5  $\mu\text{m}$ ) on skin cell functionality, hemocompatibility, thrombogenicity and the immune response. The titania nanotube arrays were fabricated using a simple anodization process. Material surface characteristics including morphology, nano-architecture, crystallinity, hydrophobicity, hardness and its ability to withstand surface delamination were evaluated using SEM, AFM, XRD, contact angle, nano-indentation and micro-scratch testing respectively. The results identify a hydrophilic nano-architecture composed of two crystalline phases (anatase and rutile). These characteristics enable improved cellular integration, additional surface area and structural stability on the interface. In addition, these interfaces provide a reduced scratch resistance and hardness comparable to that of biomedical grade titanium, evidencing a surface with appropriate mechanical properties for soft tissue interface.

Skin cell functionality for human epidermal keratinocytes (HEK) and human dermal fibroblasts (HDF) was investigated in terms of adhesion, proliferation, orientation, viability, cytoskeletal organization, differentiation and morphology. Cellular functionality was investigated for up to 4 days of culture using fluorescence microscope imaging, a cell viability assay, indirect immunofluorescence and scanning electron microscopy. The results reported in this study indicate increased dermal fibroblast and decreased epidermal keratinocyte adhesion, proliferation and differentiation on titania nanotube arrays. Thus, the nanotube architecture provides a favorable template for the growth and maintenance of dermal fibroblasts while preventing differentiation of epidermal keratinocytes. Such cellular behavior is extremely important for inducing fibroblast matrix formation, enabling quick healing and wound closure after device

implantation. This will enable primary integration between the dermis and the transcutaneous implantable device, followed by secondary epidermal integration based on subsequent cell signaling and cell-cell attachment.

The hemocompatibility of titania nanotube arrays was investigated through the adsorption of key blood serum proteins (albumin, fibrinogen and immunoglobulin-g), platelet adhesion and activation and the clotting kinetics of whole human blood. Protein adsorption was evaluated using micro-BCA and XPS. The adhesion and activation of human platelets, isolated from whole human blood, were investigated using live-cell staining, MTT assay and SEM imaging. The clotting kinetics of whole human blood was evaluated by measuring the free hemoglobin concentration and further imaging by SEM to visualize the clot formation. The results identify comparable whole blood clotting kinetics, and increased blood serum protein adsorption, platelet adhesion and activation. This evidences an altered hemocompatibility on titania nanotube arrays.

The thrombogenicity of titania nanotube arrays was investigated by incubation in whole human plasma. Thus, platelet/leukocyte adhesion, activation and interaction, morphology, complement activation, contact activation, platelet release reaction, fibrinogen expression and material cytotoxicity were evaluated to determine the *in vitro* thrombogenicity. Platelet/leukocyte adhesion, evaluated using fluorescence microscope images, indicates a significant decrease in the total number of platelets and leukocytes as well as the total cellular coverage on titania nanotube arrays. In addition, SEM images and enzyme immunoassays show limited surface-induced activation and morphology on titania nanotube arrays. A significant increase in contact activation was further identified on titania nanotube arrays, likely resulting from their increased surface area. Enzyme

immunoassays indicate slightly decreased levels of complement activation and a slightly increased degree of free fibrinogen expressed on titania nanotube arrays, showing a decrease in surface induced fibrin clot formation. These results suggest improved blood-compatibility of titania nanotube arrays, identifying this nanoarchitecture as a potential interface for promoting the long-term success of blood-contacting implants. The results presented here indicate a decrease in thrombogenic effects with the use of titania nanotube arrays as compared to biomedical grade titanium after 2 hours of contact with whole blood plasma.

The short- and long-term immune response with titania nanotube arrays was evaluated by incubation in whole blood lysate after 2 hours, 2 and 7 days. The results presented here identify a physiologically relevant representation of the immune response on titania nanotube arrays, as whole human blood lysate includes a cell population similar to that of *in vivo* immune responses. Immune cell functionality was evaluated by cellular adhesion, proliferation, viability, morphology, nitric oxide release and cytokine / chemokine expression with and without LPS. Short- and long-term monocyte, macrophage and neutrophil viability, adhesion and proliferation, as shown by an MTT assay and fluorescence microscope images, show a reduction in cell/nano-biomaterial interaction on titania nanotube arrays. After 7 days of culture, fluorescence microscope and SEM images identify extreme elongation and the formation of FBGCs on biomedical grade titanium, substantially absent on titania nanotube arrays. A Griess reaction shows significantly increased amounts of NO present on the nanotube arrays. Long-term cytokine and chemokine expression are shown to be significantly increased for MIP-1 $\beta$ , MCP-1, IL-6 and IL-8 on the control substrates, likely resulting from the cellular fusion

and overall increased activation on the biomedical grade titanium substrates. These results indicate a decrease in short- and long-term monocyte, macrophage and neutrophil functionality, further identifying a reduced immune response on titania nanotube arrays.

The results of this work suggest the improved biocompatibility of titania nanotube arrays. The findings indicate enhanced dermal matrix production, altered hemocompatibility, reduced thrombogenicity and a deterred immune response on this specific nanoarchitecture. This evidences promising implications with respect to the use of titania nanotube arrays as beneficial interfaces for the successful implantation of biomedical devices.

## **7.2 Future Work**

The simple fabrication, physiologically relevant architecture, strong mechanical properties and promising cellular interactions identify titania nanotube arrays as advantageous interfaces for implantable biomedical devices. There is a precise correlation between the anodization voltage and nanotube pore size, thus by varying the voltage and anodization time, nanotubes with different diameters and lengths can be fabricated. The cellular response may be tuned and optimized by varying the size parameters of titania nanotube arrays. Further studies will be targeted towards understanding the effects of altered anodization processes on structural and mechanical nanotube characteristics. In addition, future research will focus on evaluating the effects of these modified anodization parameters such as variable nanotube dimensions and altered mechanical properties on cellular functionality. The ability to modulate the

natural protein and cellular interactions with the implantable biomedical devices will prove to be implemental in the success of long-term implants.

Implications of this work, and the potential for titania nanotube arrays as interfaces for use in implantable devices, will require the development of mathematical models and *in vivo* studies. Mathematical models will enable consistent, situation specific answers to fundamental questions of the long-term ability to produce viable tissue/nano-biomaterial integration. *In vivo* studies will investigate the long-term effect of titania nanotube arrays on healthy tissue development including vascularization and ECM production as opposed to adverse physiological effects such as thrombosis, the release of super oxides and dense fibrous encapsulation. In addition, further investigation will be necessary regarding biomolecular modifications and localized drug delivery to enhance the long-term use of implantable biomedical devices. This future research will provide answers to fundamental questions regarding the long-term functionality of titania nanotube arrays in highly representative scenarios. Future research will help direct the use of these interfaces for appropriate clinical applications.